

โครงสร้างและพลวัตของน้ำ: การศึกษาเชิงเปรียบเทียบการจำลองพลวัตเชิง
โมเลกุลที่ผสมผสานกลศาสตร์ควอนตัมและกลศาสตร์โมเลกุลแบบดั้งเดิม
และบนพื้นฐานของวิธีไอเนียม-เอกซ์เอส

นางสาวสุคนทิพย์ เถาว์โมลา

วิทยานิพนธ์นี้เป็นส่วนหนึ่งของการศึกษาตามหลักสูตรปริญญาวิทยาศาสตรดุษฎีบัณฑิต
สาขาวิชาเคมี
มหาวิทยาลัยเทคโนโลยีสุรนารี
ปีการศึกษา 2554

**STRUCTURE AND DYNAMICS OF LIQUID WATER:
A COMPARATIVE STUDY OF CONVENTIONAL
QM/MM AND ONIOM-XS MD SIMULATIONS**

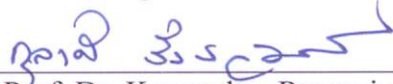
Sukhontip Thaomola

**A Thesis Submitted in Partial Fulfillment of the Requirements for the
Degree of Doctor of Philosophy in Chemistry
Suranaree University of Technology
Academic Year 2011**

**STRUCTURE AND DYNAMICS OF LIQUID WATER: A
COMPARATIVE STUDY OF CONVENTIONAL QM/MM
AND ONIOM-XS MD SIMULATIONS**

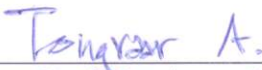
Suranaree University of Technology has approved this thesis submitted in partial fulfillment of the requirements for the Degree of Doctor of Philosophy.

Thesis Examining Committee



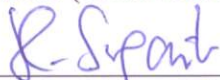
(Asst. Prof. Dr. Kunwadee Rangriwatananon)

Chairperson



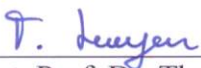
(Assoc. Prof. Dr. Anan Tongraar)

Member (Thesis Advisor)



(Prof. Dr. Krittana Sagarik)

Member



(Asst. Prof. Dr. Thanaporn Manyum)

Member



(Asst. Prof. Dr. Teerakiat Kerdcharoen)

Member



(Prof. Dr. Sukit Limpijumngong)

Vice Rector for Academic Affairs



(Assoc. Prof. Dr. Prapun Manyum)

Dean of Institute of Science

สุคนทิพย์ เถาว์โมลา : โครงสร้างและพลวัตของน้ำ: การศึกษาเชิงเปรียบเทียบการจำลอง
พลวัตเชิงโมเลกุลที่ผสมผสานกลศาสตร์ควอนตัมและกลศาสตร์โมเลกุลแบบดั้งเดิมและ
บนพื้นฐานของวิธีไอเนียม-เอกซ์เอส (STRUCTURE AND DYNAMICS OF LIQUID
WATER: A COMPARATIVE STUDY OF CONVENTIONAL QM/MM AND
ONIOM-XS MD SIMULATIONS) อาจารย์ที่ปรึกษา : รองศาสตราจารย์ ดร.
อนันต์ ทองระอา, 121 หน้า.

การจำลองพลวัตเชิงโมเลกุลที่ผสมผสานกลศาสตร์ควอนตัมและกลศาสตร์โมเลกุลแบบ
ดั้งเดิม (conventional QM/MM MD) และบนพื้นฐานของวิธีไอเนียม-เอกซ์เอส (ONIOM-XS MD)
ได้ถูกดำเนินการเพื่อศึกษาสมบัติเชิงโครงสร้างและเชิงพลวัตของน้ำ โดยเทคนิคการจำลองพลวัต
เชิงโมเลกุลขั้นสูงนี้ ส่วนที่ให้ความสนใจมากที่สุดได้แก่บริเวณพื้นที่ทรงกลมขนาดเล็กที่
ประกอบด้วยน้ำที่จุดศูนย์กลางทรงกลมจำนวนหนึ่ง โมเลกุลและน้ำที่อยู่รอบๆ น้ำที่จุดศูนย์กลางอีก
จำนวนหนึ่งซึ่งจะถูกอธิบายโดยใช้กลศาสตร์ควอนตัมในระดับฮาร์ตรี-ฟอก (HF) โดยใช้เบซิสเซต
ชนิด DZP ในขณะที่ส่วนที่เหลือของระบบจะถูกอธิบายโดยใช้ฟังก์ชันศักย์ของน้ำแบบยืดหยุ่นชนิด
BJH-CF2 ผลการศึกษาที่ได้จากการจำลองพลวัตเชิงโมเลกุลทั้งสองประเภท พบว่า การจัดเรียงตัว
ของพันธะไฮโดรเจนในน้ำมีความยืดหยุ่นค่อนข้างสูง โดยน้ำที่กระจายอยู่รอบๆ น้ำที่จุดศูนย์กลาง
ทรงกลมจะยึดเหนี่ยวกับน้ำที่จุดศูนย์กลางทรงกลมทั้งในลักษณะแบบหลวมๆ และแบบแข็งแรง
ลักษณะดังกล่าว ส่งผลให้เกิดกลไกการแลกเปลี่ยนน้ำทั้งในแบบที่ใช้เวลาสั้นๆ และแบบที่ใช้
เวลานาน รวมถึงส่งผลต่อการกวัดแกว่งของจำนวนพันธะไฮโดรเจนในน้ำที่สามารถเกิดขึ้นได้
ตั้งแต่ 2 ถึง 6 พันธะ โดยมีค่าความถี่สูงสุดเป็นลักษณะ 4 พันธะ เมื่อพิจารณาผลการจำลองพลวัต
เชิงโมเลกุลที่ได้จากเทคนิคไอเนียม-เอกซ์เอส (เปรียบเทียบกับผลการจำลองโดยเทคนิค QM/MM
MD แบบดั้งเดิม) พบว่า จำนวนพันธะไฮโดรเจนในน้ำในลักษณะที่เป็นแบบ 4 พันธะมีส่วน
ลดลงอย่างมีนัยสำคัญ ในขณะที่การจัดเรียงตัวของน้ำที่สอดคล้องกับการเกิดพันธะไฮโดรเจน
จำนวน 2 และ 3 พันธะ มีสัดส่วนเพิ่มขึ้นอย่างชัดเจน เมื่อพิจารณาผลการเปรียบเทียบระหว่างการ
จำลองพลวัตเชิงโมเลกุลทั้งสองประเภทในภาพรวมทั้งหมด กล่าวได้ว่า ผลการศึกษาที่แตกต่างกัน
นั้น แสดงให้เห็นถึงความสำคัญของการประยุกต์เทคนิค ONIOM-XS สำหรับการศึกษาเพื่อทำความเข้าใจ
เกี่ยวกับสมบัติเชิงโครงสร้างและเชิงพลวัตของน้ำ

สาขาวิชาเคมี
ปีการศึกษา 2554

ลายมือชื่อนักศึกษา อโณทัย
ลายมือชื่ออาจารย์ที่ปรึกษา

SUKHONTIP THAOMOLA : STRUCTURE AND DYNAMICS OF
LIQUID WATER: A COMPARATIVE STUDY OF CONVENTIONAL
QM/MM AND ONIOM-XS MD SIMULATIONS. THESIS ADVISOR :
ASSOC. PROF. ANAN TONGRAAR, Ph.D. 121 PP.

LIQUID WATER/ QM/MM/ ONIOM-XS

Molecular dynamics (MD) simulations based on conventional QM/MM scheme and ONIOM-XS method have been performed to investigate the structural and dynamical properties of liquid water. The region of highest interest, *i.e.*, a sphere which contains a central water molecule and its nearest-neighbor waters, was treated at the Hartree-Fock (HF) level of theory using DZP basis set, while the rest of the system was described by the flexible BJH-CF2 model. With regard to both the HF/MM and ONIOM-XS trajectories, the arrangement of hydrogen bonds (HBs) in liquid water is found to be rather flexible, in which the nearest-neighbors are either “loosely” or “tightly” bound to the central water molecule. Consequently, this leads to numerous water exchange mechanisms, with either “short-live” or “long-live” exchange periods, as well as to large fluctuations in the number of HBs, ranging from 2 to 6, with the prevalent value of 4. By means of the ONIOM-XS simulation, it is observed that the structural arrangement of liquid water with respect to 4 HBs decreases significantly and that the distributions of 2- and 3-fold HB species become more visible, *i.e.*, compared to the HF/MM results. Overall, the observed differences

between the HF/MM and ONIOM-XS simulations clearly indicate the important treatment of the ONIOM-XS method in describing the properties of liquid water.

School of Chemistry

Academic Year 2011

Student's Signature Sukhontip T.

Advisor's Signature Tongrart An

ACKNOWLEDGEMENTS

I wish to express my deep gratitude to all of people who gave me the possibility to complete this thesis. First of all, most of credits in this thesis should justifiably go to my advisor, Assoc. Prof. Dr. Anan Tongraar, for his guidance, valuable suggestions, kindness and encouragement throughout the course of my graduate. I would like to thank Prof. Dr. Kritsana Sagarik and all lecturers at School of Chemistry, Institute of Science, Suranaree University of Technology (SUT), for their encouragement and help. I would like to thank all committee members for their time and useful comments and suggestions. Furthermore, I am thankful to Prof. Dr. Wesley D. Allen for his kindness and sincere suggestions for my research work and life when I visited his research group at University of Georgia, United States of America.

During the course of my work at SUT, I was supported by grant under the program “Strategic Scholarships for Frontier Research Network from the Commission on Higher Education”, Thailand. Special thanks should go to School of Chemistry, Institute of Science, SUT, for powerful research facilities. I would also like to thank all of my friends for their friendship. Although I cannot name all of them, but of course, I will always remember them.

Finally, I would like to express my deepest gratitude to my parents, brother, husband and daughter for their unconditional love and all supports.

Sukhontip Thaomola

CONTENTS

	Page
ABSTRACT IN THAI.....	I
ABSTRACT IN ENGLISH	II
ACKNOWLEDGEMENTS.....	IV
CONTENTS.....	V
LIST OF TABLES.....	VIII
LIST OF FIGURES	IX
LIST OF ABBREVIATIONS.....	XIII
CHAPTER	
I INTRODUCTION.....	1
1.1 Literature reviews.....	1
1.2 Research objectives.....	7
1.3 Scope and limitation of the study.....	7
1.4 References.....	8
II THEORETICAL AND COMPUTATIONAL METHODS	15
2.1 Quantum mechanics.....	15
2.1.1 Schrödinger equation	15
2.1.2 Born-Oppenheimer approximation	17
2.1.3 Independent electron approximation and Hartree products.....	18
2.1.4 The antisymmetry principle and Slater determinants	20

CONTENTS (Continued)

	Page
2.1.5 The Hartree-Fock approximation.....	22
2.1.6 Basis set	24
2.1.7 Electron correlation.....	29
2.2 Computational methods	30
2.2.1 Introduction to molecular dynamics (MD) simulation	30
2.2.2 Intermolecular potentials	32
2.2.3 Time integration algorithms.....	33
2.2.4 Statistical mechanics.....	38
2.2.5 The periodic box	41
2.2.6 Non-bonded neighbor lists.....	45
2.2.7 Long-range interactions	46
2.3 Research methodology.....	48
2.3.1 Conventional QM/MM MD scheme.....	48
2.3.2 QM/MM MD based on ONIOM-XS method	50
2.4 References.....	53
III RESEARCH PROCEDURES	57
3.1 Selection of QM method, QM size and basis set.....	57
3.2 Simulation details.....	61
3.3 Determination of system's properties	63
3.3.1 Structural properties.....	63

CONTENTS (Continued)

	Page
3.3.2 Dynamical properties	64
3.4 References	65
IV RESULTS AND DISCUSSION	68
4.1 Structural properties	68
4.2 Dynamical properties	80
4.2.1 Hindered translational motions	81
4.2.2 Librational motions	83
4.2.3 Vibrational motions	88
4.2.4 Self-diffusion coefficient (D)	92
4.2.5 Water exchange processes	93
4.3 References	99
V CONCLUSION	103
APPENDICES	104
APPENDIX A LIST OF PRESENTATIONS	105
APPENDIX B MANUSCRIPT	106
CURRICULUM VITAE	121

LIST OF TABLES

Table	Page
3.1 Basis set superposition error of (H ₂ O) ₃ complex, calculated at HF, B3LYP, MP2 and CCSD levels of accuracy using two different basis sets	61
4.1 Structural parameters of liquid water, as obtained by various QM/MM MD simulations and experiments	71
4.2 Vibrational frequencies (Q_1 , Q_2 and Q_3) of liquid water, as obtained by various MD simulations and experiments (numbers in parenthesis correspond to the shoulders)	90
4.3 Mean residence times ($\tau_{H_2O}^*$) of water molecules, calculated within first minimum of the HF/MM and ONIOM-XS's O-O _w RDFs	99

LIST OF FIGURES

Figure	Page
2.1 The Slater-type and Gaussian-type for 1s orbital	26
2.2 The STO-3G basis set representing the desired STO	27
2.3 The scheme of molecular dynamics simulation	31
2.4 Comparison of macroscopic and microscopic systems	39
2.5 The periodic box in two dimensions	42
2.6 The discontinuity of energy curve when the potential is truncated.....	43
2.7 The effect of a switching function applied to the Lennard-Jones potential	45
2.8 The non-bonded neighbor list.....	46
2.9 The QM/MM scheme	48
2.10 QM/MM MD based on ONIOM-XS method.....	51
3.1 Requirements of CPU times for HF, B3LYP, MP2 and CCSD force calculations of (H ₂ O) _n , n=1,15 complexes using DZP basis set	58
3.2 Requirements of CPU times for HF force calculations of (H ₂ O) _n , n=1- 15 complexes using DZP and AUG-cc-pVDZ basis sets.....	59
3.3 Geometry of (H ₂ O) ₃ complex.....	60
4.1 a) O-O, b) O-H, c) H-O and d) H-H radial distribution functions and their corresponding integration numbers, as obtained by the HF/MM and ONIOM-XS MD simulations.....	70

LIST OF FIGURES (Continued)

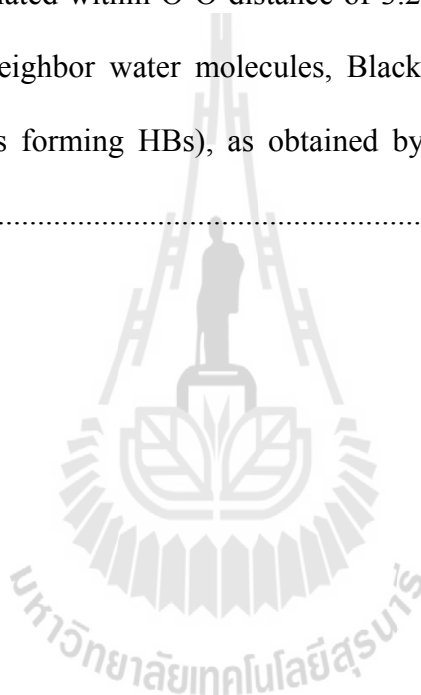
Figure	Page
4.2 Distributions of coordination numbers, calculated within first minimum of the HF/MM and ONIOM-XS MD's O-O RDFs	73
4.3 Distributions of number of HBs, calculated according to the three geometrical criteria of the H-bond formation	75
4.4 Some selected HB structures in liquid water at any simulation times, as observed in the ONIOM-XS simulation	77
4.5 Distributions of O---O---O angles, calculated within first minimum of the HF/MM and ONIOM-XS MD's O-O RDFs (<i>i.e.</i> , within O---O distance of 3.2 Å).....	79
4.6 Distributions of a) O-H---O and b) O---H-O angles, calculated within first minimum of the HF/MM and ONIOM-XS MD's H-O and O-H RDFs (<i>i.e.</i> , within H---O and O---H distances of 2.5 Å).....	79
4.7 Scheme of a distorted water molecule	80
4.8 Velocity autocorrelation functions of the center-of-mass of first-shell water system	82
4.9 Fourier transforms of the translational motions of first-shell waters, calculated from the center-of-mass VACFs of waters.....	83
4.10 Definition of three librational motions; $R_{\xi} = W_1 - W_2$ (rotation around approximated x axis), $R_{\eta} = R_1 + R_2$ (rotation around approximated y axis) and $R_{\zeta} = R_1 - R_2$ (rotation around approximated z axis).....	84

LIST OF FIGURES (Continued)

Figure	Page
4.11 Velocity autocorrelation functions of water approximated instantaneous librational motions around the ξ , η and ζ axes, for the water system.....	86
4.12 Fourier transforms of the librational motions of water molecules, calculated from the VACFs of water approximated around the ξ , η and ζ axes.....	87
4.13 Velocity autocorrelation functions for the three intramolecular vibrations of water, as obtained from the conventional HF/MM and ONIOM-XS MD simulations.....	91
4.14 Fourier transforms of the hydrogen velocity autocorrelation functions (Q_1 , Q_2 and Q_3), as obtained from a) HF/MM and b) ONIOM-XS MD simulations.....	92
4.15 Time dependence of a) H1---O, b) H2---O and c) O---H distances, together with d) number of water molecules surrounding the central H ₂ O (<i>i.e.</i> , calculated within O-O distance of 3.20 Å; Red line: number of all nearest-neighbor water molecules, Black line: number of only water molecules forming HBs), as obtained by the HF/MM MD simulation.....	95

LIST OF FIGURES (Continued)

Figure	Page
4.16 Time dependence of a) H1---O, b) H2---O and c) O---H distances, together with d) number of water molecules surrounding the central H ₂ O (<i>i.e.</i> , calculated within O-O distance of 3.20 Å; Red line: number of all nearest-neighbor water molecules, Black line: number of only water molecules forming HBs), as obtained by the ONIOM-XS MD simulation	96



LIST OF ABBREVIATIONS

Å	=	Angstrom
ADF	=	Angular distribution function
au	=	Atomic unit
Aug-cc-pVDZ	=	Additional diffuse basis function and correlation consistent polarized valence double zeta
B3LYP	=	Becke three-parameter hybrid functional combined with Lee-Yang-Parr correlation function
BJH	=	Flexible water model developed by Bopp, Jancsó and Heinzinger
BLYP	=	Becke hybrid functional combined with Lee-Yang-Parr correlation function
BO	=	Born-Oppenheimer
BOMD	=	Born-Oppenheimer molecular dynamics
BSSE	=	Basis set superposition error
CC	=	Coupled cluster
CCSD	=	Coupled cluster calculations using both single and double substitutions from Hartree-Fock determinant
CF2	=	Central force model version 2
CHARMM	=	Chemistry at Harvard molecular mechanics
CI	=	Configuration interaction

LIST OF ABBREVIATIONS (Continued)

cm^{-1}	=	Wavenumber
CN	=	Coordination number
CND	=	Coordination number distribution
CP-MD	=	Car-Parrinello molecular dynamics
CPU	=	Central processing unit
D	=	Self-diffusion coefficient
DFT	=	Density functional theory
DZP	=	Double zeta polarization
e	=	Electron charge
E_{tot}	=	Total interaction energy
E_{MM}	=	Interaction within MM region
E_{QM-MM}	=	Interaction between QM and MM regions
ECP	=	Effective core potential
<i>etc</i>	=	et cetera
F_i	=	Force acting on each particle
F_{MM}	=	MM force
F_{QM}	=	QM force
fs	=	Femtosecond
FT-IR	=	Fourier transform infrared spectroscopy
GGA	=	Generalized gradient approximation

LIST OF ABBREVIATIONS (Continued)

GTO	=	Gaussian-type orbital
\hat{H}	=	Hamiltonian operator
HB	=	Hydrogen bond
HF	=	Hartree-Fock
IR	=	Infrared spectroscopy
K	=	Kelvin
kcal/mol	=	Kilocalorie per mole
l	=	Number of particles in the switching layer
LCAO-MO	=	Linear combination of atomic orbitals to molecular orbitals
M	=	Molarity
m	=	Mass
MC	=	Monte Carlo
MD	=	Molecular dynamics
m_e	=	Mass of electron
m_k	=	Mass of nucleus
MO	=	Molecular orbital
MP2	=	Second-order Møller-Plesset
MRT	=	Mean residence times
n_1	=	Number of particle in the QM sphere

LIST OF ABBREVIATIONS (Continued)

n_2	=	Number of particle in the MM region
ND	=	Neutron diffraction
N_{ex}	=	Number of exchange events
NMR	=	Nuclear magnetic resonance
NVE	=	Microcanonical ensemble
NVT	=	Canonical ensemble
ONIOM	=	Own N-layered Integrated molecular Orbital and molecular Mechanics
ONIOM-XS	=	An extension of the ONIOM method for molecular simulation in condensed phase
ps	=	Picosecond
QCDF	=	Quasi-component distribution functions
QM/MM	=	Quantum mechanics/molecular mechanics
QMSTAT	=	Quantum mechanics/statistical mechanics
r_0	=	Distance characterizing the end of QM region
r_1	=	Distance characterizing the start of QM region
r_{ab}	=	Distance between particles a and b
RDF	=	Radial distribution function
RHF	=	Restricted Hatree-Fock
r_{max}	=	First maximum of RDF peak

LIST OF ABBREVIATIONS (Continued)

r_{min}	=	First minimum of RDF peak
RWK	=	Reimers–Watts–Klein
R_{ξ}	=	Rotation around approximated x axis
R_{η}	=	Rotation around approximated y axis
R_{ζ}	=	Rotation around approximated z axis
S	=	Velocity of the center-of-mass
SCF	=	Self-consistent field
S_{ex}	=	Sustainability coefficient
$S_m(r)$	=	Smoothing function
SPC/E	=	Simple point charge effective pair water model
SPC/E	=	Extended simple point charge
STO	=	Slater-type orbital
t^*	=	Time for observing the number of exchange water
TIP4P	=	Four-point transferable intermolecular potential
TIP5P	=	Five-point transferable intermolecular potential
t_{sim}	=	Simulation time
UHF	=	Unrestricted open-shell Hatree-Fock
V	=	Potential field
VACF	=	Velocity autocorrelation functions
XAS	=	X-ray absorption spectroscopy

LIST OF ABBREVIATIONS (Continued)

XD	=	X-ray diffraction
XES	=	X-ray emission spectroscopy
Z	=	Atomic number
μ	=	Chemical potential
μVT	=	Grand canonical ensemble
Φ	=	Trial function
Ψ	=	Wavefunction
$(\Psi_{QM} \hat{H} \Psi_{QM})$	=	Interaction within QM region
h	=	Planck's constant
$^{\circ}$	=	Degree
τ_{H_2O}	=	MRT of water molecules
λ	=	Wavelength
ξ	=	x axis
η	=	y axis
ζ	=	z axis
$\chi(x)$	=	Spin orbital
∇^2	=	Laplacian operator
Φ	=	Trial function

CHAPTER I

INTRODUCTION

1.1 Literature reviews

Water, the most abundant substance on earth, is known to play a central role in many areas of science, including physics, chemistry, biology and geology. In solid phase, each water molecule simply conducts four-hydrogen bonds with its neighboring water molecules, forming a well-defined tetrahedral structure. In liquid phase, however, the pattern of hydrogen bond structure and its dynamics properties are not fully understood. During the past decades, numerous experimental techniques and theoretical approaches have been employed to elucidate the properties of liquid water. However, significant differences among the experimental results, as well as between the experimental and theoretical observations, were often found, leading to strong debate in describing the properties of liquid water.

In terms of experimental observations, several techniques such as X-ray diffraction (XD), neutron diffraction (ND), nuclear magnetic resonance (NMR) measurements, X-ray absorption spectroscopy (XAS), X-ray emission spectroscopy (XES) and infrared spectroscopy (IR) have been applied to obtain detailed knowledge of liquid water. There are many experimental review articles that try to explain the arrangement of water molecules in liquid phase (Fu, Bienenstock, and Brennan, 2009; Ludwig, 2001; Nilsson *et al.*, 2010; Weinhardt *et al.*, 2010). As a matter of fact that the time scales for hydrogen bond forming and breaking of liquid water are extremely

fast, *i.e.*, in femto to picosecond (Tokmakoff, 2007), it should be noted that there is no single experimental technique that can provide a complete set of structural and dynamical data of water. For example, X-ray and neutron scattering techniques are only useful in providing structural details, while the IR and Raman techniques are instead preferred in order to obtain dynamics information. Numerous X-ray and neutron scattering experiments have been carried out to investigate the structural properties of liquid water (Head-Gordon and Hura, 2002; Hura, Sorenson, Glaeser, and Head-Gordon, 2000; Okhulkov, Demianets, and Gorbaty, 1994; Soper, 2000; Soper, Bruni, and Ricci, 1997; Sorenson, Hura, Glaeser, and Head-Gordon, 2000), most of which reported the tetrahedral structure with coordination number near 4. Smith and coworkers made use of Raman spectroscopy to interpret the structure of liquid water, in which the results supported the fully tetrahedrally hydrogen bonded model (Head-Gordon and Johnson, 2006; Smith *et al.*, 2005). Recently, the interpretation of the structure of water through a Compton scattering study (Hakala *et al.*, 2006) supplied information that each water molecule contains about 3.9 hydrogen bonds.

However, this standard picture of liquid water has been challenged by Wernet and co-workers (Wernet *et al.*, 2004), who used XAS and XES techniques to investigate the structure of liquid water. Of particular interest, they reported that, at room temperature, 80% of water molecules in liquid phase form only two strong hydrogen bonds with one donor and one acceptor, consisting mainly of chain or ring structures, while the remaining 20% of water molecules being made up of tetrahedral-like hydrogen bonded structures. These observations are in good accord with an early XAS study by Myneni and coworkers in 2002, who suggested a water coordination

number as small as 2.4 (Myneni *et al.*, 2002). In addition, a more recent experiment by high resolution XES technique (Tokushima *et al.*, 2008) reported that the liquid water consists of distorted structure and tetrahedral structure with ratio of 2:1. As a consequence, this is the starting point that sparks many researchers to re-check the structural properties of liquid water. In very recent discussion on the behavior of liquid water (Nilsson and Pettersson, 2011), it has been demonstrated that water is inhomogeneous with a fluctuating hydrogen-bond network around two types of structures, strongly tetrahedral and strongly hydrogen-bond distorted. In this respect, most water molecules favor a closer packing than tetrahedral, with strongly distorted hydrogen bonds. With regard to these observed discrepancies, some researchers (Holt, 2008) claimed that the results may be affected by the specifics of each experimental technique. For example, X-ray and neutron scattering provide bulk structure measurements involving static averaging over small and large length scale structure in liquid water, whereas XAS investigate instantaneous, small length scale structure, which may not be persistent outcome.

In terms of theoretical investigations, many attempts have been made to elucidate the properties of liquid water. In the first period, there are many research groups started from studying the properties of small water clusters, *i.e.*, the first step in describing the properties of bulk water (Gregory and Clary, 1996; Maheshwary, Patel, Sathyamurthy, Kulkarni, and Gadre, 2001; Schutz, Rauhut, and Werner, 1998). Later, several water models have been proposed and employed in molecular dynamics (MD) and Monte Carlo (MC) simulations. In this respect, the potential functions that describe hydrogen bond interactions of liquid water have been developed varying from very simple assumptions based on atomic point charge and rigid bonds to more

sophisticated models that include molecular flexibility and polarization effects (Lopes, Roux, and MacKerell, 2009). Popular water models include extended simple point charge (SPC/E) (Berendsen, Grigera, and Straatsma, 1987), four-point transferable intermolecular potential (TIP4P) (Jorgensen, Chandrasekhar, Madura, Impey, and Klein, 1983), five-point transferable intermolecular potential (TIP5P) (Mahoney and Jorgensen, 2000), Reimers-Watts-Klein (RWK) model (Reimers, Watts, and Klein, 1982), as well as other polarizable empirical potentials (Bukowski, Szalewicz, Groenenboom, and van der Avoird, 2008; Caldwell, Dang, and Kollman, 1990; Cieplak, Kollman, and Lybrand, 1990; Fanourgakis and Xantheas, 2008; Kozack and Jordan, 1992; Stern, Rittner, Berne, and Friesner, 2001; Svishchev, Kusalik, Wang, and Boyd, 1996). During the past decades, these water models have been widely used, providing good correlations with experimental data. Nevertheless, some serious problems, such as effects of many-body contributions, still exist since most of potential functions employed in the simulations are usually derived with respect to water dimer, *i.e.*, based on pairwise-additive approximations. In addition, such potentials can not be used for describing bond-breaking and bond-forming behaviors.

Nowadays, as a consequence of the rapid development in computer capacity and performance, these problems can be solved by performing quantum-mechanics-based MD simulations, in which the force on each particle in the system can be computed directly from the first principle calculations (Stone, 2007). In terms of the Car-Parrinello (CP) MD technique (Car and Parrinello, 1985), the whole system is treated quantum mechanically using density functional theory (DFT), with common exchange correlation function BLYP and PBE. Recently, several CP-MD simulations

have been performed for systems of 32 and 64 water molecules (Grossman, Schwegler, Draeger, Gygi, and Galli, 2004; Izvekov and Voth, 2002; Kühne, Krack, and Parrinello, 2009; Lee and Tuckerman, 2006, 2007). With regard to the CP-MD results, however, it has been reported that some properties of liquid water are rather sensitive to the density functional models chosen. At ambient conditions, it has been demonstrated that the CP-MD technique is limited to study the structural properties of liquid water, *i.e.*, due to the overestimation of water-water interactions (Lee and Tuckerman, 2006; Yoo, Zeng, and Xantheas, 2009). Consequently, some dynamics properties obtained from the CP-MD simulations, such as self-diffusion coefficients, showed significantly smaller value than that of experiments. Recently, it has been shown that liquid water simulated by the CP-MD technique under ambient condition is super-cooled or glassy (Lee and Tuckerman, 2007).

Besides the CP-MD technique, an alternative approach is to apply a so-called combined quantum mechanics/molecular mechanics (QM/MM) technique. According to the QM/MM technique, the most important part of the system is treated by quantum mechanics, while the rest of the system is described by appropriate molecular mechanical (MM) potentials. Recently, a series of QM/MM MD simulations, namely HF/MM, B3LYP/MM and MP2/MM, have been performed for studying liquid water (Xenides, Randolph, and Rode, 2005, 2006). Comparing between the HF, B3LYP and MP2 methods employed in the QM/MM MD simulations, they found that the use of HF method with enlarged QM size can provide simulation results in good agreement with those obtained by the correlated MP2 calculations, while the B3LYP method predicted a too rigid water structure as well as too slow exchange rates. Regarding the analogous HF/MM simulation with enlarged QM size

(Tongraar and Rode, 2004; Xenides, Randolph, and Rode, 2005, 2006), the results clearly indicated an enormous flexibility of the HB network in liquid water, suggesting that each water molecule forms (on average) only 2.8 HBs. In this respect, the tetrahedral-coordinated water seems most accepted at the present time, but it is apparent that a mixture of a minority of higher (4-linked) and a majority of lower (2-linked) hydrogen bond coordinated water in good accord with the experimental data (Leetmaa *et al.*, 2008).

According to the conventional QM/MM MD technique, however, only the exchanging particles are treated by a smoothing function when they are crossing the QM/MM boundary. In practice, this is not realistic since the immediate addition or deletion of a particle in the QM region due to the interchange also affects the forces acting on the remaining QM particles. Furthermore, the conventional QM/MM framework cannot clearly define the energy expression during the exchange process. To solve these problems, a more sophisticated QM/MM MD technique based on ONIOM-XS method (which will be abbreviated throughout this work as “ONIOM-XS MD”) has been proposed (Kerdcharoen and Morokuma, 2003). The ONIOM method, originally developed by Morokuma and co-workers (Svensson *et al.*, 1996) can handle not only the QM + MM combinations (which is implemented in the conventional QM/MM scheme), but also the QM + QM combinations. In the present work, an interest is therefore to apply the ONIOM-XS technique for studying the hydrogen bond structure and dynamics of liquid water. The results obtained by the ONIOM-XS simulation can be expected to provide more reliable data of liquid water, *i.e.*, compared to those obtained by the conventional QM/MM scheme, leading to further understanding the properties of this peculiar liquid in many areas of science.

1.2 Research objectives

1. To apply a more sophisticated ONIOM-XS MD technique for studying the hydrogen bond structure and dynamics of liquid water.

2. To compare the ONIOM-XS results with those obtained by the conventional QM/MM MD scheme, in order to validate the conventional QM/MM technique for the treatment of such hydrogen bond system.

1.3 Scope and limitation of the study

Conventional QM/MM and ONIOM-XS MD simulations will be performed to investigate the structural and dynamical properties of liquid water. By the QM/MM technique, the system consists of a “high-level” QM sphere which contains a central water molecule and its nearest-neighbor water molecules embedded inside a cube of “low-level” MM water molecules. For the QM treated-region, the QM size with a diameter of 8.8 Å was chosen, consisting of a central water molecule and about 10-14 nearest-neighbor waters. All interactions inside the QM region are treated at Hartree-Fock (HF) level of accuracy using DZP basis set. In the MM region, all interactions are described by means of a flexible BJH-CF2 model (Bopp, Jancsó, and Heinzinger, 1983). The structural properties of water will be analyzed through a set of radial distribution functions (RDFs) and their corresponding integration numbers, together with detailed analyses on angular distribution functions (ADFs) and orientations of water molecules surrounding the central H₂O. The dynamics details will be analyzed with respect to mean residence times (MRTs) of water molecules surrounding the central H₂O, as well as to the water exchange processes at the central reference water. The results obtained by the conventional QM/MM and ONIOM-XS MD simulations

will be compared and discussed with respect to the previous simulation results, as well as to the available experimental data.

1.4 References

- Berendsen, H. J. C., Grigera, J. R., and Straatsma, T. P. (1987). The missing term in effective pair potentials. **The Journal of Physical Chemistry**. 91: 6269-6271.
- Bopp, P., Jancsó, G., and Heinzinger, K. (1983). An improved potential for non-rigid water molecules in the liquid phase. **Chemical Physics Letters**. 98: 129-133.
- Bukowski, R., Szalewicz, K., Groenenboom, G. C., and van der Avoird, A. (2008). Polarizable interaction potential for water from coupled cluster calculations. I. Analysis of dimer potential energy surface. **The Journal of Chemical Physics**. 128: 94313-94315.
- Caldwell, J., Dang, L. X., and Kollman, P. A. (1990). Implementation of nonadditive intermolecular potentials by use of molecular dynamics: Development of a water-water potential and water-ion cluster interactions. **Journal of the American Chemical Society**. 112: 9144-9147.
- Car, R., and Parrinello, M. (1985). Unified approach for molecular dynamics and density-functional theory. **Physical Review Letters**. 55: 2471.
- Cieplak, P., Kollman, P., and Lybrand, T. (1990). A new water potential including polarization: Application to gas-phase, liquid, and crystal properties of water. **The Journal of Chemical Physics**. 92: 6755-6760.
- Fanourgakis, G. S., and Xantheas, S. S. (2008). Development of transferable interaction potentials for water. V. Extension of the flexible, polarizable, Thole-type model potential (TTM3-F, v. 3.0) to describe the vibrational

- spectra of water clusters and liquid water. **The Journal of Chemical Physics**. 128: 74506-74511.
- Fu, L., Bienenstock, A., and Brennan, S. (2009). X-ray study of the structure of liquid water. **The Journal of Chemical Physics**. 131: 234702-234710.
- Gregory, J. K., and Clary, D. C. (1996). Structure of water clusters. The contribution of many-body forces, monomer relaxation, and vibrational zero-point energy. **The Journal of Physical Chemistry**. 100: 18014-18022.
- Grossman, J. C., Schwegler, E., Draeger, E. W., Gygi, F., and Galli, G. (2004). Towards an assessment of the accuracy of density functional theory for first principles simulations of water. **The Journal of Chemical Physics**. 120: 300-311.
- Hakala, M., Nygard, K., Manninen, S., Huotari, S., Buslaps, T., Nilsson, A., Pettersson, L. G. M., and Hamalainen, K. (2006). Correlation of hydrogen bond lengths and angles in liquid water based on Compton scattering. **The Journal of Chemical Physics**. 125: 84504-84507.
- Head-Gordon, T., and Hura, G. (2002). Water structure from scattering experiments and simulation. **Chemical Reviews**. 102: 2651-2670.
- Head-Gordon, T., and Johnson, M. E. (2006). Tetrahedral structure or chains for liquid water. **Proceedings of the National Academy of Sciences**. 103: 7973-7977.
- Holt, J. (2008). Methods for probing water at the nanoscale. **Microfluidics and Nanofluidics**. 5: 425-442.

- Hura, G., Sorenson, J. M., Glaeser, R. M., and Head-Gordon, T. (2000). A high-quality X-ray scattering experiment on liquid water at ambient conditions. **The Journal of Chemical Physics**. 113: 9140-9148.
- Izvekov, S., and Voth, G. A. (2002). Car-Parrinello molecular dynamics simulation of liquid water: New results. **The Journal of Chemical Physics**. 116: 10372-10376.
- Jorgensen, W. L., Chandrasekhar, J., Madura, J. D., Impey, R. W., and Klein, M. L. (1983). Comparison of simple potential functions for simulating liquid water. **The Journal of Chemical Physics**. 79: 926-935.
- Kerdcharoen, T., and Morokuma, K. (2003). Combined quantum mechanics and molecular mechanics simulation of Ca^{2+} /ammonia solution based on the ONIOM-XS method: Octahedral coordination and implication to biology. **The Journal of Chemical Physics**. 118: 8856-8862.
- Kozack, R. E., and Jordan, P. C. (1992). Polarizability effects in a four-charge model for water. **The Journal of Chemical Physics**. 96: 3120-3130.
- Kühne, T. D., Krack, M., and Parrinello, M. (2009). Static and dynamical properties of liquid water from first principles by a novel Car-Parrinello-like approach. **Journal of Chemical Theory and Computation**. 5: 235-241.
- Lee, H.-S., and Tuckerman, M. E. (2006). Structure of liquid water at ambient temperature from ab initio molecular dynamics performed in the complete basis set limit. **The Journal of Chemical Physics**. 125: 154507-154514.
- Lee, H.-S., and Tuckerman, M. E. (2007). Dynamical properties of liquid water from ab initio molecular dynamics performed in the complete basis set limit. **The Journal of Chemical Physics**. 126: 164501-164516.

- Leetmaa, M., Wikfeldt, K. T., Ljungberg, M. P., Odelius, M., Swenson, J., Nilsson, A., and Pettersson, L. G. M. (2008). Diffraction and IR/Raman data do not prove tetrahedral water. **The Journal of Chemical Physics**. 129: 84502-84513.
- Lopes, P., Roux, B., and MacKerell, A. (2009). Molecular modeling and dynamics studies with explicit inclusion of electronic polarizability: Theory and applications. **Theoretical Chemistry Accounts: Theory, Computation, and Modeling (Theoretica Chimica Acta)**. 124: 11-28.
- Ludwig, R. (2001). Water: From clusters to the bulk. **Angewandte Chemie International Edition**. 40: 1808-1827.
- Maheshwary, S., Patel, N., Sathyamurthy, N., Kulkarni, A. D., and Gadre, S. R. (2001). Structure and stability of water clusters (H₂O)_n, n = 8-20: An *ab Initio* investigation. **The Journal of Physical Chemistry A**. 105: 10525-10537.
- Mahoney, M. W., and Jorgensen, W. L. (2000). A five-site model for liquid water and the reproduction of the density anomaly by rigid, nonpolarizable potential functions. **The Journal of Chemical Physics**. 112: 8910-8922.
- Myneni, S., Luo, Y., Naslund, L. Å., Cavalleri, M., Ojamae, L., Ogasawara, H., Pelmenschikov, A., Wernet, P., Vaterlein, P., Heske, C., Hussain, Z., Pettersson, L. G. M., and Nilsson, A. (2002). Spectroscopic probing of local hydrogen-bonding structures in liquid water. **Journal of Physics: Condensed Matter**. 14: L213.
- Nilsson, A., Nordlund, D., Waluyo, I., Huang, N., Ogasawara, H., Kaya, S., Bergmann, U., Näslund, L.-Å., Öström, H., Wernet, P., Andersson, K. J., Schiros, T., and Pettersson, L. G. M. (2010). X-ray absorption spectroscopy

- and X-ray Raman scattering of water and ice: An experimental view. **Journal of Electron Spectroscopy and Related Phenomena**. 177: 99-129.
- Nilsson, A., and Pettersson, L. G. M. (2011). Perspective on the structure of liquid water. **Chemical Physics**. 389: 1-34.
- Okhulkov, A. V., Demianets, Y. N., and Gorbaty, Y. E. (1994). X-ray scattering in liquid water at pressures of up to 7.7 kbar: Test of a fluctuation model. **The Journal of Chemical Physics**. 100: 1578-1588.
- Reimers, J. R., Watts, R. O., and Klein, M. L. (1982). Intermolecular potential functions and the properties of water. **Chemical Physics**. 64: 95-114.
- Schutz, M., Rauhut, G., and Werner, H.-J. (1998). Local treatment of electron correlation in molecular clusters: Structures and stabilities of $(\text{H}_2\text{O})_n$, $n = 2-4$. **The Journal of Physical Chemistry A**. 102: 5997-6003.
- Smith, J. D., Cappa, C. D., Wilson, K. R., Cohen, R. C., Geissler, P. L., and Saykally, R. J. (2005). Unified description of temperature-dependent hydrogen-bond rearrangements in liquid water. **Proceedings of the National Academy of Sciences of the United States of America**. 102: 14171-14174.
- Soper, A. K. (2000). The radial distribution functions of water and ice from 220 to 673 K and at pressures up to 400 MPa. **Chemical Physics**. 258: 121-137.
- Soper, A. K., Bruni, F., and Ricci, M. A. (1997). Site-site pair correlation functions of water from 25 to 400 °C: Revised analysis of new and old diffraction data. **The Journal of Chemical Physics**. 106: 247-254.
- Sorenson, J. M., Hura, G., Glaeser, R. M., and Head-Gordon, T. (2000). What can X-ray scattering tell us about the radial distribution functions of water? **The Journal of Chemical Physics**. 113: 9149-9161.

- Stern, H. A., Rittner, F., Berne, B. J., and Friesner, R. A. (2001). Combined fluctuating charge and polarizable dipole models: Application to a five-site water potential function. **The Journal of Chemical Physics**. 115: 2237-2251.
- Stone, A. J. (2007). Chemistry: Water from first principles. **Science**. 315: 1228-1229.
- Svensson, M., Humbel, S., Froese, R. D. J., Matsubara, T., Sieber, S., and Morokuma, K. (1996). ONIOM: A multilayered integrated MO + MM method for geometry optimizations and single point energy predictions. A test for Diels-Alder reactions and $\text{Pt}(\text{P}(t\text{-Bu})_3)_2 + \text{H}_2$ oxidative addition. **The Journal of Physical Chemistry**. 100: 19357-19363.
- Svishchev, I. M., Kusalik, P. G., Wang, J., and Boyd, R. J. (1996). Polarizable point-charge model for water: Results under normal and extreme conditions. **The Journal of Chemical Physics**. 105: 4742-4750.
- Tokmakoff, A. (2007). Shining light on the rapidly evolving structure of water. **Science**. 317: 54-55.
- Tokushima, T., Harada, Y., Takahashi, O., Senba, Y., Ohashi, H., Pettersson, L. G. M., Nilsson, A., and Shin, S. (2008). High resolution X-ray emission spectroscopy of liquid water: The observation of two structural motifs. **Chemical Physics Letters**. 460: 387-400.
- Tongraar, A., and Rode, B. M. (2004). Dynamical properties of water molecules in the hydration shells of Na^+ and K^+ : *Ab initio* QM/MM molecular dynamics simulations. **Chemical Physics Letters**. 385: 378-383.
- Weinhardt, L., Fuchs, O., Blum, M., Bär, M., Weigand, M., Denlinger, J. D., Zubavichus, Y., Zharnikov, M., Grunze, M., Heske, C., and Umbach, E. (2010). Resonant X-ray emission spectroscopy of liquid water: Novel

instrumentation, high resolution, and the “map” approach. **Journal of Electron Spectroscopy and Related Phenomena**. 177: 206-211.

Wernet, P., Nordlund, D., Bergmann, U., Cavalleri, M., Odellius, M., Ogasawara, H., Naslund, L. A., Hirsch, T. K., Ojamae, L., Glatzel, P., Pettersson, L. G. M., and Nilsson, A. (2004). The structure of the first coordination shell in liquid water. **Science**. 304: 995-999.

Xenides, D., Randolph, B. R., and Rode, B. M. (2005). Structure and ultrafast dynamics of liquid water: A quantum mechanics/molecular mechanics molecular dynamics simulations study. **The Journal of Chemical Physics**. 122: 174506-174510.

Xenides, D., Randolph, B. R., and Rode, B. M. (2006). Hydrogen bonding in liquid water: An *ab initio* QM/MM MD simulation study. **Journal of Molecular Liquids**. 123: 61-67.

Yoo, S., Zeng, X. C., and Xantheas, S. S. (2009). On the phase diagram of water with density functional theory potentials: The melting temperature of ice I_h with the Perdew-Burke-Ernzerhof and Becke-Lee-Yang-Parr functionals. **The Journal of Chemical Physics**. 130: 221102-221104.

CHAPTER II

THEORETICAL AND COMPUTATIONAL METHODS

2.1 Quantum mechanics

Nowadays, there are a number of quantum mechanical methods available for obtaining the observable chemical properties. The quantum mechanical methods (Szabo and Ostlund, 1989) are based on finding solutions with respect to Schrödinger equation on molecular orbital theory. According to quantum mechanics postulates, the systems are fully described by “wave function,” Ψ , which depends on the position of electrons and nuclei in the system.

2.1.1 Schrödinger equation

The objective of all *ab initio* electronic structure theories is the solution of the time-independent Schrödinger equation, which can be expressed in a time independent form as

$$\hat{H}\Psi = E\Psi , \quad (2.1)$$

where \hat{H} is the *Hamiltonian operator*, which corresponds to the kinetic energy, \hat{T} , and potential energy, \hat{V} , of the system, the *Hamiltonian operator* will be shown in atomic units.

$$\hat{H} = \hat{T} + \hat{V} , \quad (2.2)$$

where

$$\hat{T} = -\frac{\hbar^2}{2m}\nabla^2 , \quad (2.3)$$

and thus,

$$\hat{H} = -\frac{\hbar^2}{2m}\nabla^2 + \hat{V} . \quad (2.4)$$

Then, rewriting the equation (2.1) gives

$$\left\{ -\frac{\hbar^2}{2m}\nabla^2 + \hat{V} \right\} \Psi = E\Psi , \quad (2.5)$$

where ∇^2 is the *Laplacian operator*, written as

$$\nabla^2 = \frac{\partial^2}{\partial x^2} + \frac{\partial^2}{\partial y^2} + \frac{\partial^2}{\partial z^2} . \quad (2.6)$$

Here, \hbar is Planck's constant divided by 2π . Ψ is an eigenfunction which characterizes the particle's properties, and E is the eigenvalue of the particle with respect to the eigenfunction.

2.1.2 Born-Oppenheimer approximation

For N particle system, the *Hamiltonian operator* (\hat{H}) takes into account five contributions to the total energy of a system, namely the kinetic energies of the electrons (\hat{T}_e) and nuclei (\hat{T}_n), the attraction of the electrons to the nuclei (\hat{V}_{en}), and the inter-electronic (\hat{V}_{ee}) and inter-nuclear (\hat{V}_{nn}) repulsions, as shown in equations (2.7) and (2.8),

$$\hat{H} = \hat{T}_e + \hat{T}_n + \hat{V}_{en} + \hat{V}_{ee} + \hat{V}_{nn}, \quad (2.7)$$

$$\hat{H} = -\sum_{i=1}^N \frac{1}{2} \nabla_i^2 - \sum_{A=1}^M \frac{1}{2M_A} \nabla_A^2 - \sum_{i=1}^N \sum_{A=1}^M \frac{Z_A}{r_{ij}} + \sum_{i=1}^N \sum_{j>i}^N \frac{1}{r_{ij}} + \sum_{A=1}^M \sum_{B>A}^M \frac{Z_A Z_B}{R_{AB}}, \quad (2.8)$$

where i and j represent electrons, A and B represent nuclei, M is the mass of nucleus, Z is the atomic number, r and R are the distances between particles.

The “*Born-Oppenheimer approximation*” can be used to further simplify the Schrödinger equation. This allows the equation to be separated into electronic and nuclear terms. Since the nuclei are much heavier than electrons, they move much more slowly. Therefore, one can consider the electrons in a molecule to move with respect to the field of fixed nuclei. By this approximation, the kinetic energy of the nuclei can be neglected and the last term in equation (2.8), the repulsion of nuclei, can be considered as a constant. The remaining terms in equation (2.8) are called the electronic Hamiltonian or Hamiltonian describing the motion of N electrons in the field of M point charges,

$$\hat{H}_{elec} = -\sum_{i=1}^N \frac{1}{2} \nabla_i^2 - \sum_{i=1}^N \sum_{A=1}^M \frac{Z_A}{r_{ij}} + \sum_{i=1}^N \sum_{j>i}^N \frac{1}{r_{ij}} + \sum_{A=1}^M \sum_{B>A}^M \frac{Z_A Z_B}{R_{AB}}. \quad (2.9)$$

2.1.3 Independent electron approximation and Hartree products

In practice, an exact solution to the Schrödinger equation is not possible for any molecular systems. In this respect, a number of simplifying assumptions and procedures do make an approximate solution possible for a large range of molecules. To simplify the treatment further, the next step is to assume that the electrons are non-interacting in which the appropriate functional form of the wave function for N electrons can be written as

$$\hat{H}_{elec} = \sum_{i=1}^N \hat{h}(i), \quad (2.10)$$

where $\hat{h}(i)$ is the one-electron Hamiltonian, defined by

$$\hat{h}(i) = \left(-\frac{1}{2} \nabla_i^2 - \sum_{A=1}^M \frac{Z_A}{r_{iA}} \right), \quad (2.11)$$

where M is the total number of nuclei.

Eigenfunctions of the one-electron Hamiltonian in equation (2.11) must satisfy the corresponding one-electron Schrödinger equation, as shown in equation (2.12).

$$\hat{h}(i)\chi_j(x_i) = \varepsilon_j\chi_j(x_i), \quad (2.12)$$

where $\chi_j(x_i)$ is a set of spin orbital, *i.e.*, the wave function for electron that describes both its spatial distribution and its spin,

$$\chi_j(x_i) = \begin{cases} \psi_j(r_i)\alpha(\omega_i) \\ \text{or} \\ \psi_j(r_i)\beta(\omega_i) \end{cases}. \quad (2.13)$$

Because \hat{H} is a sum of one-electron Hamiltonians, a wave function is a simple product of spin orbital wave functions for each electron, as shown in equation (2.14).

$$\Psi^{HP}(x_1, x_2, \dots, x_N) = \chi_i(x_1)\chi_j(x_2)\cdots\chi_k(x_N). \quad (2.14)$$

A wave function of the form in equation (2.14) is called a ‘Hartree product’ and it is an eigenfunction of \hat{H} with eigenvalue, E ,

$$\hat{H}\Psi^{HP} = E\Psi^{HP}, \quad (2.15)$$

where E is the sum of the spin orbital energies of each of the spin orbitals appearing in Ψ^{HP} ,

$$E = \varepsilon_i + \varepsilon_j + \cdots + \varepsilon_k. \quad (2.16)$$

2.1.4 The antisymmetry principle and Slater determinants

According to equation (2.14), however, such a wave function is not acceptable because it does not allow the property of antisymmetry. The multi-electron wave function must take into consideration the fact that electrons are indistinguishable, and therefore, interchanging electron position assignments in a wave function cannot lead to a different wave function. The antisymmetrized wave functions can be obtained as follows. Considering a two-electron case occupying the spin orbitals χ_i and χ_j , the electron-one and electron-two are put in χ_i and χ_j , respectively, as shown in equation (2.17),

$$\Psi_{12}^{HP}(x_1, x_2) = \chi_i(x_1)\chi_j(x_2). \quad (2.17)$$

On the other hand, if the electron-one and electron-two are put in χ_j and χ_i , respectively, the Hartree product is shown in equation (2.18).

$$\Psi_{12}^{HP}(x_1, x_2) = \chi_i(x_2)\chi_j(x_1). \quad (2.18)$$

Each of these Hartree products clearly distinguishes between electrons. The wave function that satisfies the requirement of the antisymmetry principle can be achieved by taking appropriate linear combination of these two Hartree products as

$$\Psi(x_1, x_2) = 2^{-1/2} [\chi_i(x_1)\chi_j(x_2) - \chi_j(x_1)\chi_i(x_2)]. \quad (2.19)$$

The factor $2^{-1/2}$ is a normalization factor. The minus sign insures that $\Psi(x_1, x_2)$ is antisymmetric with respect to the interchange of the coordinates of electrons one and two,

$$\Psi(x_1, x_2) = -\Psi(x_2, x_1). \quad (2.20)$$

From equation (2.19), it is evident that the wave function vanishes if both electrons occupy the same spin orbital (*i.e.*, if $i=j$). Thus, the antisymmetry requirement immediately leads to the usual statement of the *Pauli Exclusion Principle* in which no more than one electron can occupy the same spin orbital. The antisymmetric wave function of equation (2.19) can be rewritten as “*Slater determinant*,”

$$\Psi(x_1, x_2) = 2^{-1/2} \begin{vmatrix} \chi_i(x_1) & \chi_j(x_1) \\ \chi_i(x_2) & \chi_j(x_2) \end{vmatrix}. \quad (2.21)$$

For N electron system, the generalization of equation (2.21) is written as

$$\Psi(x_1, x_2, \dots, x_N) = \frac{1}{\sqrt{N!}} \begin{vmatrix} \chi_i(x_1) & \chi_j(x_1) & \cdots & \chi_k(x_1) \\ \chi_i(x_2) & \chi_j(x_2) & \cdots & \chi_k(x_2) \\ \vdots & \vdots & \vdots & \vdots \\ \chi_i(x_N) & \chi_j(x_N) & \cdots & \chi_k(x_N) \end{vmatrix}. \quad (2.22)$$

Here, the factor $1/\sqrt{N!}$ ensures that the wave function is normalized. The short-hand notation for a normalized Slater determinant only shows the diagonal elements of determinant,

$$\Psi(x_1, x_2, \dots, x_N) = |\chi_i(x_1)\chi_j(x_2)\cdots\chi_k(x_N)\rangle. \quad (2.23)$$

2.1.5 The Hartree-Fock approximation

In practice, many-electron Schrödinger equation cannot be solved exactly, even for a simple two electron system such as helium atom or hydrogen molecule. Therefore, some approximations are required for solving the Schrödinger equation. By the variation method, the simplest antisymmetry wave function, which describes the ground state of N electron system, is a diagonal Slater determinant,

$$|\Psi_0\rangle = |\chi_i(x_1)\chi_j(x_2)\cdots\chi_k(x_N)\rangle. \quad (2.24)$$

According to the variation principle, the best sets of spin orbital correspond to the one that gives the lowest expectation value of energy. In this respect, the expectation value of the energy obtained by this wave function never lies below the exact energy of the ground state, which can be expressed in mathematical terms as

$$E_0 \leq \langle \Psi_0 | \hat{H} | \Psi_0 \rangle. \quad (2.25)$$

Consequently, the appropriate sets of spin orbital can be solved from the Hartree-Fock (HF) equation,

$$\hat{f}(i)\chi(x_i) = \varepsilon\chi(x_i), \quad (2.26)$$

where $f(i)$ is an effective one-electron operator, called the Fock operator, which can be written as

$$\hat{f}(i) = -\frac{1}{2}\nabla_i^2 - \sum_{A=1}^M \frac{Z_A}{r_{iA}} + v^{HF}(i), \quad (2.27)$$

where $v^{HF}(i)$ is the average potential or Hartree-Fock potential experienced by the i^{th} electron due to the present of other electrons. The essence of the Hartree-Fock approximation is to replace the complicated many-electron problem by a one-electron problem in which the electron-electron repulsion is treated in an average way. Thus, the Hartree-Fock equation (2.26) is nonlinear and must be solved iteratively. The procedure for solving the Hartree-Fock equation is called the self-consistent-field (SCF) method.

The idea of the SCF method is simple. By making an initial guess at spin orbitals, one can calculate the average field ($v^{HF}(i)$) seen by each electron and then solve the eigenvalue equation (2.26) for a new set of spin orbitals. Using these new spin orbitals, one can obtain new fields and repeat the procedure until self-consistency is reached.

2.1.6 Basis set

A conceptually appealing model for the (trial) wave function of our molecular system can be constructed from molecular orbitals (MO). The molecular orbitals (ψ) can be built from the atomic orbitals by using a so-called “*Linear Combination of Atomic Orbitals to Molecular Orbitals* (LCAO-MO)” method. This is one of the most important and widely used ideas in quantum chemistry. The LCAO-MO can be expressed as

$$\psi_i = \sum_{\mu=1}^n c_{\mu i} \phi_{\mu}, \quad (2.28)$$

where $c_{\mu i}$ are the molecular orbital expansion coefficients, and n is the number of atomic basis function. Here, the set of n function ϕ_{μ} is called *basis set*. The $c_{\mu i}$ can be calculated using various approaches, most of which are based on the linear variation methods.

The common types of basis function, or called atomic orbital, used in the electronic structure calculation are Slater Type Orbitals (STOs) (Slater, 1930) and Gaussian Type Orbitals (GTOs) (Boys, 1950).

The formalism of the STOs can be presented as

$$\phi_i(\zeta, n, l, m; r, \theta, \phi) = N r^{n-1} e^{-\zeta r} Y_{lm}(\theta, \phi), \quad (2.29)$$

where N is a normalization constant and ζ is an exponent. The r , θ , and ϕ are spherical coordinates, and Y_{lm} is the angular momentum part. The n , l , and m are quantum numbers referring to principal, angular momentum and magnetic quantum number, respectively. The STOs screening constants are calculated for small model molecules using rigorous self-consistent field methods, and then being generated for use with actual molecules of interest. The accuracy of STOs can be improved by combining two or more STOs (*i.e.*, with two different ζ values) into a single one-electron wavefunction (double ζ basis set).

The STOs are usually applied for atomic and diatomic system, which high accuracy, such as in semi-empirical methods where all three- and four-center integrals are neglected and in density functional methods that do not include exact exchange and that the coulomb energy is calculated by fitting the density into a set of auxiliary functions. However, the STOs do not satisfy in two-electron integral problem. The feasible basis functions is GTOs, which are functions of the form

$$\phi_i(\alpha, l, m, n; x, y, z) = Ne^{-\alpha r^2} x^l y^m z^n, \quad (2.30)$$

where N is a normalization constant, and α is an exponent. The x , y , and z are Cartesian coordinates. The l , m , and n are now not quantum numbers but simply the integral exponents at Cartesian coordinates and $r^2 = x^2 + y^2 + z^2$. The advantage of GTOs is that the product of two Gaussians at different centers is equivalent to a single Gaussian function centered at a point between the two centers. Therefore, the two-electron integral problem on three and four or more different atomic centers can be

reduced to integrals over two different centers. However, the GTO gives an inferior representation of the orbitals at the atomic nuclei, which can be considered at 1s-orbital. A 1s-orbital of STO has a *cusp* at the atomic nucleus but a GTO does not, as shown in Figure 2.1. In this respect, the larger basis set must be used to achieve the accuracy comparable to that obtained from STOs.

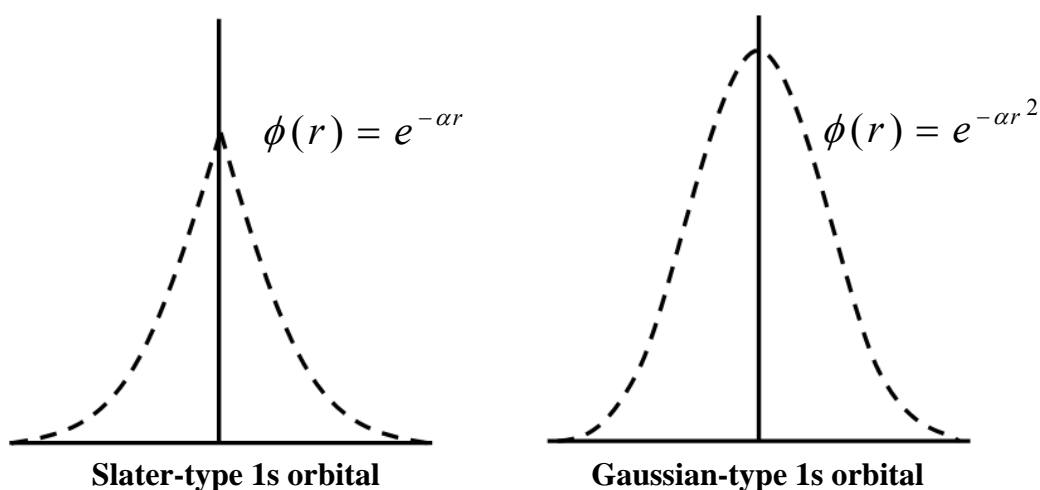


Figure 2.1 The Slater-type and Gaussian-type for 1s orbital.

The most important factor for creating the molecular orbital is a set of parameters applied to the basis function, called *basis set*. The smallest number of function possible for constructing the molecular orbital is called a *minimum basis set*. The improvement of the basis set can be made by replacing two basis functions into each basis function in the minimal basis set, called *double zeta* (DZ). The larger basis set is a *triple zeta* (TZ), where three basis functions are used to represent each of the minimal basis set. The compromise between the DZ and TZ basis sets is called a *split*

valence (SV) basis set, in which each valence atomic orbital is represented by two basis functions while each core orbital is represented by a single basis function.

In 1969, Pople and coworkers (Hehre, Stewart, and Pople, 1969) designed the basis set by expanding the STO in terms of n primitive Gaussians, called STO- n G basis set. The primitive Gaussian has been derived for $n = 2-6$. However, the STO-3G basis set is a widely used minimal basis set, as shown in Figure 2.2. The STO-3G basis set partially represents the *cusp* of s-type orbital at the atomic nuclei.

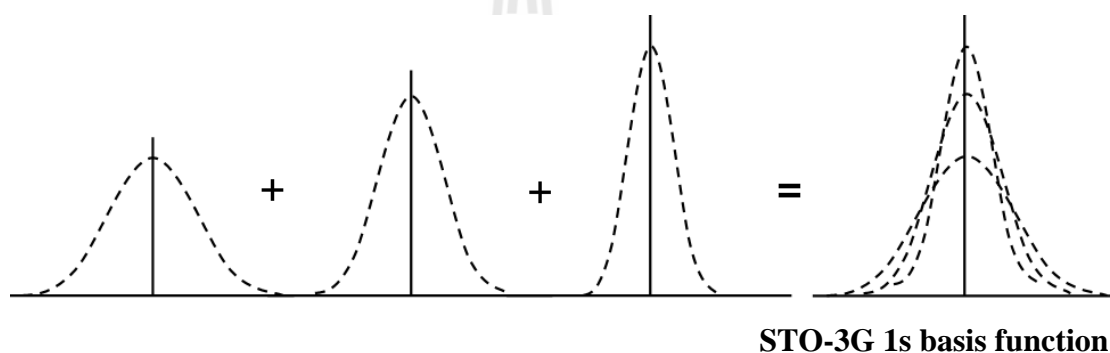


Figure 2.2 The STO-3G basis set representing the desired STO.

In addition, Pople and coworkers have applied the split valence to obtain flexibility in the basis set, which can be designed as $k-nlm$ G basis set. The first parameter (k) indicates the number of primitives used in the contracted core, while the two values (nl) refer to a split valence, and three values (nlm) refer to a triple split valence, such as 6-311G. For the triple split valence basis, the core orbitals are a contraction of six primitives and the valence splits into three functions, represented by three, one and one primitive GTOs, respectively. The Pople's style basis sets may include diffuse and/or polarization functions. The diffuse function can be denoted as +

or ++ before the G, in which the first + indicates one set of diffuse s- and p-function adding on heavy atoms and the second + refer to the inclusion of diffuse s-function for hydrogen atom. The polarization function can be put after the G, which separates designation for heavy and hydrogen atoms. For example, 6-31+G(d) basis set refers to a split valence with additional diffuse sp-functions and a single d-type polarization function only on heavy atoms. The largest standard Pople style basis set is 6-311++G(3df,3pd). In addition, the polarization function can be replaced with * notation, for example, the 6-311G* basis set is identical to 6-311G(d) and 6-311G** basis set is identical to 6-311G(d,p).

Since several GTOs are often grouped together, the *contracted Gaussian function* has been applied to *Dunning-Huzinaga (DZ)* basis set (Dunning, 1970, 1971; Huzinaga, 1965). The DZ basis set can be made by a contraction such as the (9s5p) primitive GTOs to [4s, 2p]. The contraction scheme is 6,1,1,1 for s-functions and 4,1 for the p-functions. In addition, the development of basis set by Dunning and coworkers for recovering the correlation energy of the valence electrons is known as the *correlation consistent (cc)* basis sets. The general formulation can be written as cc-pVnZ, where n = D for double zeta, T for triple zeta, Q for quadruple zeta, and so on.

For the systems involving a large number of core electron elements, it is necessary to use a large number of basis functions for describing them. However, since the deep core electrons are not much important in a chemical sense, this leads to an approximation by replacing the core electrons with analytical functions, called an *Effective Core Potential (ECP)* or *Pseudopotentials*. In practice, such basis set is

reasonably accurate and efficient, representing the combined nuclear-electronic core to the remaining electrons.

2.1.7 Electron correlation

It is known that motions of electrons are correlated and they tend to repel each electron to give a lower energy. According to the HF method, each electron moves in the static electric field created by all of the other electrons in the system. On the other hand, the electron cannot see other electrons during the HF calculation. Thus, the significant deficiency of the HF method is that it fails to adequately treat the correlation between motions of electrons. The effects of electron correlation are usually neglected in the Hamiltonian in the previous section. This leads to limitation of the HF energy calculations. The difference between HF and exact (non-relativistic) energies is the correlation energy,

$$E_{exact} = E_{HF} + E_{correlation} \quad (2.31)$$

In several cases, the neglect of electron correlation effects can lead to some anomaly of qualitative information. As a consequence, the Ψ and E cannot be used to correctly predict atomic properties without somewhere accounting for electron correlation.

The electron correlation methods calculate the coefficient in front of the other determinants in different way, such as *configuration interaction* (CI) (Sherrill and Schaefer III, 1999), *many-body perturbation* (MP) (Møller and Plesset, 1934), *coupled cluster* (CC) (Bartlett, 1989) and *density functional theory* (DFT).

2.2 Computational methods

2.2.1 Introduction to molecular dynamics (MD) simulation

The essential tools for theoretical study of large molecular system are molecular dynamics (MD) and Monte Carlo (MC) simulations. In particular for MD, this technique is widely used for studying properties of various molecular systems, providing details related to time dependent behavior of the system. The MD method was first introduced by Alder and Wainwright in the late 1950's (Alder and Wainwright, 1957, 1959) for studying the interactions of hard-sphere systems. The next major advancement was in 1964 when Rahman (Rahman, 1964) carried out the first simulation using a realistic potential for liquid argon. The first MD simulation of a realistic system was done by Rahman and Stillinger in their simulations of liquid water in 1974 (Stillinger and Rahman, 1974). Nowadays, MD technique has widely been applied for studying various molecular systems.

The MD simulation technique is based on Newton's second law, $F = ma$, when F is the force on the particle, m is its mass, and a is its acceleration. With regard to the force on each atom, it is possible to determine the acceleration of each atom in the system. Integration of the equations of motion then yields a trajectory that describes the positions, velocities and accelerations of the particles as they vary with time. From this trajectory, the average values of properties can be determined. The method is deterministic, *i.e.*, once the positions and velocities of each atom are known, the state of the system can be predicted at any time in the future or the past. The common scheme to perform MD simulations is summarized in Figure 2.3.

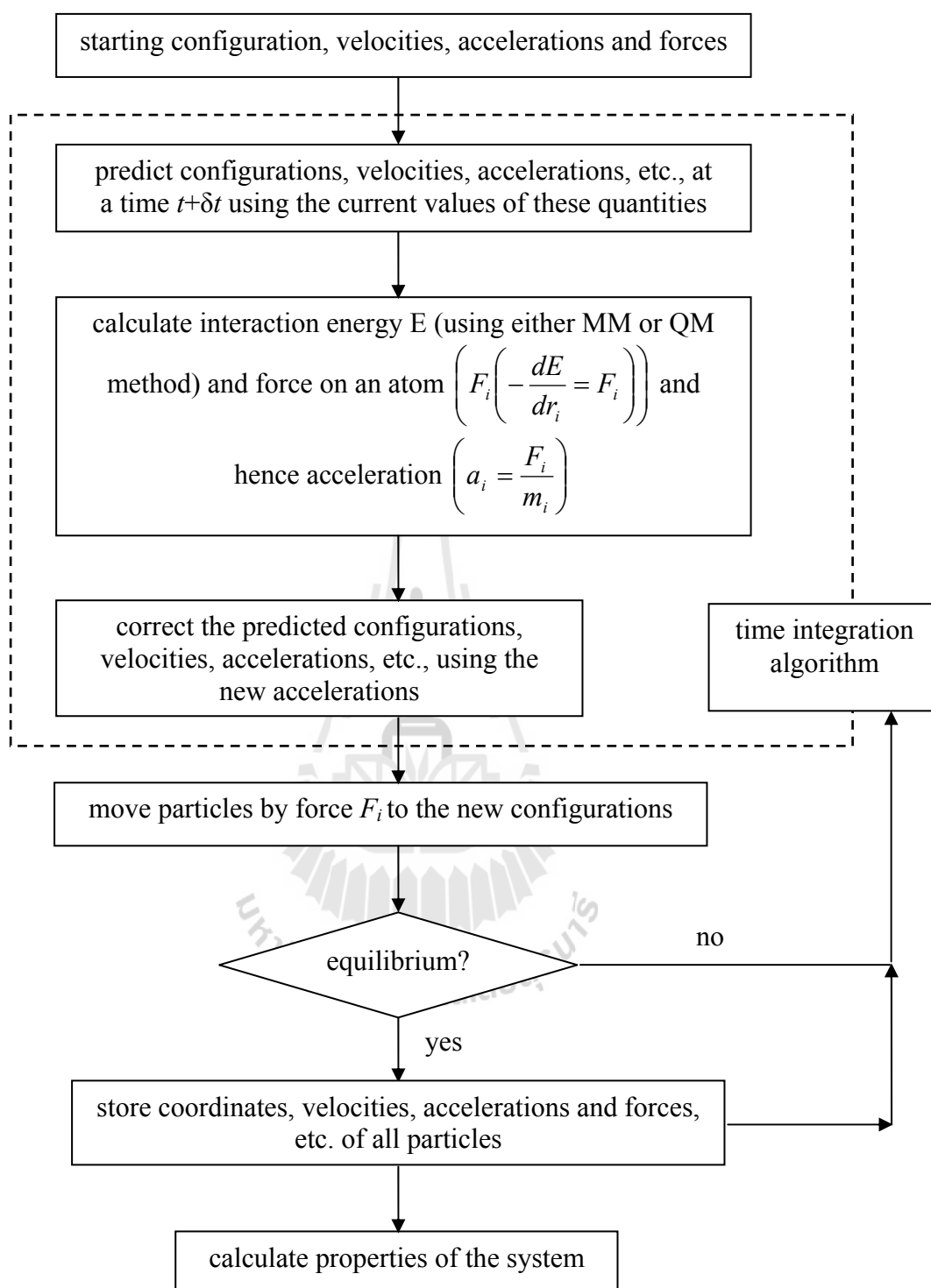


Figure 2.3 The scheme of molecular dynamics simulation.

The MD simulation starts with reading the initial configuration, velocities, accelerations and forces. The initial configuration can be obtained either from a random configuration or a lattice. The essential condition of the simulation is that there are no explicitly time-dependent or velocity-dependent forces that shall act on the system. In practice, the trajectories cannot be directly obtained from Newton's equation of motion. Therefore, the *time integration algorithm* will be used to obtain the knowledge of positions, velocities and accelerations of two successive time steps. The energy of the system can be calculated through molecular mechanics (MM) or quantum mechanics (QM) method. The force on each atom in the system can be obtained from the derivative of the energy with respect to the change in the atom's position. All particles in the system will be moved by their new forces to the new configurations. This process will be repeated until the system reaches its equilibrium. After that, the coordinates, velocities, accelerations, forces and so on of all particles will be collected for further structural and dynamical property calculations. In practice, only positions and velocities are usually stored since most important and interesting properties of the system can be obtained from these two quantities.

2.2.2 Intermolecular potentials

In general, the forces on each particle in MD simulation are usually derived from the potential energy function, V . The potential energy function is the total intermolecular interaction energy comprising all of pair, three-body, four-body, and so on up to N-body interactions,

$$V_{total} = \sum V(i, j) + \sum V(i, j, k) + \dots + \sum V(i, j, k, \dots, N). \quad (2.32)$$

With regard to equation (2.32), the upper terms are usually assumed to converge slowly and tend to have alternating signs (Kistenmacher, Popkie, and Clementi, 1974). Thus, only the summation of pair interaction has been used to describe the system's interactions, known as *pairwise additive approximations*. The pair potential functions can be constructed from experimental data. However, the popular way in obtaining the pair potential functions is to construct with respect to *ab initio* calculations.

2.2.3 Time integration algorithms

The engine of MD simulation is its time integration algorithm. The time integration algorithms are based on finite difference methods, in which the MD trajectories can be generated with continuous potential models. The essential idea is that the integration is divided into many small steps, each separated by a fixed time interval δt . The total force on each particle at time t can be calculated from the sum of interactions from other particles. Once the force is known, the accelerations of the particles can be determined, which are then combined with the positions and velocities at a time t to calculate the positions and velocities at a time $t + \delta t$.

There are many algorithms for integrating the equations of motion using finite difference methods, most of which assume that the positions and dynamics properties (velocities, accelerations, etc.) can be approximated in Taylor series expansions,

$$r(t + \delta t) = r(t) + v(t)\delta t + \frac{1}{2}a(t)\delta t^2 + \frac{1}{6}b(t)\delta t^3 + \frac{1}{24}c(t)\delta t^4 + \dots \quad (2.33)$$

$$v(t + \delta t) = v(t) + a(t)\delta t + \frac{1}{2}b(t)\delta t^2 + \frac{1}{6}c(t)\delta t^3 + \dots \quad (2.34)$$

$$a(t + \delta t) = a(t) + b(t)\delta t + \frac{1}{2}c(t)\delta t^2 + \dots \quad (2.35)$$

$$b(t + \delta t) = b(t) + c(t)\delta t + \dots, \quad (2.36)$$

where v is the velocity (the first derivative of the position with respect to time), a is the acceleration (the second derivative), b is the third derivative, and so on. Two popular integration methods for MD calculations are Verlet (Verlet, 1967) and predictor-corrector algorithms (Gear, 1971).

The Verlet algorithm is the most broadly used method for integrating the trajectories of motion in MD simulations. This algorithm uses the positions and accelerations at time t and the positions from the previous step, $r(t - \delta t)$, to calculate the new positions at time $t + \delta t$. We can write down the following equations between these quantities and the velocities at time t ,

$$r(t + \delta t) = r(t) + v(t)\delta t + \frac{1}{2}a(t)\delta t^2 \quad (2.37)$$

$$r(t - \delta t) = r(t) - v(t)\delta t + \frac{1}{2}a(t)\delta t^2. \quad (2.38)$$

The summation of these two equations gives

$$r(t + \delta t) = 2r(t) - r(t - \delta t) + a(t)\delta t^2. \quad (2.39)$$

The velocities do not explicitly appear in the Verlet integration algorithm. However, these values can be calculated by dividing the difference in positions at time $t + \delta t$ and $t - \delta t$ by $2\delta t$,

$$v(t) = [r(t + \delta t) - r(t - \delta t)] / 2\delta t. \quad (2.40)$$

However, the weakness of Verlet algorithm is that the calculation of the velocities cannot be obtained until the positions at the next step are known. Thus, it is not a self-starting algorithm. To overcome this point, some variants of the Verlet algorithm have been developed. For example, the *leap-frog* algorithm (Hockney, 1970), which uses the following expansions,

$$r(t + \delta t) = r(t) + v(t + \frac{1}{2}\delta t)\delta t \quad (2.41)$$

$$v(t + \frac{1}{2}\delta t) = v(t - \frac{1}{2}\delta t) + a(t)\delta t. \quad (2.42)$$

By this scheme, the velocities $v(t + \frac{1}{2}\delta t)$ are firstly calculated from the velocities at time $(t - \frac{1}{2}\delta t)$, and the accelerations at time t . The positions at time $t + \delta t$ are then deduced from the velocities just calculated together with the positions at time t using equation (2.41). The velocities at time t can be calculated from

$$v(t) = \frac{1}{2} \left[v\left(t + \frac{1}{2} \delta t\right) + v\left(t - \frac{1}{2} \delta t\right) \right]. \quad (2.43)$$

The advantage of this algorithm is that the velocities are explicitly calculated. However, some disadvantages exist, such as they are not calculated at the same time as the positions.

An even better implementation of the same basic algorithm is the *velocity Verlet* algorithm (Swope, Andersen, Berens, and Wilson, 1982), which gives positions, velocities and accelerations at the same time and does not compromise precision,

$$r(t + \delta t) = r(t) + v(t)\delta t + \frac{1}{2} a(t)\delta t^2 \quad (2.44)$$

$$v(t + \delta t) = v(t) + \frac{1}{2} [a(t) + a(t + \delta t)]\delta t. \quad (2.45)$$

Another integration method is Beeman's algorithm (Beeman, 1976), which is related to the Verlet method, and can be expressed as

$$r(t + \delta t) = r(t) + v(t)\delta t + \frac{2}{3} a(t)\delta t^2 - \frac{1}{6} a(t - \delta t)\delta t^2 \quad (2.46)$$

$$v(t + \delta t) = v(t) + \frac{1}{3} a(t)\delta t + \frac{5}{6} a(t)\delta t - \frac{1}{6} a(t - \delta t)\delta t. \quad (2.47)$$

The Beeman's algorithm uses a more accurate expression for the velocities and gives better energy conservation. However, the performance of this algorithm is more complicate, as well as more expensive.

For the predictor-corrector algorithm, this method has three basic steps. First, the new positions, velocities, accelerations and higher-order terms are predicted according to the Taylor expansion, as shown in equations (2.33)-(2.36). Second, the forces are then evaluated at the new positions to give the accelerations, $a(t + \delta t)$. These accelerations are compared with the accelerations predicted from the Taylor series expansion ($a^c(t + \delta t)$). In this respect, the difference between the predicted and the calculated accelerations is an *error signal*,

$$\Delta a(t + \delta t) = a^c(t + \delta t) - a^p(t + \delta t). \quad (2.48)$$

Lastly, an error signal is used to correct positions and their derivatives. All the corrections are proportional to the error signal, the coefficient of proportionality being a magic number determined to maximize the stability of the algorithm,

$$r^c(t + \delta t) = r^p(t + \delta t) + c_0 \Delta a(t + \delta t) \quad (2.49)$$

$$v^c(t + \delta t) = v^p(t + \delta t) + c_1 \Delta a(t + \delta t) \quad (2.50)$$

$$a^c(t + \delta t) = a^p(t + \delta t) + c_2 \Delta a(t + \delta t) \quad (2.51)$$

$$b^c(t + \delta t) = b^p(t + \delta t) + c_3 \Delta a(t + \delta t), \quad (2.52)$$

where the superscript p represents as predicted values, r and v stand for the complete set of positions and velocities, respectively, a represents the accelerations and b denotes all the third time derivatives of r .

2.2.4 Statistical mechanics

In general, MD simulations generate information at the microscopic level, including atomic positions and velocities. The conversion of this microscopic information to macroscopic observables requires statistical mechanics. Detailed information with respect to statistical mechanics can be found in numerous excellent text books (David, 1987; McQuarrie, 1976; Wilde and Singh, 1998).

In MD simulation, one often wishes to explore the macroscopic properties of a system through microscopic simulations. The connection between microscopic simulations and macroscopic properties is made via statistical mechanics, which provides the rigorous mathematical expressions that relate macroscopic properties to the distribution and motion of the atoms and molecules of the N -body system. In this respect, MD simulations provide the means to solve the equation of motion of the particles and evaluate these mathematical formulas. According to MD simulations, both thermodynamic and time dependent (kinetic) properties of the system can be obtained.

The thermodynamic state of a system is usually defined by a small set of parameters, for example, the temperature (T), the pressure (P), and the number of particles (N). Other thermodynamic properties may be derived from the equations of state and other fundamental thermodynamic equations. The mechanical or microscopic state of a system is defined by the atomic positions (q), and momenta (p). These can also be considered as coordinates in a multidimensional space, called phase space. For a system of N particles, this space has $6N$ dimensions. A single point in phase space, denoted by Γ , describes the state of the system. The collection of points in phase space is known as an ensemble.

An ensemble is a collection of all possible systems which have different microscopic states, but have an identical macroscopic or thermodynamic state. There are many different ensembles with different characteristics. For example, microcanonical ensemble (NVE) in which the thermodynamic state are characterized by fixed number of atoms (N), fixed volume (V), and fixed energy (E). Canonical ensemble (NVT) refers to a collection of all systems whose thermodynamic state is characterized by fixed number of atoms (N), volume (V), and temperature (T). Isobaric-isothermal ensemble (NPT) is characterized by fixed number of atoms (N), pressure (P) and temperature (T). Grand canonical ensemble (μVT) is characterized by fixed chemical potential (μ), volume (V), and temperature (T).

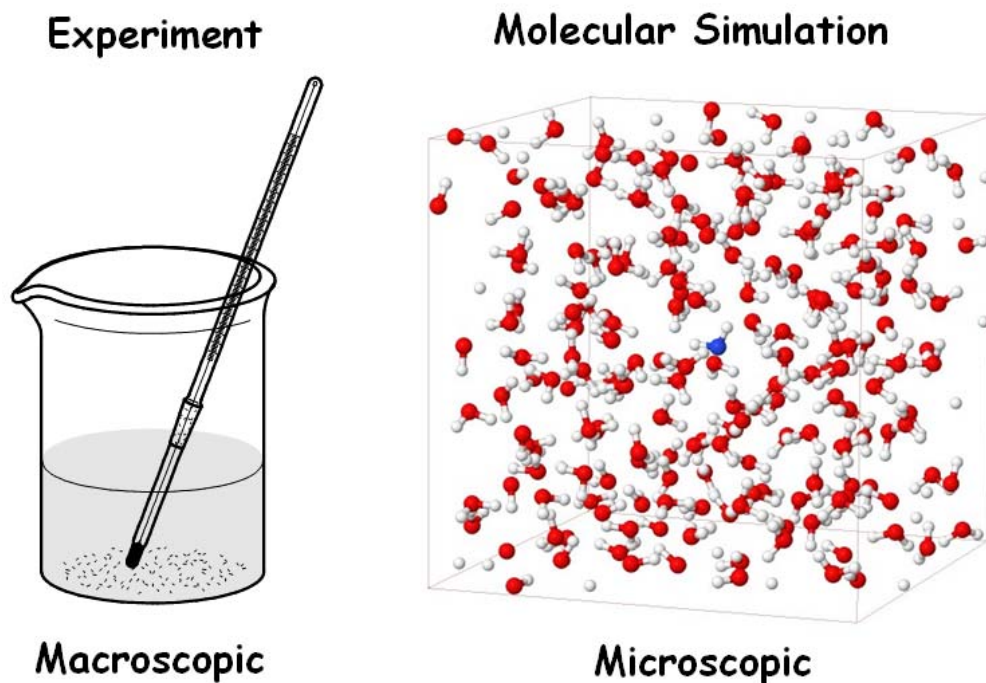


Figure 2.4 Comparison of macroscopic and microscopic systems.

An experiment is usually made on a macroscopic sample that contains an extremely large number of atoms or molecules sampling an enormous number of conformations, as shown in Figure 2.4. With regard to statistical mechanics, averages corresponding to experimental observables are defined in terms of ensemble averages; one justification for this is that there has been good agreement with experiment. An ensemble average is average taken over a large number of replicas of the system considered simultaneously, which can be expressed as

$$\langle A \rangle_{ensemble} = \iint dp^N dr^N A(p^N, r^N) \rho(p^N, r^N), \quad (2.53)$$

where $A(p^N, r^N)$ is the observable of interest and it is expressed as a function of the momenta, p , and the position, r , of the system. The integration is over all possible variables of r and p . The probability density of the ensemble is given by

$$\rho(p^N, r^N) = \frac{1}{Q} \exp\left[-\hat{H}(p^N, r^N)/k_B T\right], \quad (2.54)$$

where \hat{H} is the Hamiltonian, T is the temperature, k_B is Boltzmann's constant and Q is the partition function,

$$Q = \iint dp^N dr^N \exp\left[-\hat{H}(p^N, r^N)/k_B T\right]. \quad (2.55)$$

In practice, this integral is extremely difficult to calculate since it must calculate all possible states of the system. By means of statistical mechanics, the experimental observables are defined in terms of time averages of property A which can be measured throughout infinite time,

$$\langle A \rangle_{time} = \lim_{\tau \rightarrow \infty} \frac{1}{\tau} \int_0^{\tau} A(p^N(t), r^N(t)) dt \approx \frac{1}{M} \sum_{t=1}^M A(p^N, r^N), \quad (2.56)$$

where τ is the simulation time, M is the number of time steps in the simulation and $A(p^N, r^N)$ is the instantaneous value of A .

The relationship between time averages and ensemble averages can be achieved using the Ergodic hypothesis, which states that the time averages equals the ensemble average, *i.e.*, the estimation of time average can be obtained over an enormous number of replicas of the system considered simultaneously,

$$\langle A \rangle_{time} = \langle A \rangle_{ensemble}. \quad (2.57)$$

2.2.5 The periodic box

The periodic boundary condition is employed to solve the effects of surface, especially for the simulation of small system size where the interactions between particles and the wall could reflect in wrong system's properties.

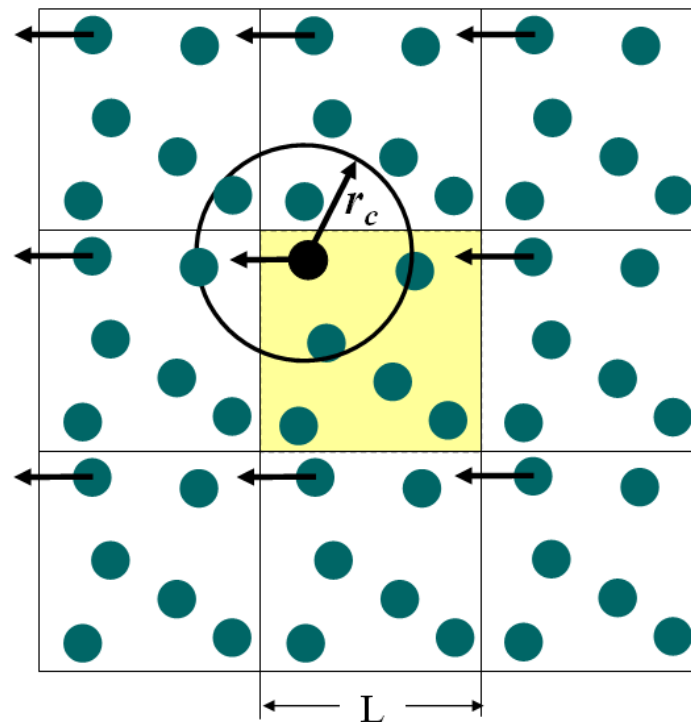


Figure 2.5 The periodic box in two dimensions.

The periodic box concept is illustrated in Figure 2.5, showing a two dimensional of a small portion of the system (the central box with yellow background) and the copies (the others with white background). Each copy is identical at the atomic level, and each atom undergoes the same time development as its image in every other copy. As the black atom (top left, central cell) leaves the central cell, its images enter from an adjoining copy (shown by the vector displacements in the figure) to keep the density constant. There are no effects due to the walls because each atom in the central cell is under the influence of every other atom in the central cell and in all copy cells.

Considering the black atom (top left in the central cell), the knowledge of force on this atom is required in order to understand its time development. First, we

sum the pair potential of the atom with every other atom. Then, differentiation of the potential with respect to the coordination of black atom gives the force on the particle.

To calculate the interactions of this particular case, there is no great problem because the Lennard-Jones potential (L-J) is short range potential. However, to solve this problem, the *minimum image criterion* is introduced in which only the nearest images of distinguishable particles are taken into account. This operating condition is commonly used and greatly simplified for setting up simulation programs. In practice, most short range interactions usually fall off rapidly and can be neglected beyond the distance called the *cut-off limit*. In general, the cut-off limit should be no more than half of the box length ($r_c \leq L/2$).

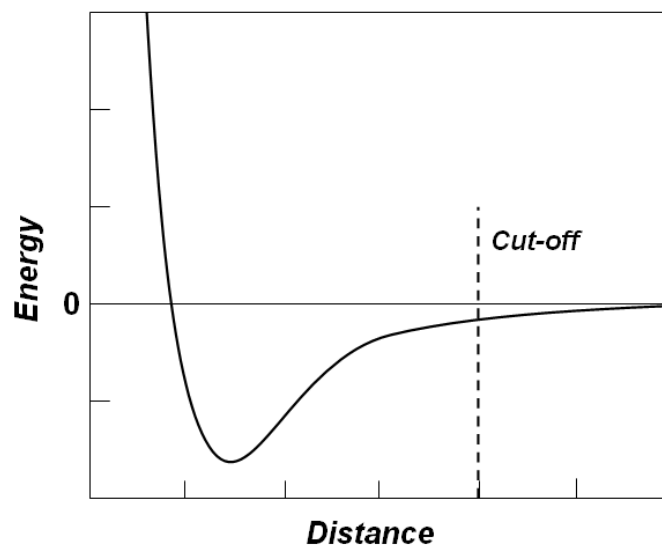


Figure 2.6 The discontinuity of energy curve when the potential is truncated.

According to the use of cut-off limit, this reflects in the discontinuity in both the potential energy and the force after the cut-off value, as shown in Figure 2.6. This problem can be solved by shifting the potential function by an amount V_c ,

$$V'(r) = \begin{cases} V(r) - V_c & \text{if } r \leq r_c \\ 0 & \text{if } r > r_c \end{cases}, \quad (2.58)$$

where r_c is the cut-off distance and V_c corresponds to the value of the potential at the cut-off distance. In this respect, although the energy conservation can be improved by the shifted potential, the discontinuity in the force with the shifted potential still exists. At the cut-off distance, since the force will have a finite value, a suitable shifted potential would be of the form

$$V'(r) = \begin{cases} V(r) - V_c - \left(\frac{dV(r)}{dr} \right)_{r=r_c} (r - r_c) & \text{if } r \leq r_c \\ 0 & \text{if } r > r_c \end{cases}. \quad (2.59)$$

However, the application of shifted potential is not easy for inhomogeneous systems containing many different types of atom. An alternative way is to eliminate discontinuities in the energy and force by using a *switching function*. The switched potential ($V^{SF}(r)$) is related to the true potential ($V(r)$) as

$$V'(r) = V(r)S(r). \quad (2.60)$$

Some switching functions are applied to the entire range of the potential up to the cut-off point. In general, the switching function has a value of 1 at $r = 0$ and a value of 0 at $r = r_c$, while the switching function values between two

cut-offs are varied. The example of a switching function applied to the Lennard-Jones potential is given in Figure 2.7.

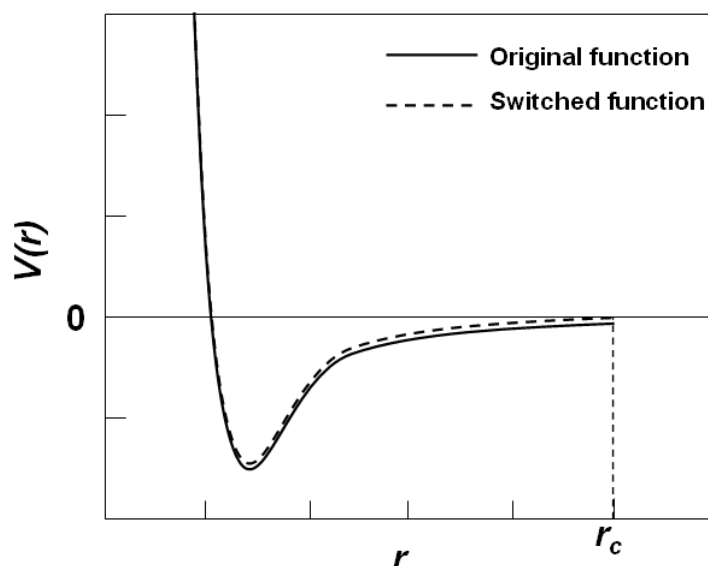


Figure 2.7 The effect of a switching function applied to the Lennard-Jones potential.

2.2.6 Non-bonded neighbor lists

The use of cut-off and minimum image convention is not actually reduce the time for calculating the non-bonded interactions, since the distance between every pair of atoms still have to be calculated in each simulation step. In practice, since most of atoms move within a time step of less than 0.2 \AA , the local neighbors of a given atom remain almost the same for many time steps. In this regard, the *non-bonded neighbor list* as shown in Figure 2.8 is employed. The first non-bonded neighbor list has been proposed by Verlet (Verlet, 1967). The Verlet neighbor list stores all atoms within the cut-off distance (r_c) and atoms are slightly further away than the cut-off distance (r_m). The neighbor list will frequently be updated throughout

the simulation. With regard to this point, the distance used to calculate each atom's neighbors should be slightly larger than the actual cut-off distance in order to ensure that the atoms outside the cut-off will not move closer than the cut-off distance before the neighbor list is updated again.

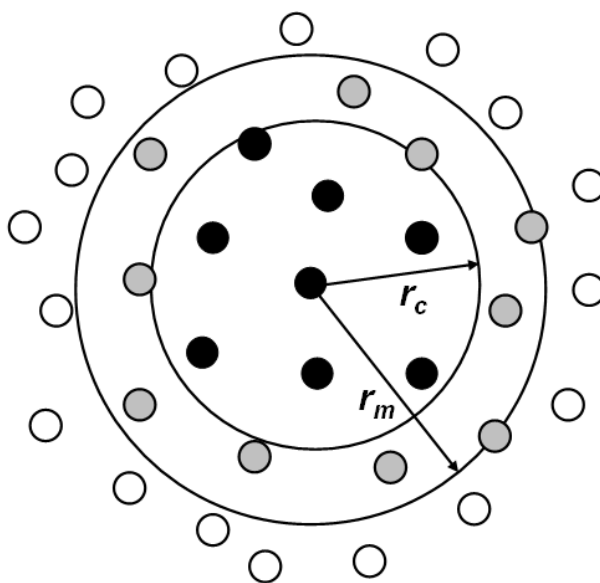


Figure 2.8 The non-bonded neighbor list.

2.2.7 Long-range interactions

The neglect of interactions beyond the cut-off distance, especially for the strong interacting systems, may result in an incorrect description of molecular properties. One simple way to treat the long-range interactions is to use a large simulation cell, but this reflects in more time-consuming. There are many suitable methods for the treatment of long-range interactions. The first method is the Ewald summation method, which derived by Ewald in 1921 (Ewald, 1921). This method studies the energetic of ionic crystals, *i.e.*, a particle interacts with all the other

particles in the simulation box and with all of their images in an infinite array of periodic cells. The charge-charge contribution to the potential energy of the Ewald summation method could be of the form

$$V = \frac{1}{2} \sum'_{|n|=0} \sum_{i=1}^N \sum_{j=1}^N \frac{q_i q_j}{4\pi\epsilon_0 |r_{ij} + n|}, \quad (2.61)$$

where the prime on the first summation indicates that the series does not include the interaction $i = j$ for $n = 0$, q_i and q_j are charges and n is a cubic lattice point. The Ewald summation method is the most correct way to accurately include all the effects of long-range forces in the computer simulation. However, this method is rather expensive to implement since the equation (2.61) converges extremely slowly.

Another method for the treatment of long-range interactions is the *reaction field method* (Foulkes and Haydock, 1989). This method constructs the sphere around the molecule with a radius equal to the cut-off distance. By this scheme, all interactions within the sphere are calculated explicitly, while those outside of the sphere are modeled as a homogeneous medium of dielectric constant (ϵ_s). The electrostatic field due to the surrounding dielectric is given by

$$E_i = \frac{2(\epsilon_s - 1)}{\epsilon_s + 1} \left(\frac{1}{r_c^3} \right) \sum_{j: r_{ij} \leq r_c} \mu_j, \quad (2.62)$$

where μ_j are the dipoles of the neighboring molecules that are located within the cut-off distance (r_c) of the molecules i . The interaction between molecule i and the reaction field equals to $E_i \cdot \mu_i$.

2.3 Research methodology

2.3.1 Conventional QM/MM MD scheme

According to the conventional QM/MM MD technique, the system is partitioned into two parts, namely QM and MM regions. The QM region, *i.e.*, a sphere which contains a set of particles of highest interest, is treated by quantum mechanics, while the rest of the system is described by classical MM potentials. The schematic details of QM/MM are shown in Figure 2.9.

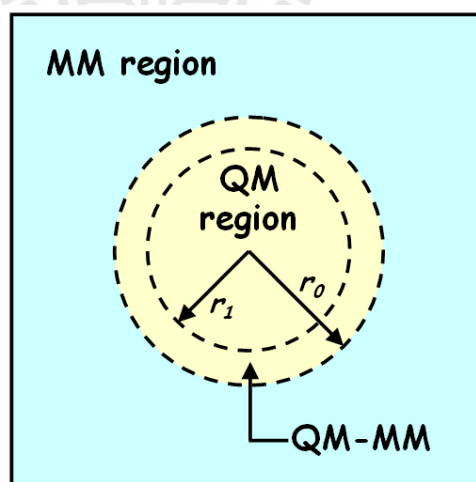


Figure 2.9 The QM/MM scheme.

The total energy (E_{tot}) of the system can be obtained from the summation of three component parts, namely the interactions within the QM, in the MM and between the QM and MM regions,

$$E_{total} = \langle \Psi_{QM} | \hat{H} | \Psi_{QM} \rangle + E_{MM} + E_{QM-MM}, \quad (2.63)$$

where $\langle \Psi_{QM} | \hat{H} | \Psi_{QM} \rangle$ refers to the interactions within the QM region, E_{MM} is the interactions within the MM region and E_{QM-MM} is the interactions between the QM and MM regions.

During the QM/MM simulation, exchanges of water molecules between the QM and MM regions can occur frequently. With regard to this point, the force acting on each particle in the system is switched according to which region the water molecule is entering or leaving the QM region and is defined as

$$F_i = S_m(r)F_{QM} + (1 - S_m(r))F_{MM}, \quad (2.64)$$

where F_{QM} and F_{MM} are quantum mechanical and molecular mechanical forces, respectively. $S_m(r)$ is a smoothing function described by

$$\begin{aligned} S_m(r) &= 1 && \text{for } r \leq r_1 \\ S_m(r) &= \frac{(r_0^2 - r^2)^2 (r_0^2 + 2r^2 - 3r_1^2)}{(r_0^2 - r_1^2)^3} && \text{for } r_1 < r \leq r_0, \\ S_m(r) &= 0 && \text{for } r > r_0 \end{aligned} \quad (2.65)$$

where r_1 and r_0 are the distances characterizing the start and the end of the QM region, applied within an interval of 0.2 Å to ensure a continuous change of forces at the transition between the QM and MM regions.

2.3.2 QM/MM MD based on ONIOM-XS method

The conventional QM/MM technique is a very useful tool for studying various condensed-phase systems. However, some unsolved problems have been demonstrated. First, only the exchanging particles which crossings between QM and MM regions are treated by a smoothing function. With regards to this point, it is not realistic since immediate addition or deletion of a particle in the QM region due to the solvent exchange also affects the forces acting on the remaining particles in the QM region. Consequently, the conventional QM/MM simulation may provides numerical instability of forces whenever the solvent exchange process occurs in the system. Second, the conventional scheme cannot clearly define the appropriate energy expression when the solvent exchange process occurs during the simulation.

To solve these problems, a more sophisticated QM/MM technique based on ONIOM-XS method has been proposed (Kerdcharoen and Morokuma, 2003). The ONIOM (Own N-layered Integrated molecular Orbital and molecular Mechanics) method was originally proposed by Morokuma *et al.* (Svensson *et al.*, 1996). The extension of the ONIOM method for the treatment of condensed-phase system was firstly applied by Kerdcharoen and co-worker, called ONIOM-XS (XS = eXtension to Solvation)

According to the QM/MM MD technique based on ONIOM-XS method, the system is comprised of a “high-level” QM sphere, *i.e.*, a sphere which

contains a central reference molecule and its nearest-neighbors, and the remaining “low-level” MM bulk solvents. A thin switching shell located between the QM and MM regions is then introduced in order to smooth the transition of force due to the solvent exchange.

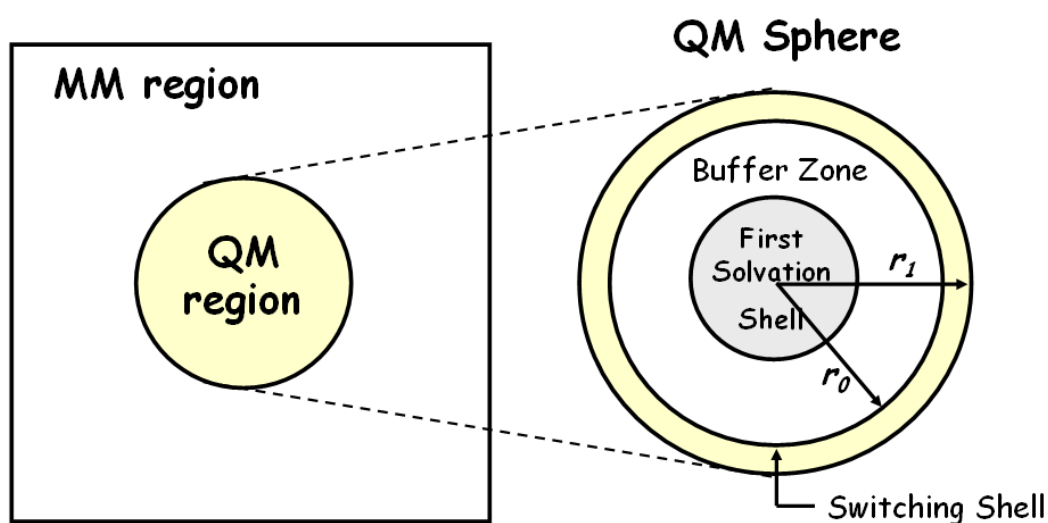


Figure 2.10 QM/MM MD based on ONIOM-XS method.

Given n_1 , l and n_2 as number of particles in the QM sphere, the switching layer and the MM region, respectively, and $N(= n_1+l+n_2)$ as the total number of particles, the potential energy of the system can be written in two ways based on the ONIOM extrapolation scheme (Svensson *et al.*, 1996). If the switching layer is included into the high-level (QM) calculation, the energy expression is written as

$$E^{ONIOM}(n_1 + l; N) = E^{QM}(n_1 + l) - E^{MM}(n_1 + l) + E^{MM}(N). \quad (2.66)$$

If the switching layer is considered as part of the low-level (MM) region, the energy expression is written as

$$E^{ONIOM}(n_1; N) = E^{QM}(n_1) - E^{MM}(n_1) + E^{MM}(N). \quad (2.67)$$

The potential energy of the entire system is taken as a hybrid between both energy terms (2.66) and (2.67),

$$E^{ONIOM-XS}(\{r_i\}) = (1 - \bar{s}(\{r_i\})) \cdot E^{ONIOM}(n_1 + l; N) + \bar{s}(\{r_i\}) \cdot E^{ONIOM}(n_1 + N), \quad (2.68)$$

where $\bar{s}(\{r_i\})$ is an average over a set of switching functions for individual exchanging particle in the switching layer $s_i(x_i)$,

$$\bar{s}(\{r_i\}) = \frac{1}{l} \sum_{i=1}^l s_i(x_i). \quad (2.69)$$

The switching function in equation (3.69) can have any form. In the present study, a polynomial form is employed,

$$s_i(x_i) = 6\left(x_i - \frac{1}{2}\right)^5 - 5\left(x_i - \frac{1}{2}\right)^3 + \frac{15}{8}\left(x_i - \frac{1}{2}\right) + \frac{1}{2}, \quad (2.70)$$

where $x_i = ((r_i - r_0)/(r_1 - r_0))$, r_0 and r_1 are the radius of inner and outer surfaces of the switching shell, respectively, and r_i is the distance between the center of mass of the exchanging particle and the center of the QM sphere. The switching function has an S-shape and converges to 0 and 1 at r_0 and r_1 , respectively. The gradient of the energy can be written as

$$\begin{aligned} \nabla_R E^{ONIOM-XS}(\{r_l\}) = & (1 - \bar{s}(\{r_l\})) \cdot \nabla_R E^{ONIOM}(n_l + l; N) + \bar{s}(\{r_l\}) \\ & \cdot \nabla_R E^{ONIOM}(n_1; N) + \frac{1}{(r_1 - r_0)} \nabla \bar{s}(\{r_l\}) \\ & \cdot (E^{ONIOM}(n_1; N) - E^{ONIOM}(n_1 + l; N)) \end{aligned} \quad (2.71)$$

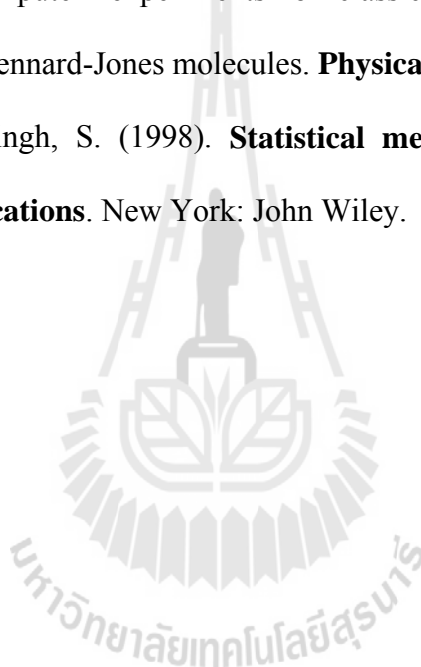
2.4 References

- Alder, B. J., and Wainwright, T. E. (1957). Phase transition for a hard sphere system. **The Journal of Chemical Physics**. 27: 1208-1209.
- Alder, B. J., and Wainwright, T. E. (1959). Studies in molecular dynamics. I. General method. **The Journal of Chemical Physics**. 31: 459-466.
- Bartlett, R. J. (1989). Coupled-cluster approach to molecular structure and spectra: a step toward predictive quantum chemistry. **The Journal of Physical Chemistry**. 93: 1697-1708.
- Beeman, D. (1976). Some multistep methods for use in molecular dynamics calculations. **Journal of Computational Physics**. 20: 130-139.
- Boys, S. F. (1950). Electronic wave functions. I. A general method of calculation for the stationary states of any molecular system. **Proceedings of the Royal**

- Society of London. Series A. Mathematical and Physical Sciences.** 200: 542-554.
- David, C. (1987). **Introduction to modern statistical mechanics.** New York: Oxford University Press.
- Dunning, J. T. H. (1970). Gaussian basis functions for use in molecular calculations. I. Contraction of (9s5p) atomic basis sets for the first-row atoms. **The Journal of Chemical Physics.** 53: 2823-2833.
- Dunning, J. T. H. (1971). Gaussian basis functions for use in molecular calculations. III. Contraction of (10s6p) atomic basis sets for the first-row atoms. **The Journal of Chemical Physics.** 55: 716-723.
- Ewald, P. P. (1921). Die berechnung optischer und elektrostatischer gitterpotentiale. **Annalen der Physik.** 369: 253-287.
- Foulkes, W. M. C., and Haydock, R. (1989). Tight-binding models and density-functional theory. **Physical Review B.** 39: 12520-12536.
- Gear, C. W. (1971). The automatic integration of ordinary differential equations. **Communications of the ACM.** 14: 176-179.
- Hehre, W. J., Stewart, R. F., and Pople, J. A. (1969). Self-consistent molecular-orbital methods. I. Use of gaussian expansions of slater-type atomic orbitals. **The Journal of Chemical Physics.** 51: 2657-2664.
- Hockney, R. W. (1970). Potential calculation and some applications. **Methods in Computational Physics.** 9: 135-211.
- Huzinaga, S. (1965). Gaussian-type functions for polyatomic systems. I. **The Journal of Chemical Physics.** 42: 1293-1302.

- Kerdcharoen, T., and Morokuma, K. (2003). Combined quantum mechanics and molecular mechanics simulation of Ca^{2+} /ammonia solution based on the ONIOM-XS method: Octahedral coordination and implication to biology. **The Journal of Chemical Physics**. 118: 8856-8862.
- Kistenmacher, H., Popkie, H., and Clementi, E. (1974). Study of the structure of molecular complexes. VIII. Small clusters of water molecules surrounding Li^+ , Na^+ , K^+ , F^- and Cl^- ions. **The Journal of Chemical Physics**. 61: 799-815.
- McQuarrie, D. A. (1976). **Statistical mechanics**. New York: Harper & Row.
- Møller, C., and Plesset, M. S. (1934). Note on an approximation treatment for many-electron systems. **Physical Review**. 46: 618-622.
- Rahman, A. (1964). Correlations in the motion of atoms in liquid argon. **Physical Review**. 136: A405-A411.
- Sherrill, C. D., and Schaefer III, H. F. (1999). The configuration interaction method: Advances in highly correlated approaches. **Advances in Quantum Chemistry**. 34: 143-269.
- Slater, J. C. (1930). Atomic shielding constants. **Physical Review**. 36: 57-64.
- Stillinger, F. H., and Rahman, A. (1974). Improved simulation of liquid water by molecular dynamics. **The Journal of Chemical Physics**. 60: 1545-1557.
- Svensson, M., Humbel, S., Froese, R. D. J., Matsubara, T., Sieber, S., and Morokuma, K. (1996). ONIOM: A multilayered integrated MO + MM method for geometry optimizations and single point energy predictions. A test for Diels-Alder reactions and $\text{Pt}(\text{P}(t\text{-Bu})_3)_2 + \text{H}_2$ oxidative addition. **The Journal of Physical Chemistry**. 100: 19357-19363.

- Swope, W. C., Andersen, H. C., Berens, P. H., and Wilson, K. R. (1982). A computer simulation method for the calculation of equilibrium constants for the formation of physical clusters of molecules: Application to small water clusters. **The Journal of Chemical Physics**. 76: 637-649.
- Szabo, A., and Ostlund, N. S. (1989). **Modern quantum chemistry: Introduction to advanced electronic structure theory**. New York: McGraw-Hill.
- Verlet, L. (1967). Computer “experiments” on classical fluids. I. Thermodynamical properties of Lennard-Jones molecules. **Physical Review**. 159: 98-103.
- Wilde, R. E., and Singh, S. (1998). **Statistical mechanics: Fundamentals and modern applications**. New York: John Wiley.



CHAPTER III

RESEARCH PROCEDURES

3.1 Selection of QM method, QM size and basis set

With regard to the QM/MM technique, the selection of QM method, as well as the size of QM region and basis set, is very crucial in order to obtain reliable results. In practice, these important parameters must be optimized, compromising between the quality of the simulation results and the requirement of CPU time. In this work, the QM region was set with respect to a sphere which contains a central water molecule and about 10-14 nearest-neighbor waters, assuming to be large enough to study the hydrogen-bonded structure and dynamics of liquid water. This QM region will be treated at HF level of accuracy using DZP basis set. Figures 3.1 and 3.2 provide supporting data for the selection of HF method and DZP basis set. As can be seen in Figure 3.1, the correlated methods, even for the MP2, with medium-size basis set, such as DZP, are rather time-consuming and therefore are not feasible for the QM treatment of more than 8 water molecules, *i.e.*, with respect to our available computational resources. As a consequence, the HF and DFT, such as B3LYP, methods seem to be the only possible choices, in conjunction with the use of medium-size DZP basis set. However, the B3LYP method is not taken into consideration since it has been shown that this method tends to overestimate the water interactions (Lee and Tuckerman, 2007; Xenides, Randolph, and Rode, 2005).

In this work, although the effects of electron correlation could be expected to play some roles on the properties of liquid water, the use of the HF method with a sufficiently large QM size and basis set is considered to be reliable enough to achieve a sufficient level of accuracy in the QM/MM MD simulations. With regard to the selection of DZP basis set, it should be noted that the use of larger basis set can provide better results, but it's also too time-consuming. As can be seen in Figure 3.2, it is apparent that the HF calculations with a relatively large basis set, like AUG-cc-pVDZ, are extremely expensive, and thus, beyond our current computational feasibility.

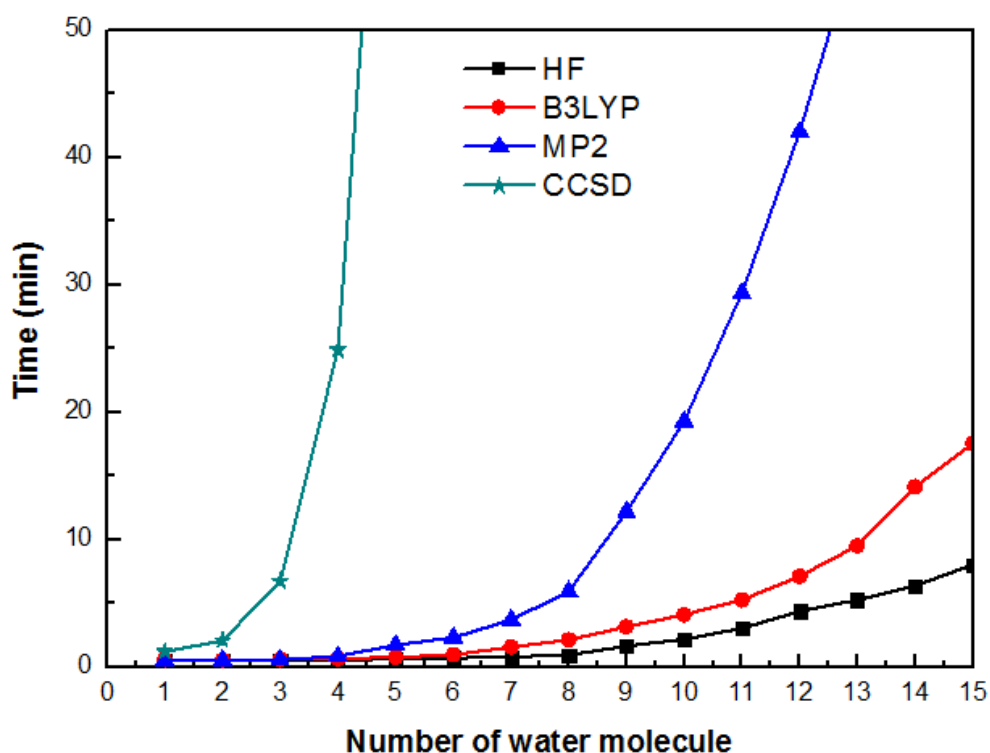


Figure 3.1 Requirements of CPU times for HF, B3LYP, MP2 and CCSD force calculations of $(\text{H}_2\text{O})_n$, $n=1,15$ complexes using DZP basis set. All calculations were performed on CCRL cluster with Intel Core^{TM2} Quad of CPU and 4GB of Ram.

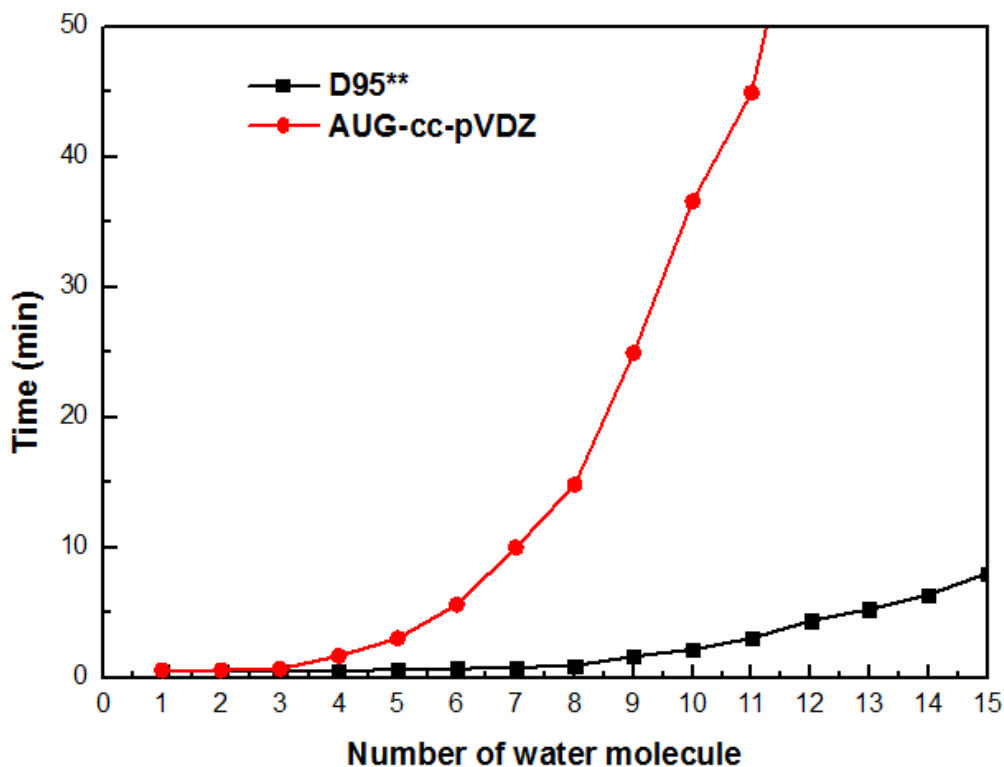


Figure 3.2 Requirements of CPU times for HF force calculations of $(\text{H}_2\text{O})_n$, $n=1-15$ complexes using DZP and AUG-cc-pVDZ basis sets. All calculations were performed on CCRL cluster with Intel Core™2 Quad of CPU and 4GB of Ram.

In the theory of intermolecular interactions, another important problem is Basis Set Superposition Error (BSSE), leading to overestimation of binding energies as well as to limit of the accuracy in the standard (finite basis) quantum chemical calculations. When the BSSE is suspected, a correction must be made in order to avoid false results, especially the global minima of stabilization energies and the corresponding molecular geometry due to the overestimation of their interaction energies. In this work, the geometry optimizations of $(\text{H}_2\text{O})_3$ complex as shown in Figure 3.3, calculated at HF, B3LYP, MP2 and CCSD levels of accuracy using two

different basis sets, namely DZP and AUG-cc-pVDZ, have been carried out, and the results are summarized in Tables 3.1.

According to the data in Tables 3.1, it is obvious that the use of correlated methods, such as MP2 and CCSD, with a relatively large AUG-cc-pVDZ basis set can provide reliable results with small BSSE values. In practice, however, the use of such correlated methods and basis set in the QM/MM MD simulations is very time-consuming. In Table 3.1, the HF calculation using DZP basis set gives rather smaller BSSE value, when compared to those of the correlated methods. In addition, the HF stabilization energy is rather close to the CCSD results. Thus, the HF method and the medium-size DZP basis set employed in this work appear to be a promising condition. With regard to the B3LYP calculations, as can be seen in Table 3.1, the results with respect to the use of DZP basis set show significant overestimation of the stabilization energy of the $(\text{H}_2\text{O})_3$ complex. These data clearly indicate the deficiency of the B3LYP method in describing the properties of liquid water.

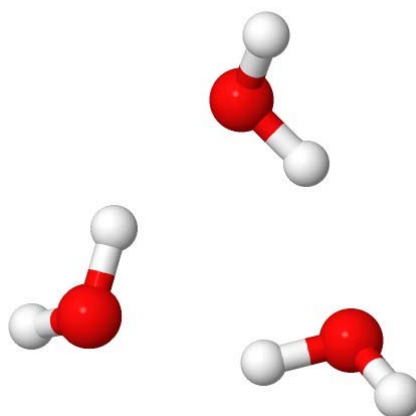


Figure 3.3 Geometry of $(\text{H}_2\text{O})_3$ complex.

Table 3.1 Basis set superposition error of (H₂O)₃ complex, calculated at HF, B3LYP, MP2 and CCSD levels of accuracy using two different basis sets.

Basis set	Uncorrected E	Corrected E (kcal.mol ⁻¹)	BSSE
DZP			
HF	-13.702	-13.396	-0.305
B3LYP	-18.802	-18.308	-0.493
MP2	-17.206	-15.543	-1.663
CCSD	-15.900	-14.327	-1.573
AUG-cc-pVDZ			
HF	-11.142	-10.416	-0.726
B3LYP	-14.083	-13.197	-0.886
MP2	-14.200	-13.908	-0.292
CCSD	-13.775	-13.637	-0.139

3.2 Simulation details

For both the conventional QM/MM and ONIOM-XS MD simulations, all interactions within the QM region were evaluated by performing *ab initio* calculations at the Hartree-Fock (HF) level of accuracy using the DZP basis set. All QM calculations were carried out using the Gaussian03 program (Frisch *et al.*, 2005). For the QM treated-region, a QM radius of 4.2 Å and a switching width of 0.2 Å were chosen, corresponding to the ONIOM-XS parameters r_0 and r_1 of 4.0 and 4.2 Å, respectively. In comparison to the conventional QM/MM scheme, these parameters correspond to the start and the end of the QM radius, *i.e.*, a defined QM/MM boundary where the smoothing applies. This QM size is assumed to be large enough to include all molecules that are forming hydrogen bonds with the central H₂O. In this

respect, it could be expected that the remaining interactions beyond the QM region are well accounted for by the MM potentials. As can be seen in the next section (Figure 4.1), the smooth shape of the O-O radial distribution functions (RDFs) between 4.0 and 4.2 Å clearly confirms that transition of water molecules between the QM and MM regions occurs smoothly. For the interactions within the MM and between the QM and MM regions, a flexible BJH-CF2 water model (Bopp, Jancsó, and Heinzinger, 1983), which describes intermolecular and intramolecular interactions, was employed. This flexible water model is employed in order to ensure a smooth transition when water molecules move from the QM region with its full flexibility to the MM region.

Both the HF/MM and ONIOM-XS MD simulations were performed in a canonical ensemble at 298 K with periodic boundary conditions. The system's temperature was kept constant using the Berendsen algorithm (Berendsen, Postma, van Gunsteren, DiNola, and Haak, 1984). A periodic box, with a box length of 18.15 Å, contains 200 water molecules, corresponding to the experimental density of pure water. The reaction-field method (Adams, Adams, and Hills, 1979) was employed for the treatment of long-range interactions. The Newtonian equations of motions were treated by a general predictor-corrector algorithm. The time step size was set to 0.2 fs, which allows for the explicit movement of the hydrogen atoms of water molecules. In this work, the HF/MM and ONIOM-XS simulations were performed independently with the system's re-equilibration for 30,000 time steps, followed by another 200,000 (HF/MM) and 150,000 (ONIOM-XS) time steps to collect configurations every 10th step.

3.3 Determination of system's properties

3.3.1 Structural properties

Detailed information on the structure of liquid water can be obtained by analyzing the MD trajectory files, *i.e.*, in terms of a set of g_{O-O} , g_{O-H} and g_{H-H} RDFs. The RDF, $g_{\alpha\beta}(r)$, is the set of site-site pair correlation functions, which describes how (on average) the atoms in the system are radially packed around each other. The RDF is useful in other ways. For example, it is something that can be deduced experimentally from X-ray or neutron diffraction studies, thus providing a direct comparison between experiments and simulations. The RDF can be expressed as

$$g_{\alpha\beta}(r) = N_{\alpha\beta}(r) / (4\pi r^2 \Delta r \rho_{\beta}), \quad (3.1)$$

where $N_{\alpha\beta}(r)$ is the average number of β sites located in the shell $(r, r+\Delta r)$ centered on site α , and $\rho_{\beta} = \frac{N_{\beta}}{V}$ is the average number density of β sites in the system.

The corresponding integration number of RDF is defined as

$$n_{\alpha\beta}(r) = 4\pi\rho_{\beta} \int_0^r g_{\alpha\beta}(r') r'^2 dr'. \quad (3.2)$$

In addition, the information with respect to the angles formed between either oxygen or hydrogen atoms of the central water molecule and the atoms of the surrounding water molecules can be obtained from the angular distribution functions

(ADFs), such as O---O---O, O-H---O and O---H-O angles. Moreover, the coordination number distributions (CNDs) and the number of hydrogen-bond distributions surrounding the central H₂O will also be presented.

3.3.2 Dynamical properties

The dynamics details of liquid water can be obtained by computing the velocity autocorrelation functions (VACFs), which can be expressed as

$$C_{vv}(t) = \frac{1}{N_\tau N} \frac{\sum_j^{N_\tau} \sum_{i=1}^N [\vec{v}_i(t_j) \vec{v}_i(t_j + t)]}{\sum_j^{N_\tau} \sum_{i=1}^N [\vec{v}_i(t_j) \vec{v}_i(t_j)]}, \quad (3.3)$$

where N_τ is the number of “time origins”, N is the number of particles and \vec{v}_i denotes the velocity of a given particle j .

In this work, the normal-coordinate analysis developed by Bopp (Bopp, 1986) was used for obtaining the vibrational and librational frequencies of liquid water. Six scalar quantities Q_2 , Q_1 , Q_3 , R_x , R_y , and R_z are defined to describe the bending vibration, symmetric and asymmetric stretching vibrations, and rotations around the three principal axes of the water molecule, respectively.

In addition, self-diffusion coefficients (D) and the mean residence times (MRTs) of water molecules will be calculated. The values of D for the central H₂O and its nearest-neighbors were calculated from their center-of-mass VACFs using the Green-Kubo relation (Spohr, Palinkas, Heinzinger, Bopp, and Probst, 1988),

$$D = \frac{1}{3} \lim_{t \rightarrow \infty} \int_0^t C_{vw}(t) dt. \quad (3.4)$$

During the HF/MM and ONIOM-XS MD simulations, trajectories of each species in the system were monitored. In this work, the rate of water exchange processes at the central water molecule was determined through the MRT of its nearest-neighbor water molecules, which calculated using a “direct” method (Hofer, Tran, Schwenk, and Rode, 2004). Based on the direct method, the whole trajectories were inspected either the leaving or entering a coordination shell of ligands and the MRT can be expressed as

$$MRT(\tau) = \frac{CN \times t_{sim}}{N_{ex}}, \quad (3.5)$$

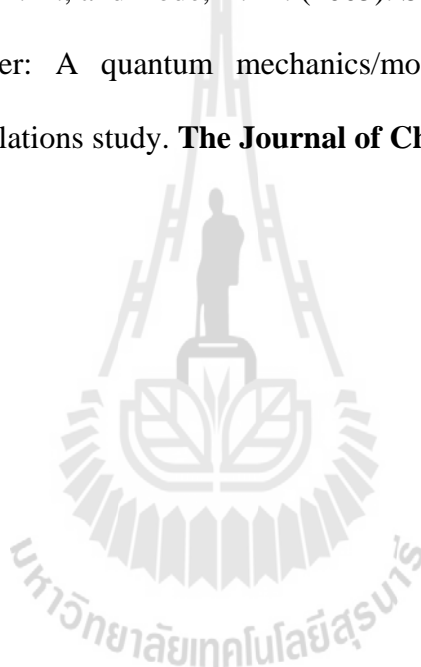
where CN is the average number of ligand in the shell, t_{sim} is the duration of the simulation and N_{ex} equals the number of events. In this work, the parameters t^* were set to 0.0 and 0.5 ps , which correspond to the lifetime of hydrogen bond and a suitable exchange of ligands in the immediate neighborhood of given molecule, respectively.

3.4 References

Adams, D. J., Adams, E. M., and Hills, G. J. (1979). The computer simulation of polar liquids. **Molecular Physics**. 38: 387-400.

- Berendsen, H. J. C., Postma, J. P. M., van Gunsteren, W. F., DiNola, A., and Haak, J. R. (1984). Molecular dynamics with coupling to an external bath. **The Journal of Chemical Physics**. 81: 3684-3690.
- Bopp, P. (1986). A study of the vibrational motions of water in an aqueous CaCl_2 solution. **Chemical Physics**. 106: 205-212.
- Bopp, P., Jancsó, G., and Heinzinger, K. (1983). An improved potential for non-rigid water molecules in the liquid phase. **Chemical Physics Letters**. 98: 129-133.
- Frisch, M. J., Trucks, G. W., Schlegel, H. B., Scuseria, G. E., Robb, M. A., Cheeseman, J. R., Zakrzewski, V. G., Montgomery, J. A., Stratmann, R. E., Burant, J. C., Dapprich, S., Millam, J. M., Daniel, A. D., Kudin, K. N., Strain, M. C., Farkas, O., Tomasi, J., Barone, V., Cossi, M., Cammi, R., Mennucci, B., Pomelli, C., Adamo, C., Clifford, S., Ochterski, J., Petersson, G. A., P.Y. Ayala, Q. C., Morokuma, K., Salvador, P., Dannenberg, J. J., Malick, D. K., Rabuck, A. D., Raghavachari, K., J. B. Foresman, Cioslowski, J., Ortiz, J. V., Baboul, A. G., Stefanov, B. B., Liu, G., Liashenko, A., Piskorz, P., Komaromi, I., Gomperts, R., Martin, R. L., Fox, D. J., T. Keith, M. A. A. L., Peng, C. Y., Nanayakkara, A., Challacombe, M., Gill, B. J., Chen, W., Wong, M. W., Gonzalez, C., and Pople, J. A. (2005). Gaussian 03 (Revision D.1) [Computer Software]. Wallingford, CT, USA: Gaussian.
- Hofer, T. S., Tran, H. T., Schwenk, C. F., and Rode, B. M. (2004). Characterization of dynamics and reactivities of solvated ions by ab initio simulations. **Journal of Computational Chemistry**. 25: 211-217.

- Lee, H.-S., and Tuckerman, M. E. (2007). Dynamical properties of liquid water from ab initio molecular dynamics performed in the complete basis set limit. **The Journal of Chemical Physics**. 126: 164501-164516.
- Spohr, E., Palinkas, G., Heinzinger, K., Bopp, P., and Probst, M. M. (1988). Molecular dynamics study of an aqueous strontium chloride solution. **The Journal of Physical Chemistry**. 92: 6754-6761.
- Xenides, D., Randolph, B. R., and Rode, B. M. (2005). Structure and ultrafast dynamics of liquid water: A quantum mechanics/molecular mechanics molecular dynamics simulations study. **The Journal of Chemical Physics**. 122: 174506-174510.



CHAPTER IV

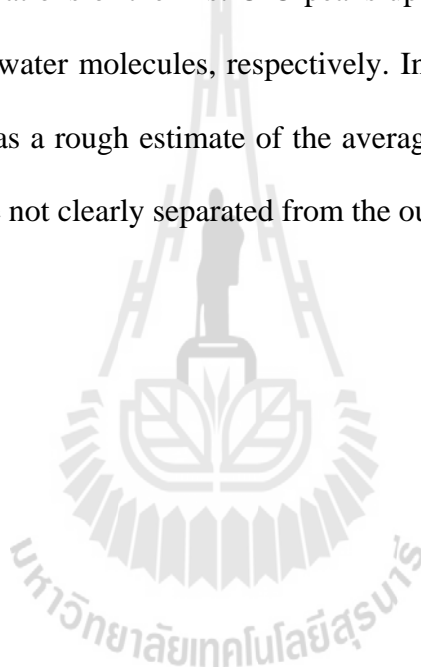
RESULTS AND DISCUSSION

4.1 Structural properties

The details with respect to the structure of liquid water can be visualized from a series of O-O, O-H, H-O and H-H RDFs, together with their corresponding integration numbers, as depicted in Figure 4.1. In this context, the first atom denotes the atoms of the central H₂O and the second one refers to the atoms of the surrounding waters, respectively. To provide useful comparison, structural parameters of liquid water, as obtained by various QM/MM MD simulations and experiments, are summarized in Table 4.1. Regarding the O-O RDFs, as shown in Figure 4.1a, both HF/MM and ONIOM-XS simulations reveal a rather well-defined first peak with maxima centered at 2.84 and 2.82 Å, respectively. These observed O-O distances are in good agreement with the corresponding values of 2.82 and 2.83 Å derived by X-ray scattering (Okhulkov, Demianets, and Gorbaty, 1994) and neutron diffraction (Soper, 1994) experiments, respectively. According to the experimental data in Table 4.1, the observed variations in the O-O distance could be ascribed to the use of different models and techniques in evaluating the collected (pre-fitted) data, which are both crucial factors affecting the results (Soper, 2000). Comparing the HF/MM and ONIOM-XS results, however, a significant difference is found in the O-O RDFs beyond 3.20 Å, in which the feature of the ONIOM-XS's O-O RDF reveals a relatively more distinct first coordination shell. Of particular interest, this observed

difference can be expected to reflect (more or less) in different structural and dynamical details of liquid water derived from these two simulation techniques.

In Figure 4.1a, the O-O RDFs from both the HF/MM and ONIOM-XS simulations do not show distinct minima after the first peak, suggesting that a number of water molecules can be located between the inner and outer coordination shell and that these water molecules are rather labile, *i.e.*, they can rapidly exchange between the two regions. Integrations of the first O-O peaks up to about 3.20 Å yield average values of 4.9 and 4.7 water molecules, respectively. In fact, these observed numbers should be considered as a rough estimate of the average coordination numbers, since the first O-O peaks are not clearly separated from the outer region.



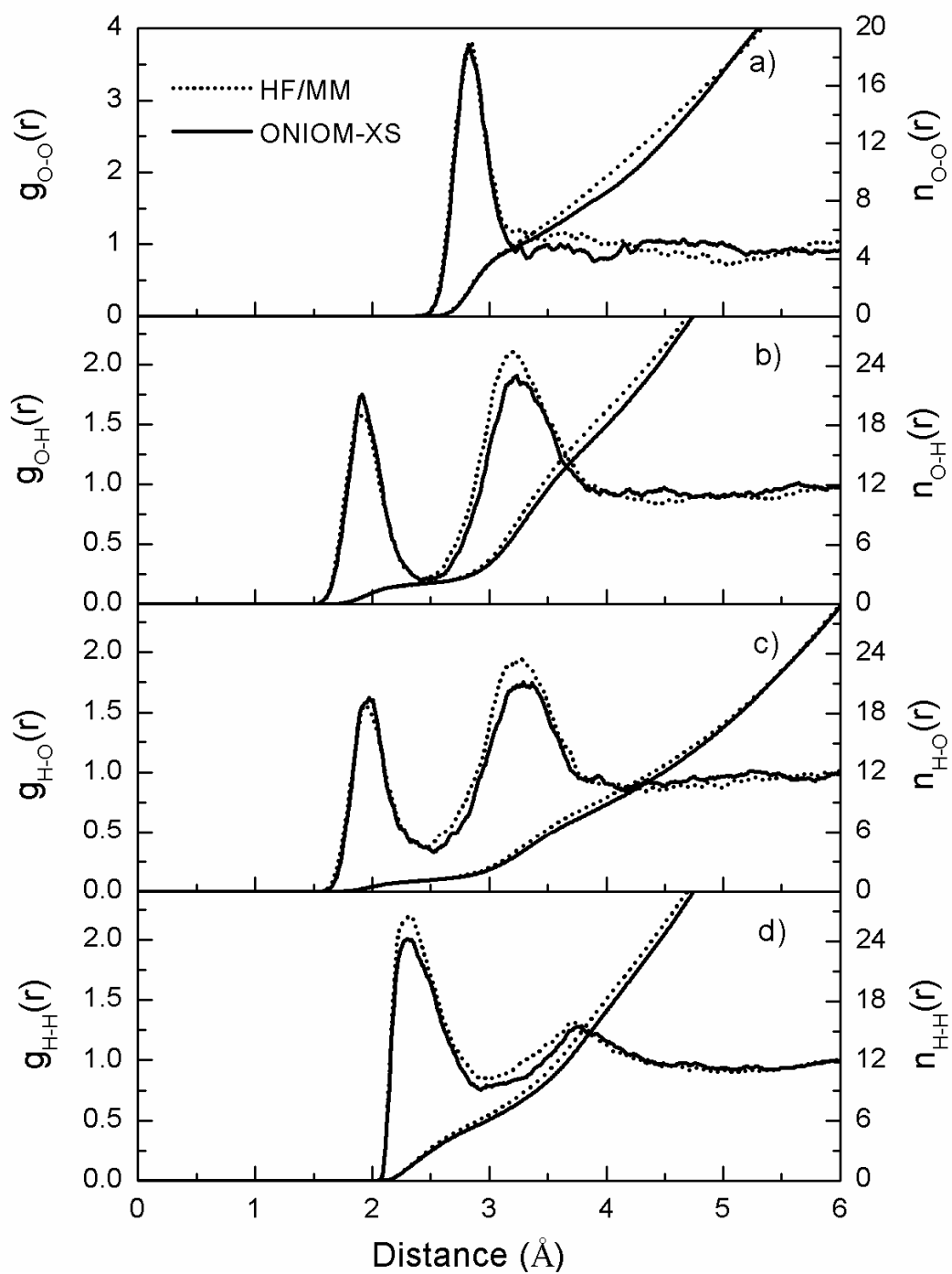


Figure 4.1 a) O-O, b) O-H, c) H-O and d) H-H radial distribution functions and their corresponding integration numbers, as obtained by the HF/MM and ONIOM-XS MD simulations.

Table 4.1 Structural parameters of liquid water, as obtained by various QM/MM MD simulations and experiments.

Method	R_{O-O} (Å)		R_{O-H} (Å)		R_{H-H} (Å)		CN
	R_{max}	R_{min}	R_{max}	R_{min}	R_{max}	R_{min}	
HF/MM MD [*]	2.84	3.20	1.90	2.46	2.37	2.98	4.9
ONIOM-XS MD [*]	2.82	3.22	1.91	2.49	2.35	2.95	4.7
HF/MM MD ^a	2.92	3.41	2.06	2.53	2.59	3.24	4.2
MP2/MM MD ^a	2.87	3.43	1.93	2.61	2.44	2.95	4.7
B3LYP/MM MD ^a	2.81	3.31	1.85	2.42	2.33	2.89	4.2
XS ^b	2.82	-	-	-	-	-	-
XS ^c	2.72	-	-	-	-	-	3.7
ND ^d	2.78	-	1.79	-	-	-	-
ND ^e	2.67	-	1.67	-	-	-	4.2
ND ^f	2.83	-	1.79	-	-	-	4.2
ND ^g	2.89	-	1.95	-	-	-	-

^{*} Present study

^a (Xenides, Randolph, and Rode, 2005)

^b (Okhulkov, Demianets, and Gorbaty, 1994)

^c (Hura, Sorenson, Glaeser, and Head-Gordon, 2000)

^d (Soper, 2000)

^e (Soper, Bruni, and Ricci, 1997)

^f (Soper, 1994)

^g (Jedlovsky, 1998)

Figure 4.2 shows the probability distributions of the coordination numbers, calculated within the O-O distance of 3.20 Å. According to both the HF/MM and ONIOM-XS simulations, the coordination numbers of 4 and 5 are dominating the first coordination shell. However, it is observed that, besides the most frequent 4- and 5-coordinated species, other entities, such as 3-, 6- and 7-fold coordinated ones, are also found in considerable amounts. The HF/MM and ONIOM-XS results are consistent with the recent QM/MM studies, which reported that each water molecule can form various coordination numbers (Xenides, Randolph, and Rode, 2005, 2006), ranging from 3 to 6, with the prevalent value of 4. With respect to the O-O RDFs in Figure 4.1a, the second O-O peaks are absent in both HF/MM and ONIOM-XS simulations, indicating that interactions of the central H₂O with its surrounding water molecules lying beyond the first coordination shell are weak (*i.e.*, less ordering). The diminution of the second O-O RDF has been reported experimentally as the system's temperature or pressure increases (Okhulkov, Demianets, and Gorbaty, 1994).

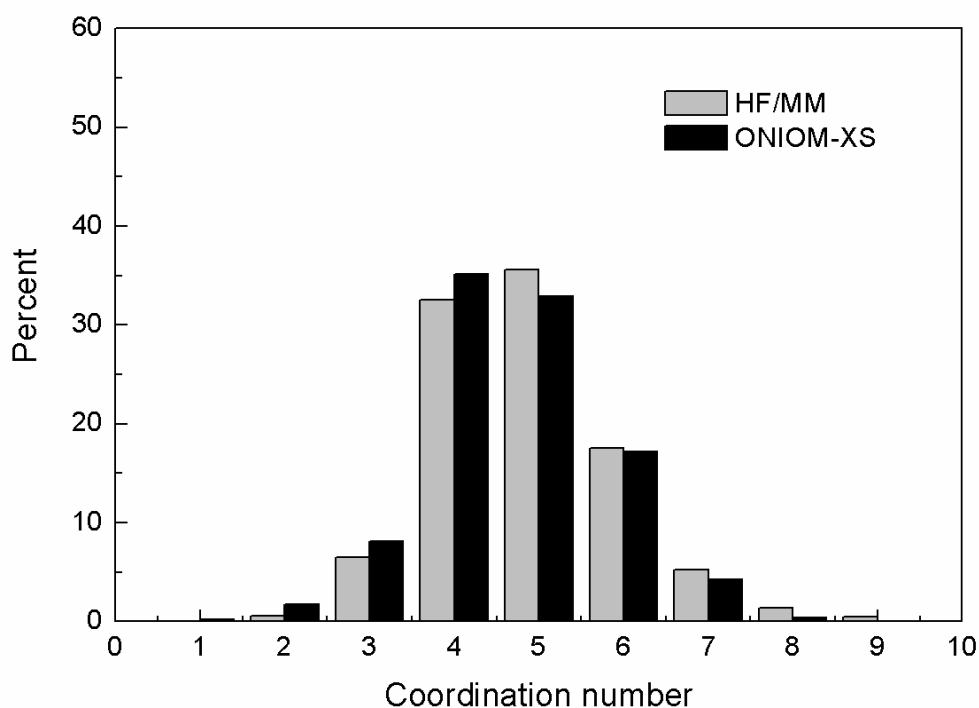


Figure 4.2 Distributions of coordination numbers, calculated within first minimum of the HF/MM and ONIOM-XS MD's O-O RDFs.

The characteristics of intermolecular hydrogen bonds (HBs) in liquid water can be analyzed through the O-H and H-O RDFs. According to Figures 4.1b and c, the first O-H and H-O peaks reflect the HBs between the central H₂O and its neighboring water molecules, *i.e.*, acting as acceptor and donor, respectively. Comparing between the HF/MM and ONIOM-XS simulations, further differences are recognizable, *i.e.*, while the first O-H and H-O RDFs are not much different, the respective second O-H and H-O peaks obtained by the ONIOM-XS simulation are significantly less pronounced than those of the HF/MM results. For the ONIOM-XS simulation, integrations up to first minimum of the O-H and H-O RDFs yield average values of 2.07 and 1.09, compared to the corresponding values of 2.00 and 1.10

obtained by the HF/MM simulation. The HF/MM and ONIOM-XS results correspond to the expectation that on average over time about four HBs (actual values are 4.20 and 4.25 for the HF/MM and ONIOM-XS simulations, respectively) are involved in the HB formation at the central reference water (*i.e.*, two HBs are formed by the central water's oxygen acting as acceptor, and another two HBs are formed by the central water's hydrogen atoms acting as donors). However, since the O-H and H-O RDFs do not show distinct minima after the first shell, the numbers of HBs which are simultaneously formed during the simulations can be evaluated through the detailed analysis of the MD trajectories.

In this work, the evaluations the numbers of HBs were carried out according to the following three geometrical criteria of the HB formation (Xenides, Randolph, and Rode, 2006), (1) the O-O distance is set with respect to the defined first O-O RDFs, *i.e.*, $2.5 \leq R_{O\cdots O} \leq 3.2 \text{ \AA}$, (2) the HB distance is limited by the first minimum of O-H and H-O RDFs, *i.e.*, $1.5 \leq R_{O\cdots H} \leq 2.5 \text{ \AA}$ and (3) the HB angle, $\angle O\cdots H-O, \geq 100^\circ$. Based on these criteria, the distributions of the number of HBs forming around the central H₂O, as obtained by the HF/MM and ONIOM-XS simulations, are plotted in Figure 4.3.

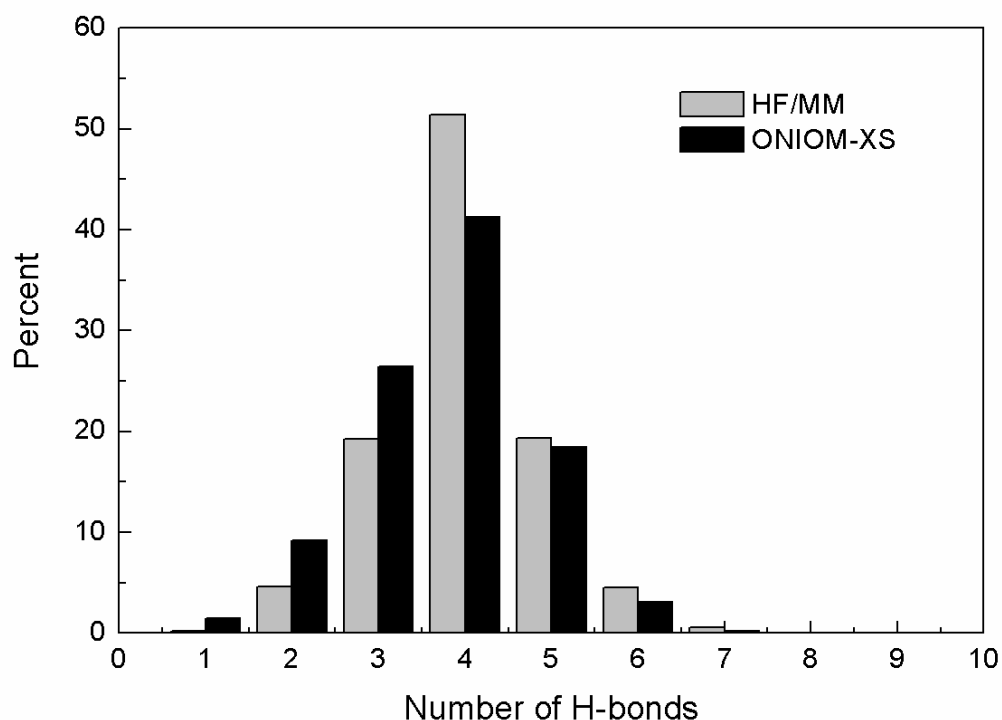


Figure 4.3 Distributions of number of HBs, calculated according to the three geometrical criteria of the H-bond formation.

According to the HF/MM and ONIOM-XS simulations, the total average values of the simultaneously formed HBs were found to be 4.0 and 3.7, respectively. As can be seen in Figure 4.3, although the most frequent number of HBs in both HF/MM and ONIOM-XS simulations is 4, the distributions of 3 and 5 HBs appear to be in considerable amounts. The results obtained by both HF/MM and ONIOM-XS simulations clearly suggests that any accurate water model used in the interpretation of the spectroscopic or other experimental data should include the 3- and 5-coordinated entities, which can simultaneously form along with the distorted tetrahedral structure. By means of the ONIOM-XS simulation, the distribution of 4 HBs is found to decrease significantly, while the formation of 2- and 3-fold HB

species becomes more visible, *i.e.*, compared to the HF/MM results. With regard to the ONIOM-XS's trajectory file, examples of different HB species formed in liquid water are given in Figure 4.4. The results obtained by the ONIOM-XS simulation are in good accord with the recent experimental observations, which reported relatively large numbers of 2- and 3-fold HB clusters in liquid water (Myneni *et al.*, 2002; Tokushima *et al.*, 2008; Wernet *et al.*, 2004). In Figure 4.1d, the characteristics of H-H RDFs are somewhat useful, providing the detailed picture with respect to the distributions of hydrogen atoms of nearest-neighbor waters surrounding the hydrogen atoms of the central H₂O.



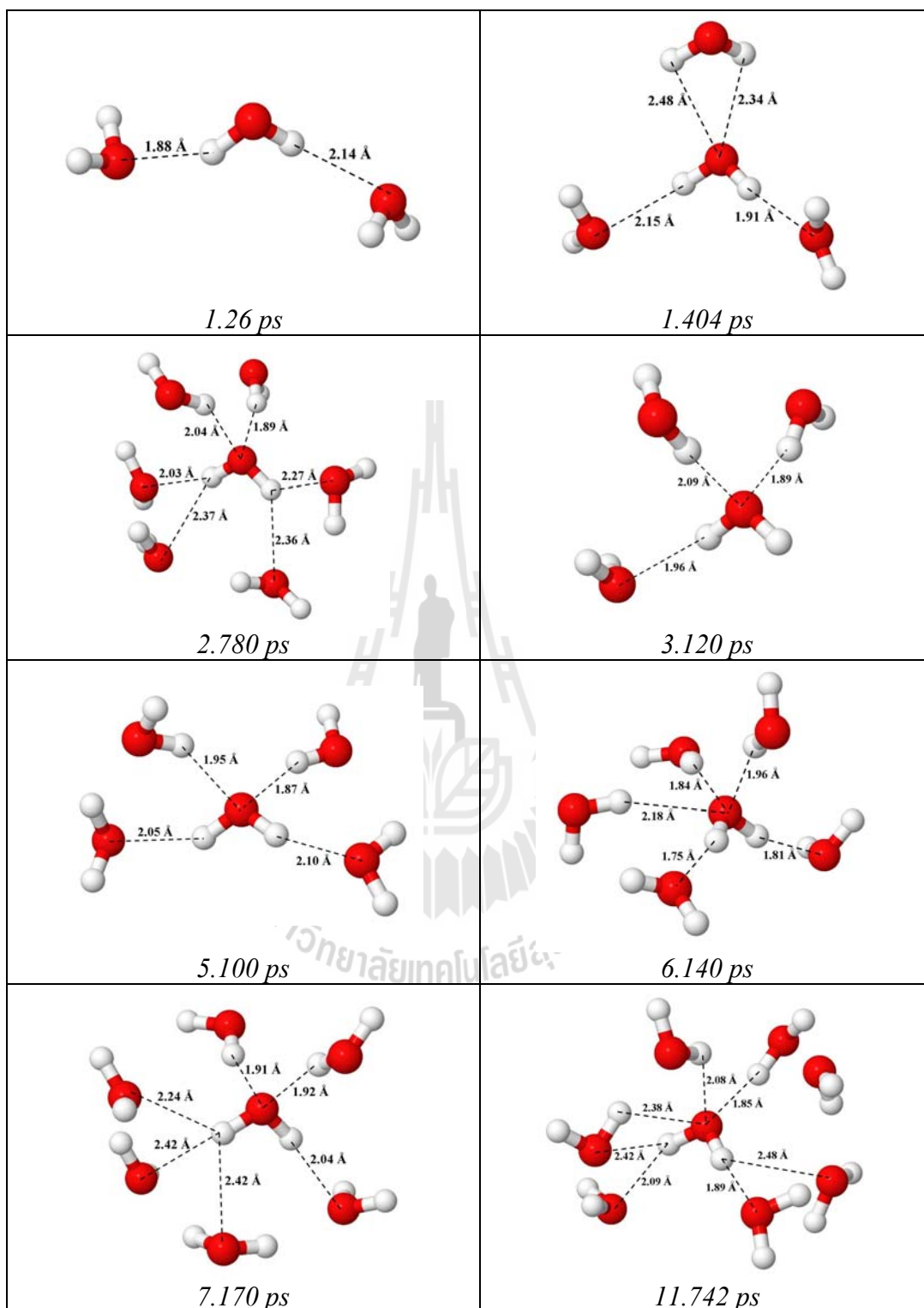


Figure 4.4 Some selected HB structures in liquid water at any simulation times, as observed in the ONIOM-XS simulation.

To further analyze the structural properties of liquid water, the probability distributions of the O---O---O angle, as well as of the O-H---O and O---H-O angles, are plotted in Figures 4.5 and 4.6, respectively. In both the HF/MM and ONIOM-XS simulations, the structure of the first coordination shell with respect to the tetrahedral arrangement is found to be a major distribution. However, this structure is rather far from a regular arrangement, by the pronounced broad peaks between 70-120°. Regarding the distributions of the graphs in Figure 4.5, the distortion from the ideally tetrahedral arrangement is more evidence in the case of the ONIOM-XS simulation. In spite of the distorted tetrahedral structure, however, both the HF/MM and ONIOM-XS simulations reveal that the HBs between water molecules are relatively strong (cf. Figure 4.6), by the pronounced peak between 150-160°. In this respect, it could be demonstrated that the tetrahedral arrangement is apparently favored for liquid water, but such an arrangement can distort frequently, *i.e.*, due to the observed large variation of the number of neighboring waters. As can be seen in Figure 4.5, the shoulder at 60° clearly indicates the arrangement of HB structures with more than four participating water molecules.

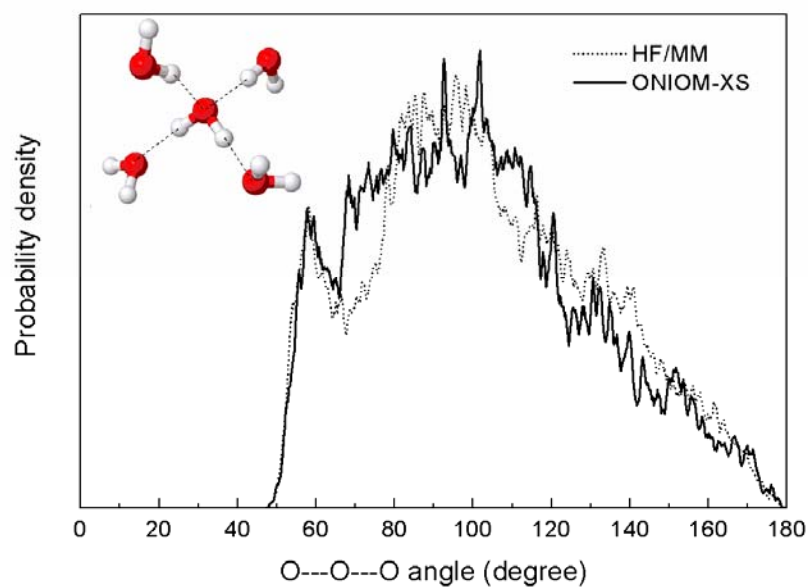


Figure 4.5 Distributions of O---O---O angles, calculated within first minimum of the HF/MM and ONIOM-XS MD's O-O RDFs (*i.e.*, within O---O distance of 3.2 Å).

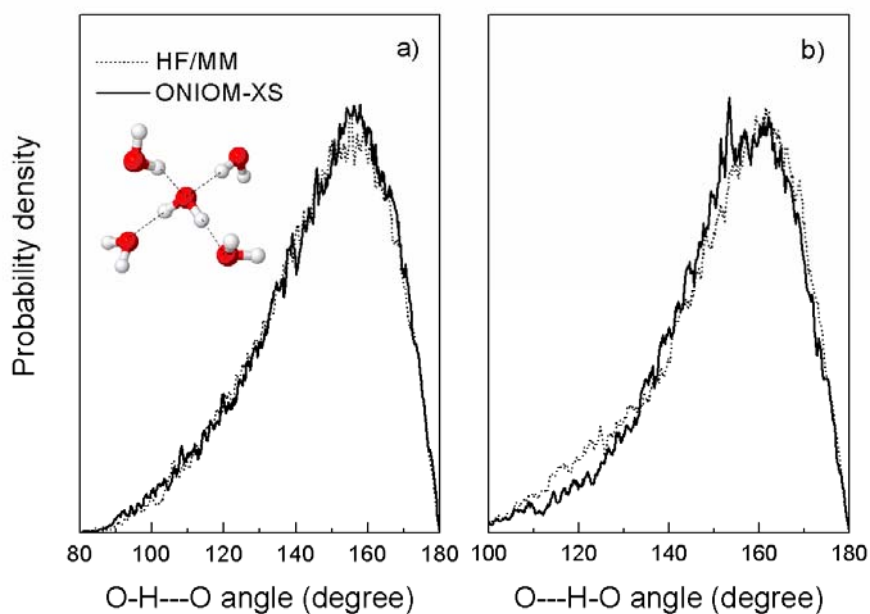


Figure 4.6 Distributions of a) O-H---O and b) O---H-O angles, calculated within first minimum of the HF/MM and ONIOM-XS MD's H-O and O-H RDFs (*i.e.*, within H--O and O---H distances of 2.5 Å).

4.2 Dynamical properties

The dynamical properties of liquid water can be observed from time correlation functions. The time correlation function of the same properties is known as time autocorrelation function. The autocorrelation functions of the particle velocities (velocity autocorrelation functions, VACFs) and their spectra density are usually employed to describe the particle motions in the liquid. For water, since a flexible water model has been used, the dynamical properties of waters can be described in terms of hindered translational motions, librational (rotational) motions and vibrational motions, respectively. The scheme for a distorted water molecule has been proposed by Bopp (Bopp, 1986), which can be represented in Figure 4.7.

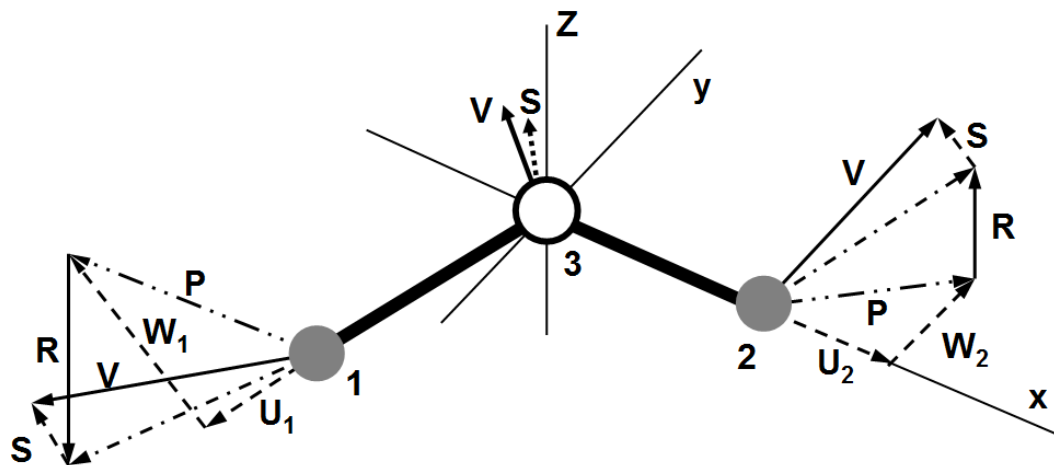


Figure 4.7 Scheme of a distorted water molecule. V: instantaneous velocity; S: velocity of the center-of-mass; R: velocity component perpendicular to the molecular plane; P: velocity component in the molecular plane; U, W: projection of P on the normalized instantaneous O-H vector and on a unit vector perpendicular to it in the molecular plane.

Then, the following six quantities can be defined using capital letters to denote the projections of the hydrogen velocities onto the corresponding unit vectors,

$$\begin{aligned}
 R_{\xi} &= W_1 - W_2 \\
 R_{\eta} &= V_1 + V_2 \\
 R_{\zeta} &= V_1 - V_2 \\
 Q_1 &= U_1 + U_2 \\
 Q_2 &= W_1 + W_2 \\
 Q_3 &= U_1 - U_2
 \end{aligned} \tag{4.1}$$

Where R_{ξ} , R_{η} , and R_{ζ} represent rotation around approximated x, y and z axis, respectively, while Q_1 , Q_2 , and Q_3 correspond to the symmetric stretching, bending and asymmetric stretching motions of water molecule, respectively.

4.2.1 Hindered translational motions

For water, the hindered translations are studied by the center-of-mass VACFs of the water molecules. These functions can be evaluated from

$$C_{VV}(t) = \frac{1}{N_{\tau} N_{H_2O}} \frac{\sum_j^{N_{\tau}} \sum_{i=1}^{N_{H_2O}} [S_i(t_j) S_i(t_j + t)]}{\sum_j^{N_{\tau}} \sum_{i=1}^{N_{H_2O}} [S_i(t_j) S_i(t_j)]}, \tag{4.2}$$

where S_j is the velocity of center-of-mass of water. The VACFs and their Fourier transformations for water molecules in the first shell, as obtained by the conventional HF/MM and ONIOM-XS simulations, are shown in Figures 4.8 and 4.9, respectively. As can be seen in Figure 4.8, the VACFs obtained from both conventional HF/MM and ONIOM-XS simulations are quite similar. Regarding the VACFs in Figure 4.8, the Fourier transformation of VACFs exhibits two pronounced peaks, with a first

maximum at about 50 cm^{-1} (for both HF/MM and ONIOM-XS simulations) and a second maximum at around 230 (HF/MM) and 250 (ONIOM-XS) cm^{-1} . These two pronounced peaks are identified as the hindered translational motions of the center-of-mass parallel and perpendicular to their dipole vectors, respectively. In this respect, the ONIOM-XS simulation supplies information that the translation of water molecules in the direction perpendicular to their dipole moments is less favorable, *i.e.*, such phenomenon is more apparent than the HF/MM simulation data.

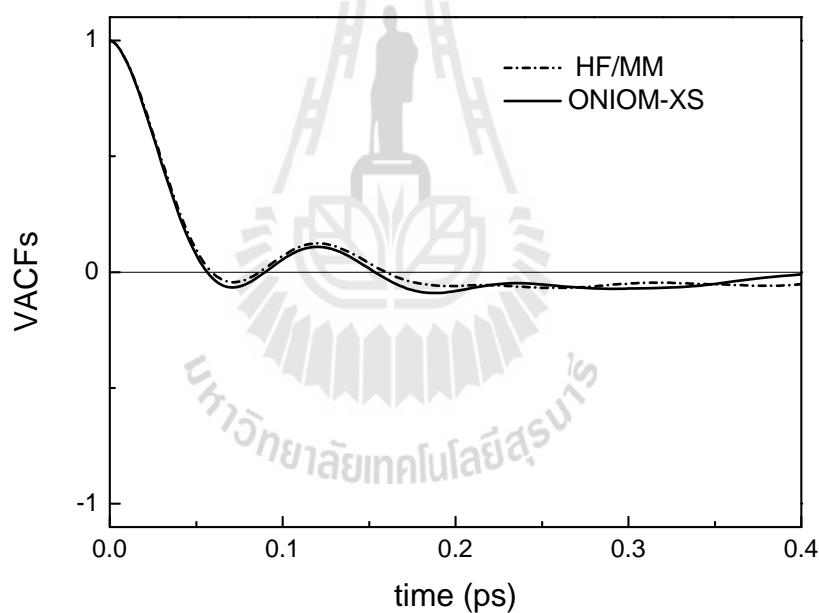


Figure 4.8 Velocity autocorrelation functions of the center-of-mass of first-shell water system.

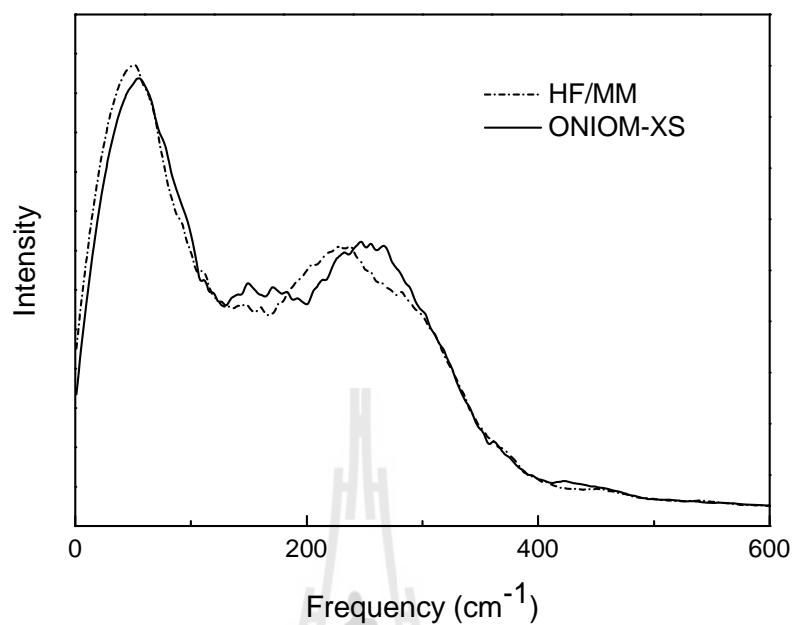


Figure 4.9 Fourier transforms of the translational motions of first-shell waters, calculated from the center-of-mass VACFs of waters.

4.2.2 Librational motions

For the librational (rotational) motions of waters, the three axis, η , ξ and ζ , were chosen to be identical to the three principal moments of inertia employed in the description of the rotations of the rigid molecule, as shown in Figure 4.10.

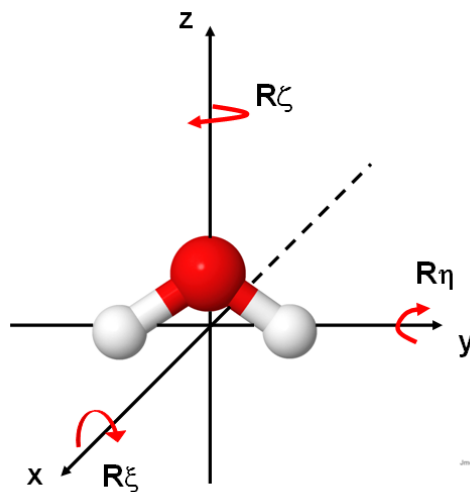


Figure 4.10 Definition of three librational motions; $R_\xi = W_1 - W_2$ (rotation around approximated x axis), $R_\eta = R_1 + R_2$ (rotation around approximated y axis) and $R_\zeta = R_1 - R_2$ (rotation around approximated z axis).

According to Figure 4.10, the three normalized autocorrelation functions can be calculated from

$$\begin{aligned}
 C_{R_\xi R_\xi}(t) &= \frac{1}{N_\tau N_{H_2O}} \frac{\sum_j^{N_\tau} \sum_{i=1}^{N_{H_2O}} [R_\xi^i(t_j) R_\xi^i(t_j + t)]}{\sum_j^{N_\tau} \sum_{i=1}^{N_{H_2O}} [R_\xi^i(t_j) R_\xi^i(t_j)]} \\
 C_{R_\eta R_\eta}(t) &= \frac{1}{N_\tau N_{H_2O}} \frac{\sum_j^{N_\tau} \sum_{i=1}^{N_{H_2O}} [R_\eta^i(t_j) R_\eta^i(t_j + t)]}{\sum_j^{N_\tau} \sum_{i=1}^{N_{H_2O}} [R_\eta^i(t_j) R_\eta^i(t_j)]} \\
 C_{R_\zeta R_\zeta}(t) &= \frac{1}{N_\tau N_{H_2O}} \frac{\sum_j^{N_\tau} \sum_{i=1}^{N_{H_2O}} [R_\zeta^i(t_j) R_\zeta^i(t_j + t)]}{\sum_j^{N_\tau} \sum_{i=1}^{N_{H_2O}} [R_\zeta^i(t_j) R_\zeta^i(t_j)]}
 \end{aligned} \tag{4.3}$$

The VACFs and their corresponding Fourier transformations for the librational motions of first shell waters are shown in Figures 4.11 and 4.12, respectively. The results obtained by both conventional HF/MM and ONIOM-XS simulations are not much difference. Both HF/MM and ONIOM-XS results suggest that the VACFs around the approximated ζ axis decay faster than the motions around the approximated ξ and η and hence give the Fourier transformations peaks at the highest frequencies.



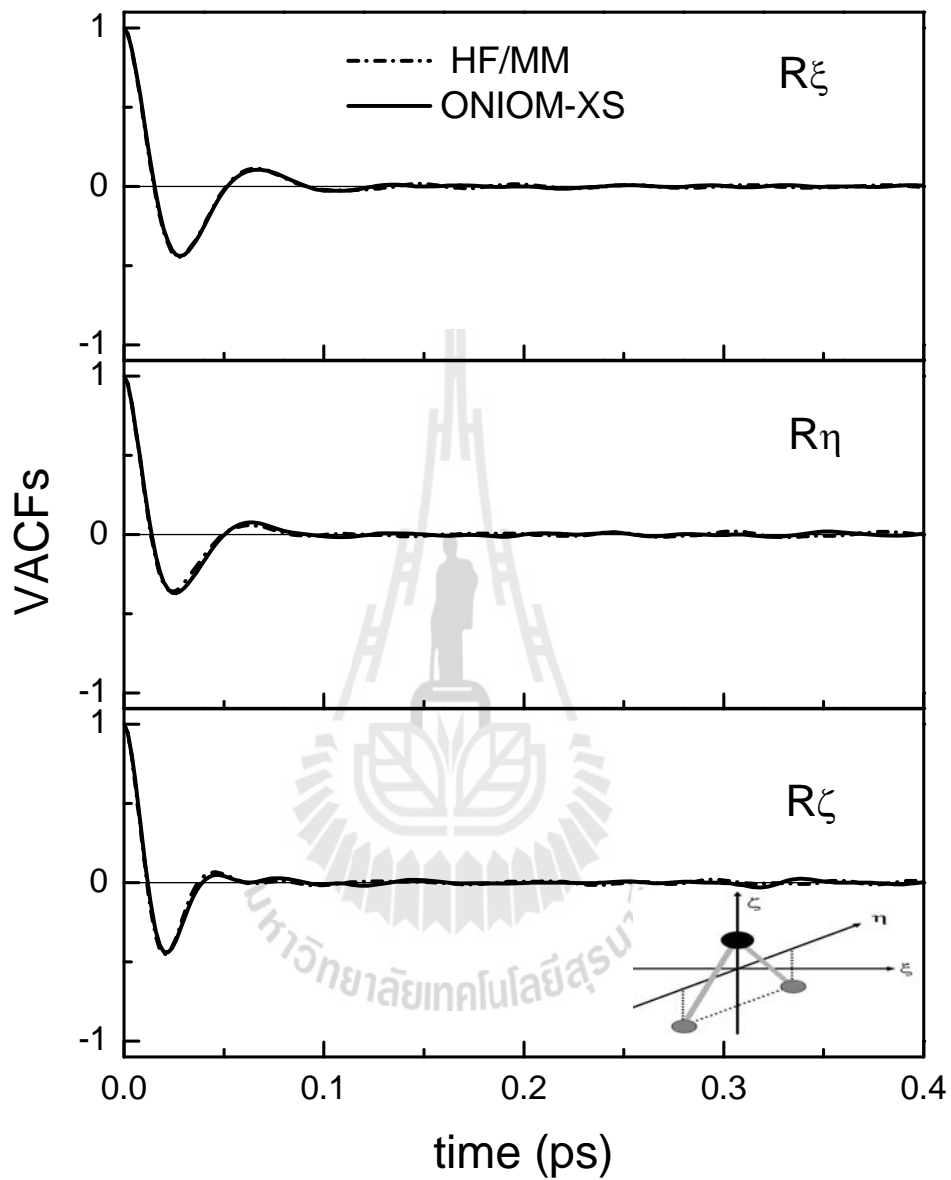


Figure 4.11 Velocity autocorrelation functions of water approximated instantaneous librational motions around the ξ , η and ζ axes, for the water system.

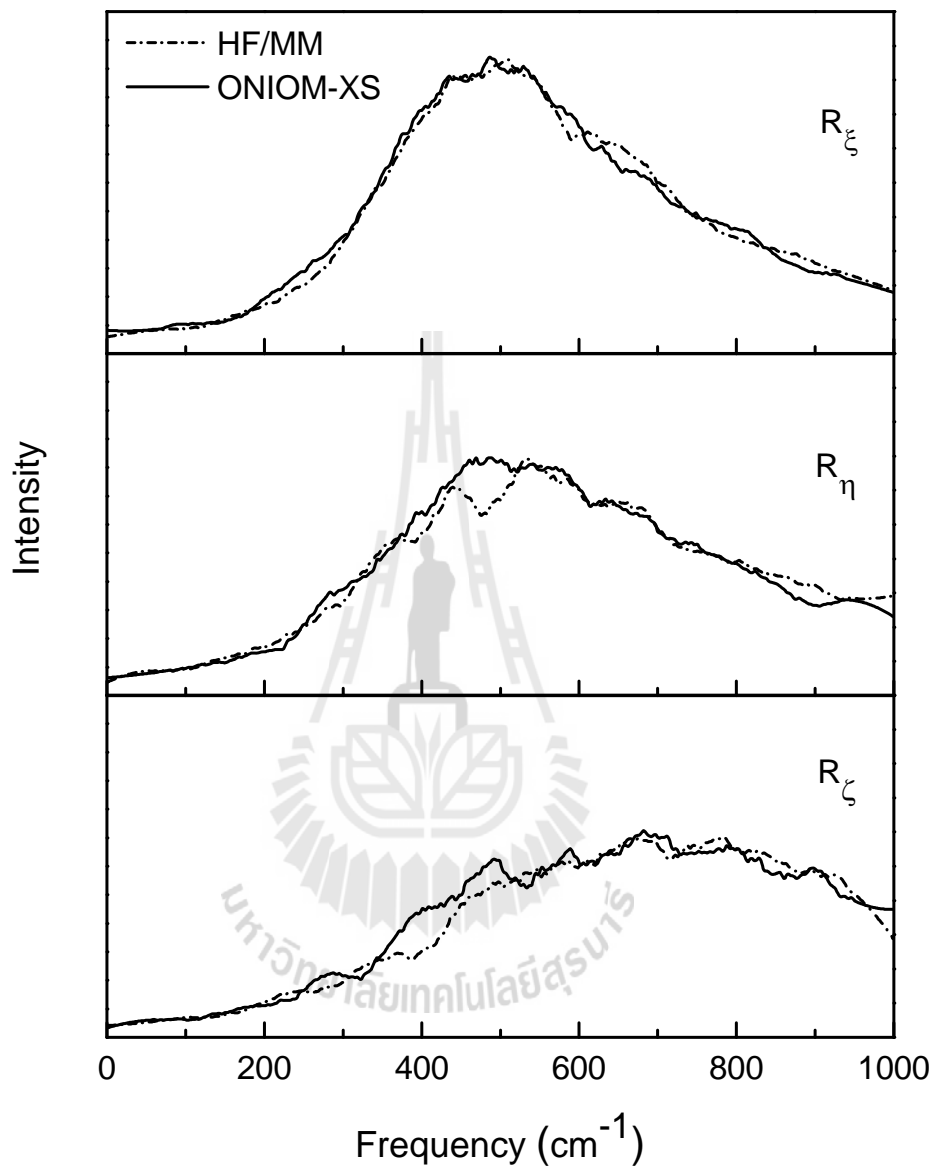


Figure 4.12 Fourier transforms of the librational motions of water molecules, calculated from the VACFs of water approximated around the ξ , η and ζ axes.

4.2.3 Vibrational motions

The vibrational motions are described by the three quantities: Q_1 , Q_2 , and Q_3 , which correspond to the symmetric stretching, bending and asymmetric stretching motions of water molecule, respectively. The three normalized autocorrelation functions can be written as

$$C_{Q_k Q_k}(t) = \frac{1}{N_\tau N_{H_2O}} \frac{\sum_j^{N_\tau} \sum_{i=1}^{N_{H_2O}} [Q_k^i(t_j) Q_k^i(t_j + t)]}{\sum_j^{N_\tau} \sum_{i=1}^{N_{H_2O}} [Q_k^i(t_j) Q_k^i(t_j)]}, \quad (4.4)$$

where $k = 1, 2, 3$.

The normalized VACFs and their Fourier transforms spectra of water in first shell, as obtained from the conventional HF/MM and ONIOM-XS simulations are shown in Figures 4.13 and 4.14, respectively. To compare with experimental data, all frequencies obtained by both HF/MM and ONIOM-XS simulations were multiplied by an appropriate scaling factor of 0.905 (Scott and Radom, 1996). The three intramolecular vibrational frequencies (Q_1 , Q_2 and Q_3) of liquid water, as obtained from various QM/MM MD simulations and experiments, are given in Table 4.2. With regard to the HF/MM and ONIOM-XS simulations, all the bending and stretching vibrational frequencies are not much different, showing the peaks with recognizable shoulders, especially for the symmetric and asymmetric vibrational modes. These observed spectra clearly supply information that several kinds of HBs, with varying strengths, can simultaneously be formed in liquid water. According to

the data in Table 4.2, large variations of the calculated frequencies are found among the various QM/MM simulations. In this respect, it should be noted that these frequencies are highly sensitive to the computational methods, rather than to the structural parameters. As compared to the results obtained at similar HF level of accuracy, our HF/MM and ONIOM-XS results show good agreement with the recent HF/MM studies (Xenides, Randolph, and Rode, 2005, 2006).



Table 4.2 Vibrational frequencies (Q_1 , Q_2 and Q_3) of liquid water, as obtained by various MD simulations and experiments (numbers in parenthesis correspond to the shoulders).

Method	Frequencies (cm ⁻¹)		
	Q_1	Q_2	Q_3
HF/MM MD [*]	3624 (3588,3662)	1670	3712 (3678,3730)
ONIOM-XS MD [*]	3606 (3650)	1660	3720 (3755)
HF/MM MD ^h	3770 (3620,3680)	1640	3775 (3615,3675)
MP2/MM MD ⁱ	3964 (3844)	1640	3964 (3847)
B3LYP/MM MD ⁱ	3580 (3460)	1622	3553 (3458)
Experiment ^j	3400 (3200)	-	-
Experiment ^k	3410 (3280)	-	-
Experiment ^l	3400	1643.5	-

^{*}Present work

^h(Xenides, Randolph, and Rode, 2006)

ⁱ(Xenides, Randolph, and Rode, 2005)

^j(Deàk, Rhea, Iwaki, and Dlott, 2000)

^k(Lock, Woutersen, and Bakker, 2001)

^l(Lock and Bakker, 2002)

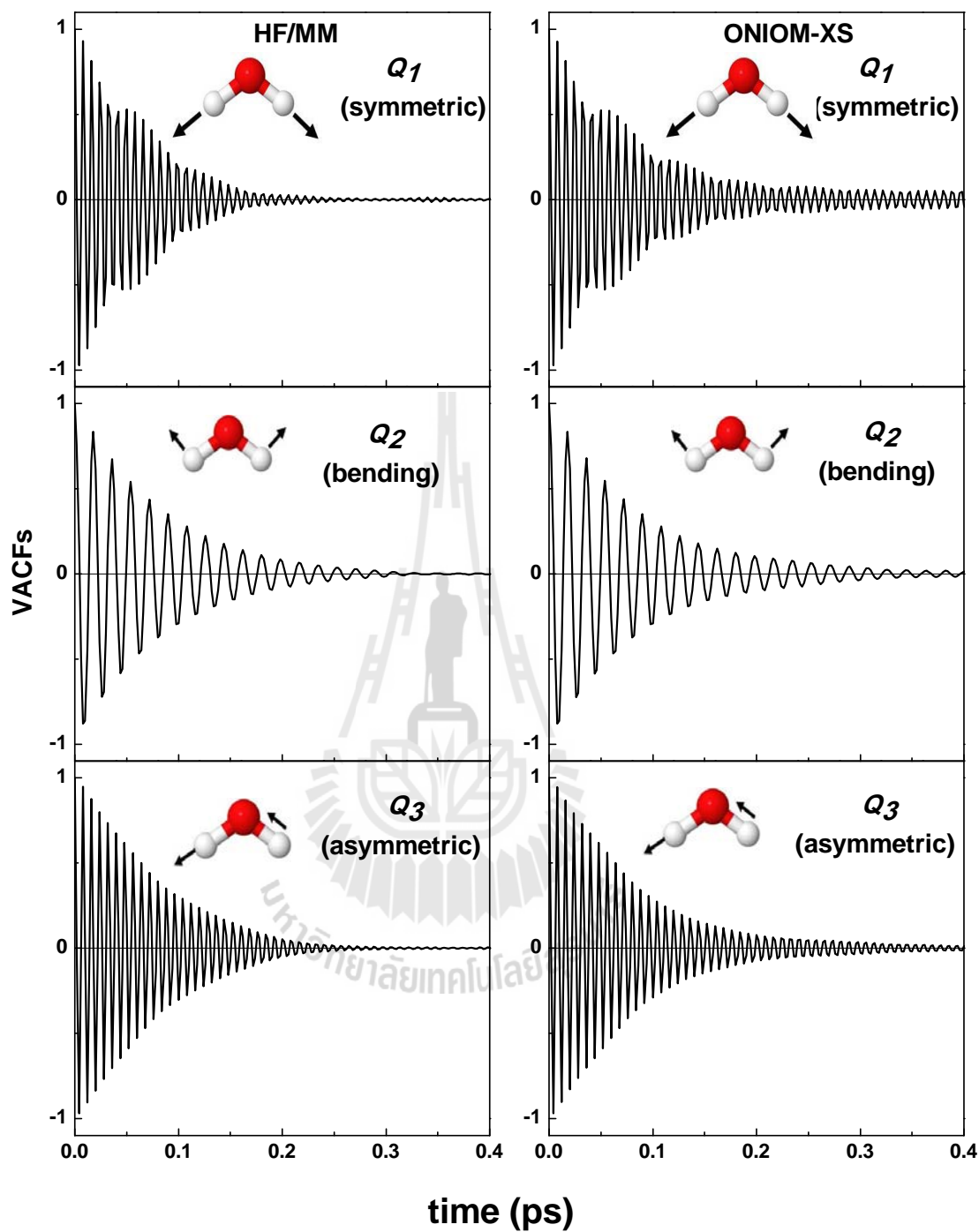


Figure 4.13 Velocity autocorrelation functions for the three intramolecular vibrations of water, as obtained from the conventional HF/MM and ONIOM-XS MD simulations.

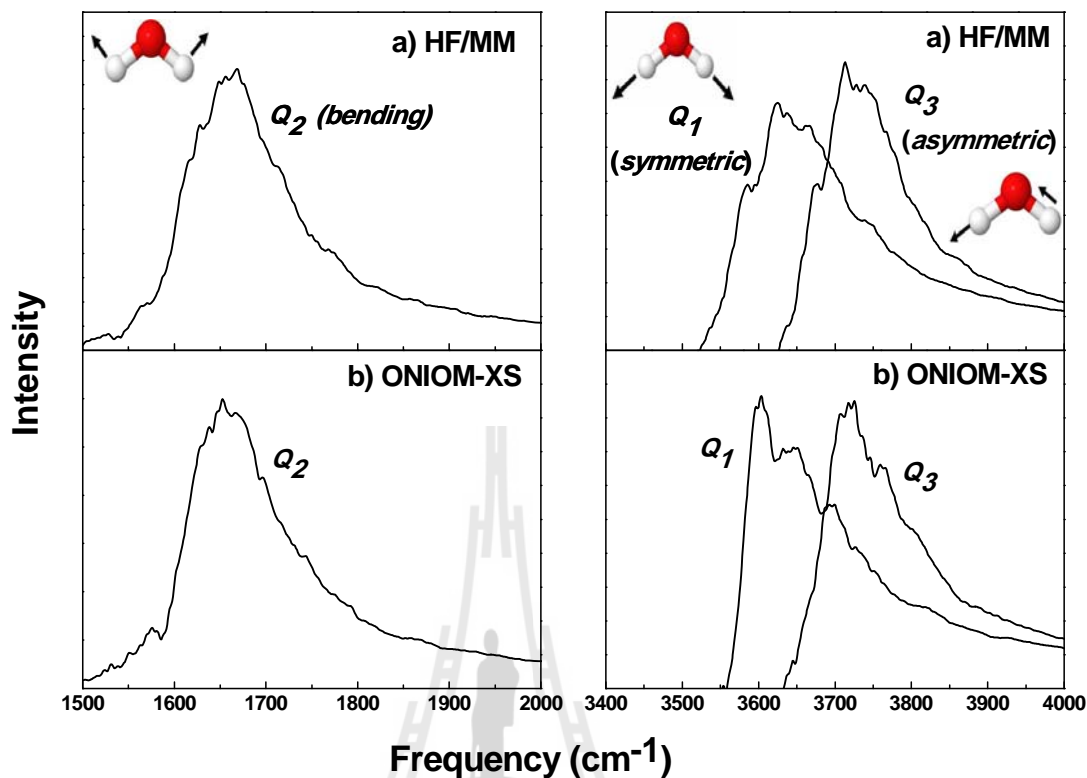


Figure 4.14 Fourier transforms of the hydrogen velocity autocorrelation functions (Q_1 , Q_2 and Q_3), as obtained from a) HF/MM and b) ONIOM-XS MD simulations.

4.2.4 Self-diffusion coefficient (D)

In addition to the detailed analyses on the hindered translational motions, the mobility of water molecules can be interpreted with respect to the self-diffusion coefficient (D). Based on the HF/MM and ONIOM-XS simulations, the D values are estimated to be 3.23×10^{-5} and $2.73 \times 10^{-5} \text{ cm}^2 \cdot \text{s}^{-1}$, respectively. As compared to the experimental value of $2.30 \times 10^{-5} \text{ cm}^2 \cdot \text{s}^{-1}$ (Kenneth, Douglass, and Hoch, 1972; Woolf, 1975), the D value resulting from the ONIOM-XS simulation is clearly in better agreement with the experimental observations. These data clearly

confirm once again the efficiency of the ONIOM-XS technique over the conventional QM/MM scheme in order to correctly describe the properties of liquid water.

4.2.5 Water exchange processes

In both the HF/MM and ONIOM-XS simulations, the nonzero first minimum of the O-O RDFs (Figure 4.1a) clearly suggests an easy exchange of water molecules between those in the first hydration shell of the central H₂O and in the outer region. Such a phenomenon corresponds to the observed large variation of the HB formations in liquid water. The exchange processes of water molecules at each of the hydrogen and oxygen atoms of the central H₂O can be visualized through the plots of the H---O and O---H distances against the simulation time, as depicted in Figures 4.15 and 4.16 for the HF/MM and ONIOM-XS simulations, respectively. According to the detailed analyses on the HF/MM and ONIOM-XS trajectories, it is observed that nearest-neighbor waters can be either “loosely” or “tightly” bound to the central H₂O, leading to several water exchange mechanisms, with either “short-lived” or “long-lived” exchange periods. In very recent discussion on the behavior of liquid water (Nilsson *et al.*, 2010; Nilsson and Pettersson, 2011), it has been demonstrated that water is inhomogeneous with a fluctuating HB network around two types of structures, strongly tetrahedral and strongly HB distorted. In this respect, most water molecules favor a closer packing than tetrahedral, with strongly distorted HBs. In Figures 4.15d and 4.16d, the variations of the number of all nearest-neighbor waters and those that form hydrogen bonding to the central H₂O, calculated within the O-O distance of 3.20 Å, are also plotted for comparison. These graphs correspond to the plots in Figures 4.2 and 4.3, showing that some of the nearest-neighbor waters are not

directly hydrogen bonded to the central H₂O. Thus, this leads to an increment of the distribution of 2- and 3-fold HB clusters in liquid water (Figure 4.3, as compared to Figure 4.2). In this regard, as can be seen in Figure 4.3, the presence of 2- and 3-fold HB species becomes more visible in the ONIOM-XS simulation, *i.e.*, compared to the HF/MM results.



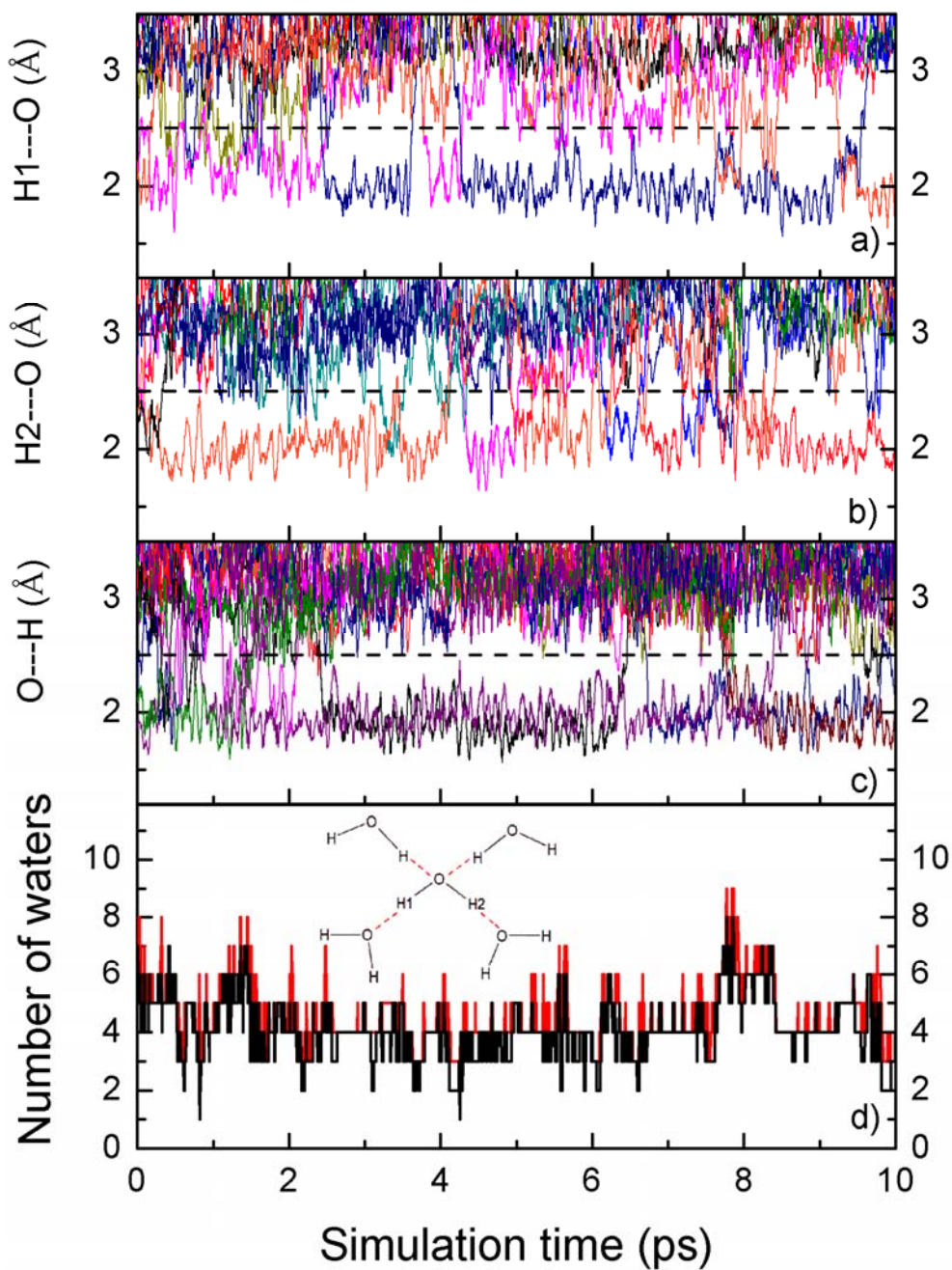


Figure 4.15 Time dependence of a) H1---O, b) H2---O and c) O---H distances, together with d) number of water molecules surrounding the central H₂O (*i.e.*, calculated within O-O distance of 3.20 Å; Red line: number of all nearest-neighbor water molecules, Black line: number of only water molecules forming HBs), as obtained by the HF/MM MD simulation.

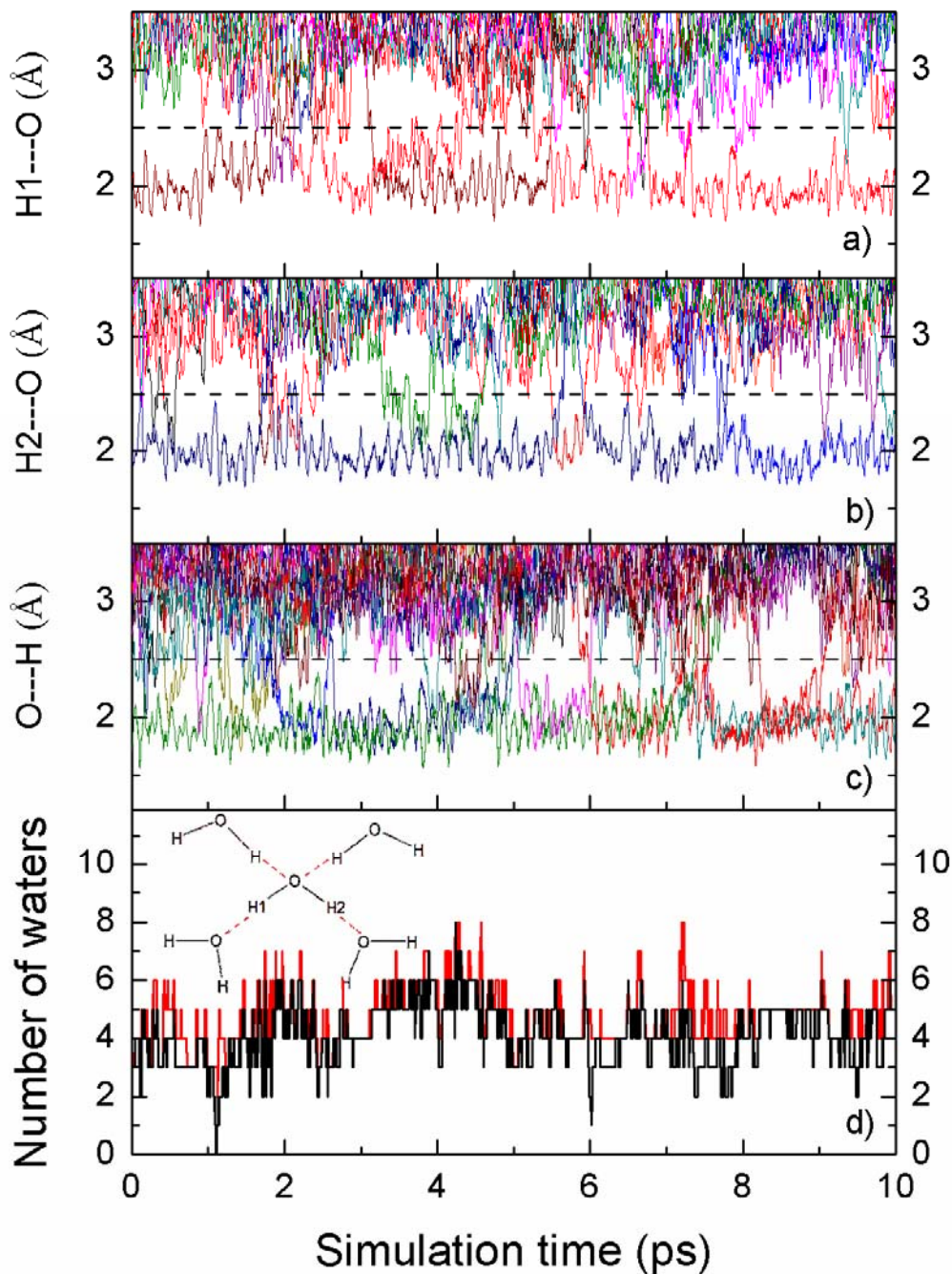


Figure 4.16 Time dependence of a) H1---O, b) H2---O and c) O---H distances, together with d) number of water molecules surrounding the central H₂O (*i.e.*, calculated within O-O distance of 3.20 Å; Red line: number of all nearest-neighbor water molecules, Black line: number of only water molecules forming HBs), as obtained by the ONIOM-XS MD simulation.

The lifetime of HBs and the water exchange processes at the central H₂O was calculated via means residence times (MRT) of the neighboring waters. In this work, the MRT data were calculated using the direct method, as the product of the average number of nearest-neighbor waters located within the first minimum of the O-O RDFs with the duration of the simulation, divided by the number of exchange events. In this work, since the first peak of the O-O RDFs is not clearly separated from the outer region (Figure 4.1a), the O-O distance of 3.2 Å was selected, assuming it to be a rough estimate of the first minimum of the O-O RDFs. With respect to time parameters t^* (*i.e.*, the minimum duration of a ligand's displacement from its original coordination shell to be accounted) of 0.0 and 0.5 ps, the calculated MRT values are summarized in Table 4.3. In general, the MRT data obtained using $t^* = 0.0$ ps are used for an estimation of HB lifetimes, whereas the data obtained with $t^* = 0.5$ ps are considered as a good estimate for sustainable water exchange processes (Hofer, Tran, Schwenk, and Rode, 2004). With respect to $t^* = 0.0$ ps, both HF/MM and ONIOM-XS simulations reveal rather similar MRT data. However, for $t^* = 0.5$ ps, the ONIOM-XS simulation reveals a relatively smaller MRT value, *i.e.*, compared to the HF/MM data. Consequently, this leads to a different average number of attempts needed to achieve one sustainable exchange event ($N_{ex}^{0.0} / N_{ex}^{0.5}$), being 11.2 and 9.3 for the HF/MM and ONIOM-XS simulations, respectively. Comparing the HF/MM and ONIOM-XS results, these observed differences clearly confirm the important treatment of the ONIOM-XS method in obtaining a more accurate description of this particular system. In this respect, the ONIOM-XS method could be expected to be highly effective for the situation where the number of particles that are crossing the QM/MM boundary is large, such as in the case of liquid water. According to the simulation data

in Table 4.3, the observed different MRT data can be ascribed to the performance of different QM methods, as well as to the use of different QM sizes and basis sets. For example, with regard to $t^* = 0.0$ ps, the HF/MM, B3LYP/MM and MP2/MM simulations using a similar QM radius (*i.e.*, 3.2 Å for HF/MM and B3LYP/MM, and 3.4 Å for MP2/MM) predicted the MRT values of 0.21, 1.07 and 0.28, respectively (Xenides, Randolph, and Rode, 2005). In addition, the HF/MM simulations using QM radii of 3.2 and 5.6 Å yielded different MRT values of 0.21 and 0.33, respectively (Xenides, Randolph, and Rode, 2005, 2006). Therefore, it should be demonstrated that, in conjunction with the performance of the more accurate ONIOM-XS technique, the QM size and basis set must also be taken into account as the crucial factors in obtaining the correct description of the HBs in liquid water.

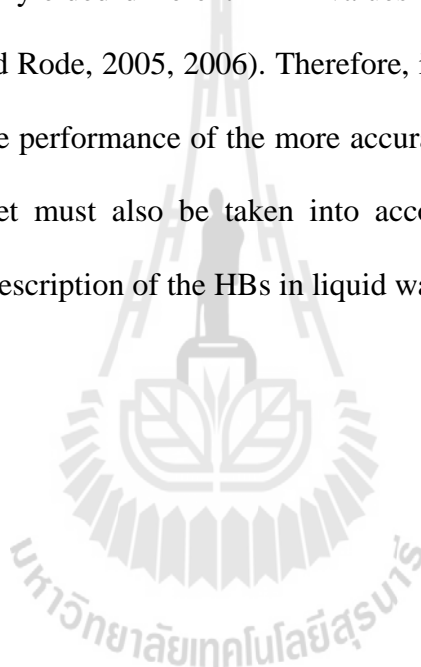


Table 4.3 Mean residence times ($\tau_{H_2O}^{t^*}$) of water molecules, calculated within first minimum of the HF/MM and ONIOM-XS's O-O RDFs.

Method	CN	t_{sim} (ps)	$t^* = 0.0$ ps		$t^* = 0.5$ ps	
			$N_{\text{ex}}^{0.0}$	$\tau_{H_2O}^{0.0}$	$N_{\text{ex}}^{0.5}$	$\tau_{H_2O}^{0.5}$
HF/MM MD [*]	4.9	40.0	944	0.21	84	2.33
ONIOM-XS MD [*]	4.7	30.0	607	0.23	65	2.17
HF/MM MD ^m	4.6	12.0	292	0.20	31	1.80
HF/MM MD ⁿ	4.2	40.0	515	0.33	112	1.51
MP2/MM MD ^o	4.6	5.0	-	0.28	-	2.45
Experiment ^p			-	0.5	-	-

^{*}Present work

^m(Tongraar and Rode, 2004)

ⁿ(Xenides, Randolph, and Rode, 2006)

^o(Xenides, Randolph, and Rode, 2005)

^p(Lock, Woutersen, and Bakker, 2001)

4.3 References

Bopp, P. (1986). A study of the vibrational motions of water in an aqueous CaCl_2 solution. **Chemical Physics**. 106: 205-212.

- Deàk, J. C., Rhea, S. T., Iwaki, L. K., and Dlott, D. D. (2000). Vibrational energy relaxation and spectral diffusion in water and deuterated water. **The Journal of Physical Chemistry A**. 104: 4866-4875.
- Hofer, T. S., Tran, H. T., Schwenk, C. F., and Rode, B. M. (2004). Characterization of dynamics and reactivities of solvated ions by ab initio simulations. **Journal of Computational Chemistry**. 25: 211-217.
- Hura, G., Sorenson, J. M., Glaeser, R. M., and Head-Gordon, T. (2000). A high-quality X-ray scattering experiment on liquid water at ambient conditions. **The Journal of Chemical Physics**. 113: 9140-9148.
- Kenneth, T. G., Douglass, D. C., and Hoch, M. J. R. (1972). Self-Diffusion in Liquid Water to -31 °C. **The Journal of Chemical Physics**. 57: 5117-5119.
- Lock, A. J., and Bakker, H. J. (2002). Temperature dependence of vibrational relaxation in liquid H₂O. **The Journal of chemical physics**. 117: 1708-1713.
- Lock, A. J., Woutersen, S., and Bakker, H. J. (2001). Ultrafast energy equilibration in hydrogen-bonded liquids. **The Journal of Physical Chemistry A**. 105: 1238-1243.
- Myneni, S., Luo, Y., Naslund, L. Å., Cavalleri, M., Ojamae, L., Ogasawara, H., Pelmenchikov, A., Wernet, P., Vaterlein, P., Heske, C., Hussain, Z., Pettersson, L. G. M., and Nilsson, A. (2002). Spectroscopic probing of local hydrogen-bonding structures in liquid water. **Journal of Physics: Condensed Matter**. 14: L213.
- Nilsson, A., Nordlund, D., Waluyo, I., Huang, N., Ogasawara, H., Kaya, S., Bergmann, U., Näslund, L.-Å., Öström, H., Wernet, P., Andersson, K. J., Schiros, T., and Pettersson, L. G. M. (2010). X-ray absorption spectroscopy

and X-ray Raman scattering of water and ice: An experimental view. **Journal of Electron Spectroscopy and Related Phenomena**. 177: 99-129.

Nilsson, A., and Pettersson, L. G. M. (2011). Perspective on the structure of liquid water. **Chemical Physics**. 389: 1-34.

Okhulkov, A. V., Demianets, Y. N., and Gorbaty, Y. E. (1994). X-ray scattering in liquid water at pressures of up to 7.7 kbar: Test of a fluctuation model. **The Journal of Chemical Physics**. 100: 1578-1588.

Scott, A. P., and Radom, L. (1996). Harmonic vibrational frequencies: An evaluation of Hartree-Fock, Møller-Plesset, quadratic configuration interaction, density functional theory, and semiempirical scale factors. **The Journal of Physical Chemistry**. 100: 16502-16513.

Soper, A. K. (1994). Orientational correlation function for molecular liquids: The case of liquid water. **The Journal of Chemical Physics**. 101: 6888-6901.

Soper, A. K. (2000). The radial distribution functions of water and ice from 220 to 673 K and at pressures up to 400 MPa. **Chemical Physics**. 258: 121-137.

Soper, A. K., Bruni, F., and Ricci, M. A. (1997). Site-site pair correlation functions of water from 25 to 400 °C: Revised analysis of new and old diffraction data. **The Journal of Chemical Physics**. 106: 247-254.

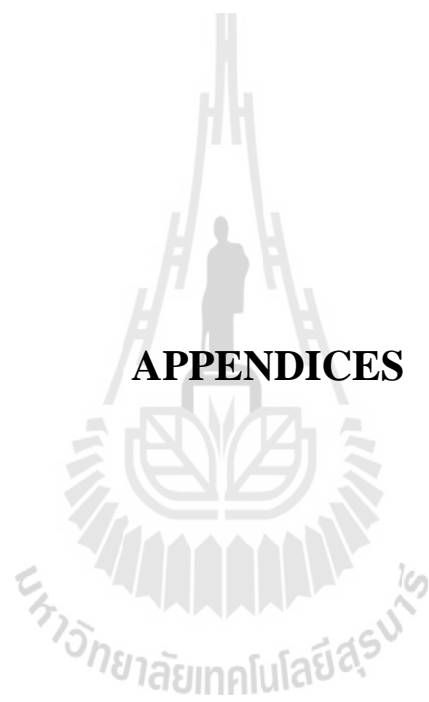
Tokushima, T., Harada, Y., Takahashi, O., Senba, Y., Ohashi, H., Pettersson, L. G. M., Nilsson, A., and Shin, S. (2008). High resolution X-ray emission spectroscopy of liquid water: The observation of two structural motifs. **Chemical Physics Letters**. 460: 387-400.

- Tongraar, A., and Rode, B. M. (2004). Dynamical properties of water molecules in the hydration shells of Na^+ and K^+ : *Ab initio* QM/MM molecular dynamics simulations. **Chemical Physics Letters**. 385: 378-383.
- Wernet, P., Nordlund, D., Bergmann, U., Cavalleri, M., Odellius, M., Ogasawara, H., Naslund, L. A., Hirsch, T. K., Ojamae, L., Glatzel, P., Pettersson, L. G. M., and Nilsson, A. (2004). The structure of the first coordination shell in liquid water. **Science**. 304: 995-999.
- Woolf, L. A. (1975). Tracer diffusion of tritiated water (THO) in ordinary water (H_2O) under pressure. **Journal of the Chemical Society, Faraday Transactions 1: Physical Chemistry in Condensed Phases**. 71: 784-796.
- Xenides, D., Randolph, B. R., and Rode, B. M. (2005). Structure and ultrafast dynamics of liquid water: A quantum mechanics/molecular mechanics molecular dynamics simulations study. **The Journal of Chemical Physics**. 122: 174506-174510.
- Xenides, D., Randolph, B. R., and Rode, B. M. (2006). Hydrogen bonding in liquid water: An *ab initio* QM/MM MD simulation study. **Journal of Molecular Liquids**. 123: 61-67.

CHAPTER V

CONCLUSION

In this work, conventional HF/MM and ONIOM-XS MD simulations have been performed to investigate the structural and dynamical properties of HBs in liquid water. Based on both HF/MM and ONIOM-XS simulations, it is observed that the HB network in liquid water is highly flexible, in which each water molecule can form various HBs, ranging from 2 to 6, with the prevalent value of 4. In addition, the detailed analyses on the HF/MM and ONIOM-XS's trajectories clearly show that nearest-neighbor waters can be either "loosely" or "tightly" bound to the central water molecule, leading to several water exchange mechanisms, with either "short-live" or "long-live" exchange periods. By means of the ONIOM-XS simulation, as compared to the HF/MM results, it is observed that the structural arrangement of liquid water with respect to 4 HBs decreases significantly and that the distributions of 2- and 3-fold HB species becomes more visible. The results obtained by the ONIOM-XS simulation correspond well to the recent experimental observations, which reported considerable amounts of 2- and 3-fold HB clusters in liquid water. In this context, the observed differences between the HF/MM and ONIOM-XS simulations clearly indicate some deficiencies of the conventional QM/MM scheme, and thus, confirm the need for more accurate simulation techniques, like the ONIOM-XS, in describing the properties of such HBs system.



APPENDICES

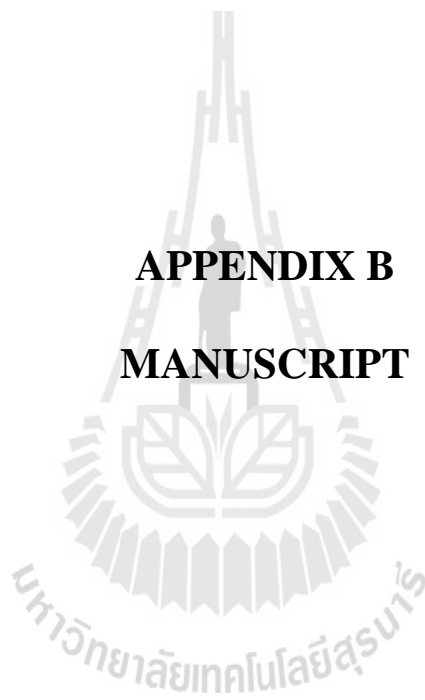
APPENDIX A

LIST OF PRESENTATIONS

1. Sukhontip Thaomola and Anan Tongraar. (September 9-11, 2010). Quantum-mechanics-based simulations of liquid water. **Commission on Higher Education Congress III: University Staff Development Consortium CHE-USDC Congress III**, Royal Cliff Beach Resort, Chonburi, Thailand.



APPENDIX B
MANUSCRIPT



Insights into the structure and dynamics of liquid water: A comparative study of conventional QM/MM and ONIOM-XS

MD simulations

Sukhontip Thaomola,¹ Anan Tongraar^{1*} and Teerakiat Kerdcharoen²

¹ School of Chemistry, Institute of Science, Suranaree University of Technology,

Nakhon Ratchasima 30000, Thailand

² Department of Physics and NANOTEC Center of Excellence, Faculty of Science,

Mahidol University, Bangkok 10400, Thailand

Abstract

Structural and dynamical properties of liquid water have been investigated through molecular dynamics (MD) simulations based on conventional QM/MM scheme and ONIOM-XS method. The region of highest interest, *i.e.*, a sphere which contains a central water molecule and its nearest-neighbor waters, was treated at the Hartree-Fock (HF) level of theory using DZP basis set, while the rest of the system was described by the flexible BJH-CF2 model. With regard to both the HF/MM and ONIOM-XS simulations, the arrangement of hydrogen bonds (HBs) in liquid water is found to be rather flexible, in which the nearest-neighbors are either “loosely” or “tightly” bound to the central water molecule. Consequently, this leads to numerous water exchange mechanisms, with either “short-live” or “long-live” exchange periods, as well as to large fluctuations in the number of HBs, ranging from 2 to 6, with the prevalent value of 4. By means of the ONIOM-XS simulation, it is observed that the structural arrangement of liquid water with respect to 4 HBs decreases significantly and that the distributions of 2- and 3-fold HB species become more visible, *i.e.*, compared to the HF/MM results. Overall, the observed differences between the HF/MM and ONIOM-XS simulations clearly indicate the important treatment of the ONIOM-XS method in describing the properties of liquid water.

* Corresponding author. E-mail: anan_tongraar@yahoo.com. fax: 0066-44-224017.

1. Introduction

Water, the most abundant substance on earth, is known to play a central role in many areas of science, including physics, chemistry, biology and geology. In solid phase, each water molecule simply conducts four hydrogen bonds (HBs) with its neighboring waters, forming a well-defined tetrahedral structure. In liquid phase, however, the pattern and dynamics of the HB network are not fully understood. Experimental techniques, such as X-ray and neutron scattering, have been carried out to investigate the structural properties of liquid water, most of which reported the tetrahedral arrangement with coordination number near 4.¹⁻⁶ This observed phenomenon is consistent with X-ray absorption spectroscopy (XAS) results by Smith and his group,⁷ which reported the XAS spectral of tetrahedral-like liquid water. However, this standard picture of liquid water has been challenged by Wernet and co-workers,⁸ who used XAS and X-ray emission spectroscopy (XES) techniques to investigate the structure of liquid water. Of particular interest, they proposed that most water molecules in liquid phase form only two strong HBs with one donor and one acceptor, consisting mainly of chain or ring structures and with very few tetrahedral structures. These observations are in good accord with an early XAS study by Myneni and coworkers,⁹ which reported a coordination number as small as 2.4. In addition, the results from a high resolution XES experiment also showed that the liquid water consists of both a distorted structure and tetrahedral structure with the ratio of 2:1.¹⁰ With regard to these observed discrepancies, some researchers claimed that the results may be affected by the specifics of each experimental technique.¹¹ In this respect, since the time scales for HBs forming and breaking in liquid water are extremely fast, *i.e.*, in femto to picoseconds, it should be realized that a complete set of structural and dynamical data of liquid water cannot be obtained from a single experimental technique.¹² For example, X-ray and neutron scattering are only useful in providing structural details, while the infrared (IR) and Raman techniques are instead preferred in order to obtain dynamics information.

In conjunction with experiments, numerous theoretical efforts have been devoted to elucidate such details. During the past decades, several water models have been proposed and employed in molecular dynamics (MD) and Monte Carlo (MC) simulations, most of which fairly provided good correlations with experimental data.¹³⁻¹⁹ However, some serious problems still exist such as the effects of many-body contributions, since most of the



potential functions employed in the simulations are usually derived from water dimer, *i.e.*, based on pairwise-additive approximations.^{20,21} Nowadays, as a consequence of the rapid development in computer capacity and performance, these problems can be solved by performing quantum-mechanics-based simulations. In terms of the Car-Parinello (CP) MD technique,²² the whole system is treated quantum mechanically using density functional theory (DFT), with common exchange correlation functions BLYP and PBE. Recently, several CP-MD simulations have been carried out for systems of 32 and 64 water molecules,²³⁻²⁷ With regard to the CP-MD results, however, it has been demonstrated that some properties of the liquid water are quite sensitive to the density functionals chosen, *i.e.*, several of them were found to overestimate the water-water interactions.^{25,28} Consequently, some dynamics properties of water obtained from numerous CP-MD simulations, such as self-diffusion coefficients, showed significantly smaller value than that of experiments, implying that the liquid water simulated by the CP-MD technique under ambient condition is super-cooled or glassy.²⁶

Besides the CP-MD technique, an alternative approach is to apply a so-called combined quantum mechanics/molecular mechanics (QM/MM) technique,²⁹⁻³² which treats the active-site region, *i.e.* a small subsystem which contains most interesting particles, quantum mechanically, while the rest of the system is described by classical molecular mechanical potentials. Recently, a series of QM/MM MD simulations, namely HF/MM, B3LYP/MM and MP2/MM, have been performed for liquid water,^{33,34} showing that the use of the HF method with enlarged QM size can provide simulation results in good agreement with those obtained by the correlated MP2 calculations, while the B3LYP method predicted a too rigid water structure as well as too slow exchange rates. Regarding the HF/MM simulation with enlarged QM size,³⁴ the results clearly indicated an enormous flexibility of the HB network in liquid water, suggesting that each water molecule forms (on average) only 2.8 HBs. These HF/MM results are in good accord with the recent experimental observations, in which the number of 4-fold HBs in liquid water is found to be rather small in comparison to 2- and 3-fold HB species.⁸⁻¹⁰

With regard to the conventional QM/MM technique, however, only the exchanging particles are treated by a smoothing function when they are crossing the QM/MM boundary. In practice, this is not realistic since the immediate addition or deletion of a

particle in the QM region due to the interchange also affects the forces acting on the remaining QM particles. Furthermore, the conventional QM/MM framework cannot clearly define the energy expression during the exchange process. To solve those problems, a more sophisticated QM/MM MD technique based on ONIOM-XS method (which will be abbreviated throughout this work as "ONIOM-XS MD") has been proposed.^{35,36} This technique allows the forces on all QM particles to be smoothed during particle exchange, and thus, clearly defines the system's energy expression. In this work, MD simulations based on the conventional QM/MM scheme and ONIOM-XS method will be performed to study the local structure and dynamics of HBs in liquid water. Of particular interest, the results obtained by the ONIOM-XS simulation can be expected to provide more reliable data of liquid water, *i.e.*, compared to those obtained by the conventional QM/MM scheme, leading to further understanding the properties of this peculiar liquid in many areas of science.

2. Methods

2.1 Conventional QM/MM MD

By the conventional QM/MM MD technique,^{29-32,37,38} the system is divided into two parts, namely the QM and MM regions. The total interaction energy of the system is defined as:

$$E_{total} = \langle \Psi_{QM} | \hat{H} | \Psi_{QM} \rangle + E_{MM} + E_{QM-MM} , \quad (1)$$

where $\langle \Psi_{QM} | \hat{H} | \Psi_{QM} \rangle$ refers to the interactions within the QM region, and E_{MM} and E_{QM-MM} represent the interactions within the MM and between the QM and MM regions, respectively. The QM region, the most interesting part which contains a central H₂O and its nearest-neighbor waters, is treated quantum mechanically, while the rest of the system (*i.e.*, the E_{MM} and E_{QM-MM}) is described by classical MM potentials. By this scheme, the total force of the system is described by the following formula:

$$F_{tot} = F_{MM}^{tot} + (F_{QM}^{QM} - F_{MM}^{QM}) , \quad (2)$$

where F_{MM}^{ev} , F_{QM}^{OM} and F_{MM}^{OM} are the MM force of the total system, the QM force in the QM region and the MM force in the QM region, respectively. In this respect, the F_{MM}^{OM} term accounts for the coupling between the QM and MM regions.

During the QM/MM simulation, since the interchange of water molecules between the QM and MM regions can take place frequently, the forces acting on each particle in the system are switched according to which region the water molecule is entering or leaving and can be defined as:

$$F_i = S_m(r)F_{QM}^{OM} + (1 - S_m(r))F_{MM}^{OM}, \quad (3)$$

where F_{QM}^{OM} and F_{MM}^{OM} are the quantum mechanical and molecular mechanical forces, respectively. $S_m(r)$ is a smoothing function,⁴⁰

$$\begin{aligned} S_m(r) &= 1, & \text{for } r \leq r_0, \\ S_m(r) &= \frac{(r_1^2 - r^2)^2 (r_1^2 + 2r^2 - 3r_0^2)}{(r_1^2 - r_0^2)^3}, & \text{for } r_0 < r \leq r_1, \\ S_m(r) &= 0, & \text{for } r > r_1, \end{aligned} \quad (4)$$

where r_0 and r_1 are the distances characterizing the start and the end of the QM region, respectively, and applied within an interval of 0.2 Å (*i.e.*, between the distances of the central H₂O's oxygen and the oxygen atoms of the surrounding waters of 4.0 – 4.2 Å) to ensure a continuous change of forces at the transition between the QM and MM regions.

2.2 ONIOM-XS MD

Based on the ONIOM-XS method,^{35,36} the system is comprised of a “high-level” QM region, *i.e.*, a sphere which contains the central H₂O and its nearest-neighbor waters, and the remaining “low-level” MM bulk waters. A thin switching shell located between the QM and MM regions is employed to detect the exchanging particles and help in smoothing the energy and forces of the combined system. Given n_1 , l and n_2 as the number of particles in the QM region, the switching layer and the MM region, respectively, and $N (= n_1 + l + n_2)$ as the total number of particles, the potential energy of the system can be written in two

ways based on the ONIOM extrapolation scheme.⁴¹ If the switching layer is included into the high-level QM sphere, the energy expression is written as

$$E^{ONIOM}(n_1 + l; N) = E^{QM}(n_1 + l) - E^{MM}(n_1 + l) + E^{MM}(N). \quad (5)$$

If the switching layer is considered as part of the “low-level” MM region, the energy expression is

$$E^{ONIOM}(n_1; N) = E^{QM}(n_1) - E^{MM}(n_1) + E^{MM}(N). \quad (6)$$

According to Eqs. (5) and (6), E^{QM} and E^{MM} terms refer to the interactions obtained by the QM calculations and by the classical MM potentials, respectively. In this respect, the interactions between the QM and MM regions are also described by means of MM potentials, and thus, these contributions are already included into the $E^{MM}(N)$. In practice, when a particle moves into the switching layer (either from QM or MM region), both Eqs. (5) and (6) must be evaluated. Then, the potential energy of the entire system is taken as a hybrid between both energy terms (5) and (6),

$$E^{ONIOM-XS}(r_i) = (1 - \bar{s}(r_i)) E^{ONIOM}(n_1 + l; N) + \bar{s}(r_i) \cdot E^{ONIOM}(n_1; N), \quad (7)$$

where $\bar{s}(r_i)$ is an average over a set of switching functions for individual exchanging particles in the switching layer $s_i(x_i)$,

$$\bar{s}(r_i) = \frac{1}{l} \sum_{i=1}^l s_i(x_i), \quad (8)$$

In general, the switching function in Eq. (8) can have any form. Here, a polynomial expression is employed,

$$s_i(x_i) = 6 \left(x_i - \frac{1}{2} \right)^3 - 5 \left(x_i - \frac{1}{2} \right) + \frac{15}{18} \left(x_i - \frac{1}{2} \right) + \frac{1}{2}, \quad (9)$$

where $x_i = (r_i - r_0)/(r_1 - r_0)$, and r_0 and r_1 are the radius of the inner and outer surfaces of the switching shell, respectively, and r_i is the distance between the center of mass of the

exchanging particle and the center of the QM sphere. The above polynomial form and parameter sets were derived to have an S-shape that converges to 0 and 1 at r_0 and r_1 , respectively.³⁵ This polynomial form is preferred over the ST2 switching function⁴² usually employed in the conventional QM/MM simulation because its first and second derivatives are both continuous. It should be noted that both energies and forces are smoothed in the ONIOM-XS scheme, whereas only forces were handled in the conventional QM/MM scheme. The gradient of the energy can be written as

$$\begin{aligned} \nabla_{\mathbf{r}} E^{\text{ONIOM-XS}}(r_1) &= (1 - \bar{s}(r_1)) \cdot \nabla_{\mathbf{r}} E^{\text{ONIOM}}(n_1 + t; N) + \bar{s}(r_1) \cdot \nabla_{\mathbf{r}} E^{\text{ONIOM}}(n_1; N) + \\ &\quad \frac{1}{(r_1 - r_0)} \nabla \bar{s}(r_1) \cdot (E^{\text{ONIOM}}(n_1; N) - E^{\text{ONIOM}}(n_1 + t; N)) \end{aligned} \quad (10)$$

2.3 Simulation details

For both the conventional QM/MM and ONIOM-XS MD simulations, all interactions within the QM region were evaluated by performing *ab initio* calculations at the Hartree-Fock (HF) level of accuracy using the DZP basis set.⁴³ In this work, although the effects of electron correlation could be expected to play some roles on the properties of the liquid water, the use of the HF method with a sufficiently large QM size and basis set is considered as suitable conditions compromising between the quality of the simulation results and the requirement of CPU time.³³ All QM calculations were carried out using the Gaussian03 program.⁴⁴ For the QM treated-region, a QM radius of 4.2 Å and a switching width of 0.2 Å were chosen, corresponding to the ONIOM-XS parameters r_0 and r_1 of 4.0 and 4.2 Å, respectively. In comparison to the conventional QM/MM scheme,³⁷⁻³⁹ these parameters correspond to the start and the end of the QM radius, *i.e.*, a defined QM/MM boundary where the smoothing applies. This QM size is assumed to be large enough to include all molecules that are forming HBs with the central H₂O. In this respect, it could be expected that the remaining interactions beyond the QM region are well accounted for by the MM potentials. As can be seen in the next section (cf. Figure 1a), the smooth shape of the O-O radial distribution functions (RDFs) between 4.0 and 4.2 Å clearly confirms that transition of water molecules between the QM and MM regions occurs smoothly. For the

interactions within the MM and between the QM and MM regions, a flexible BIH-CF2 water model, which describes intermolecular⁴⁵ and intramolecular⁴⁶ interactions, was employed. This flexible water model is employed in order to ensure a smooth transition when water molecules move from the QM region with its full flexibility to the MM region.

Both the HF/MM and ONIOM-XS MD simulations were performed in a canonical ensemble at 298 K with periodic boundary conditions. The system's temperature was kept constant using the Berendsen algorithm.⁴⁷ A periodic box, with a box length of 18.15 Å, contains 200 water molecules, corresponding to the experimental density of pure water. The reaction-field method⁴⁸ was employed for the treatment of long-range interactions. The Newtonian equations of motions were treated by a general predictor-corrector algorithm. The time step size was set to 0.2 fs, which allows for the explicit movement of the hydrogen atoms of water molecules. In this work, the HF/MM and ONIOM-XS simulations were performed independently with the system's re-equilibration for 30,000 time steps, followed by another 200,000 (HF/MM) and 150,000 (ONIOM-XS) time steps to collect configurations every 10th step.

3. Results and discussion

3.1 Structural data

The details with respect to the structure of liquid water can be visualized from a series of O-O, O-H, H-O and H-H RDFs, together with their corresponding integration numbers, as depicted in Figure 1. In this context, the first atom denotes the atoms of the central H₂O and the second one refers to the atoms of the surrounding waters, respectively. To provide useful comparison, structural parameters of liquid water, as obtained by various QM/MM MD simulations and experiments, are summarized in Table 1. Regarding the O-O RDFs (Figure 1a), both HF/MM and ONIOM-XS simulations reveal a rather well-defined first peak with maxima centered at 2.84 and 2.82 Å, respectively. These observed O-O distances are in good agreement with the corresponding values of 2.82 and 2.83 Å derived by X-ray scattering¹ and neutron diffraction⁴⁹ experiments, respectively. According to the experimental data in Table 1, the observed variations in the O-O distance could be ascribed to the use of different models and techniques in evaluating the collected (pre-fitted) data,

are not much different, the respective second O-H and H-O peaks obtained by the ONIOM-XS simulation are significantly less pronounced than those of the HF/MM results. For the ONIOM-XS simulation, integrations up to first minimum of the O-H and H-O RDFs yield average values of 2.07 and 1.09, compared to the corresponding values of 2.00 and 1.10 obtained by the HF/MM simulation. The HF/MM and ONIOM-XS results correspond to the expectation that on average over time about four HBs (actual values are 4.20 and 4.25 for the HF/MM and ONIOM-XS simulations, respectively) are involved in the HB formation at the central reference water (*i.e.*, two HBs are formed by the central water's oxygen acting as acceptor, and another two HBs are formed by the central water's hydrogen atoms acting as donors). However, since the O-H and H-O RDFs do not show distinct minima after the first shell, the numbers of HBs which are simultaneously formed during the simulations can be evaluated through the detailed analysis of the MD trajectories. In this work, the evaluations were carried out according to the following geometrical criteria of the HB formation: (1) the O-O distance is set with respect to the defined first O-O RDFs, *i.e.*, $2.5 \leq R_{O-O} \leq 3.2$ Å, (2) the HB distance is limited by the first minimum of O-H and H-O RDFs, *i.e.*, $1.5 \leq R_{O-H} \leq 2.5$ Å and (3) the HB angle, $\angle_{O-H-O} \geq 100^\circ$. Based on these criteria, the distributions of the number of HBs forming around the central H₂O, as obtained by the HF/MM and ONIOM-XS simulations, are plotted in Figure 3. According to the HF/MM and ONIOM-XS simulations, the total average values of the simultaneously formed HBs were found to be 4.0 and 3.7, respectively. As can be seen in Figure 3, although the most frequent number of HBs in both HF/MM and ONIOM-XS simulations is 4, the distributions of 3 and 5 HBs appear to be in considerable amounts. The results obtained by both HF/MM and ONIOM-XS simulations clearly suggests that any accurate water model used in the interpretation of the spectroscopic or other experimental data should include the 3- and 5-coordinated entities, which can simultaneously form along with the distorted tetrahedral structure. By means of the ONIOM-XS simulation, the distribution of 4 HBs is found to decrease significantly, while the formation of 2- and 3-fold HB species becomes more visible, *i.e.*, compared to the HF/MM results. With regard to the ONIOM-XS's trajectory file, examples of different HB species formed in liquid water are given in Figure 4. The results obtained by the ONIOM-XS simulation are in good accord with the recent experimental observations, which reported relatively large numbers

which are both crucial factors affecting the results.² Comparing the HF/MM and ONIOM-XS results, however, a significant difference is found in the O-O RDFs beyond 3.20 Å, in which the feature of the ONIOM-XS's O-O RDF reveals a relatively more distinct first coordination shell. Of particular interest, this observed difference can be expected to reflect (more or less) in different structural and dynamical details of liquid water derived from these two simulation techniques.

In Figure 1a, the O-O RDFs from both the HF/MM and ONIOM-XS simulations do not show distinct minima after the first peak, suggesting that a number of water molecules can be located between the inner and outer coordination shell and that these water molecules are rather labile, *i.e.*, they can rapidly exchange between the two regions. Integrations of the first O-O peaks up to about 3.20 Å yield average values of 4.9 and 4.7 water molecules, respectively. In fact, these observed numbers should be considered as a rough estimate of the average coordination numbers, since the first O-O peaks are not clearly separated from the outer region. Figure 2 shows the probability distributions of the coordination numbers, calculated within the O-O distance of 3.20 Å. According to both the HF/MM and ONIOM-XS simulations, the coordination numbers of 4 and 5 are dominating the first coordination shell. However, it is observed that, besides the most frequent 4- and 5-coordinated species, other entities, such as 3-, 6- and 7-fold coordinated ones, are also found in considerable amounts. The HF/MM and ONIOM-XS results are consistent with the recent QM/MM studies,^{33,34} which reported that each water molecule can form various coordination numbers, ranging from 3 to 6, with the prevalent value of 4. With respect to the O-O RDFs in Figure 1a, the second O-O peaks are absent in both HF/MM and ONIOM-XS simulations, indicating that interactions of the central H₂O with its surrounding water molecules lying beyond the first coordination shell are weak (*i.e.*, less ordering). The diminution of the second O-O RDF has been reported experimentally as the system's temperature or pressure increases.¹

The characteristics of intermolecular HBs in liquid water can be analyzed through the O-H and H-O RDFs. According to Figures 1b and c, the first O-H and H-O peaks reflect the HBs between the central H₂O and its neighboring water molecules, *i.e.*, acting as acceptor and donor, respectively. Comparing between the HF/MM and ONIOM-XS simulations, further differences are recognizable, *i.e.*, while the first O-H and H-O RDFs



of 2- and 3-fold HB clusters in liquid water.⁸⁻¹⁰ In Figure 1d, the characteristics of H-H RDFs are somewhat useful, providing the detailed picture with respect to the distributions of hydrogen atoms of nearest-neighbor waters surrounding the hydrogen atoms of the central H₂O.

To further analyze the structural properties of liquid water, the probability distributions of the O---O angle, as well as of the O-H---O and O---H-O angles, are plotted in Figures 5 and 6, respectively. In both the HF/MM and ONIOM-XS simulations, the structure of the first coordination shell with respect to the tetrahedral arrangement is found to be a major distribution. However, this structure is rather far from a regular arrangement, by the pronounced broad peaks between 70-120°. Regarding the distributions of the graphs in Figure 5, the distortion from the ideally tetrahedral arrangement is more evidence in the case of the ONIOM-XS simulation. In spite of the distorted tetrahedral structure, however, both the HF/MM and ONIOM-XS simulations reveal that the HBs between water molecules are relatively strong (cf. Figure 6), by the pronounced peak between 150-160°. In this respect, it could be demonstrated that the tetrahedral arrangement is apparently favored for liquid water, but such an arrangement can distort frequently, *i.e.*, due to the observed large variation of the number of neighboring waters. As can be seen in Figure 5, the shoulder at 60° clearly indicates the arrangement of HB structures with more than four participating water molecules.

3.2 Dynamical data

The dynamical properties of liquid water can be gained by computing the velocity autocorrelation functions (VACFs) and their Fourier transformations. In this work, the normal-coordinate analysis developed by Bopp^{51,52} was used for obtaining three quantities Q_2 , Q_1 and Q_3 , which are defined for describing bending vibration, symmetric and asymmetric stretching vibrations of water molecules, respectively. To compare with experimental data, all frequencies obtained by both HF/MM and ONIOM-XS simulations were multiplied by an appropriate scaling factor of 0.905,⁵³ as depicted in Figure 7. The intramolecular vibrational frequencies (Q_1 , Q_2 and Q_3) of liquid water, as obtained from various QM/MMMD simulations and experiments, are given in Table 2. With regard to the HF/MM and ONIOM-XS simulations, all the bending and stretching vibrational

frequencies are not much different, showing the peaks with recognizable shoulders, especially for the symmetric and asymmetric vibrational modes. These observed spectra clearly supply information that several kinds of HBs, with varying strengths, can simultaneously be formed in liquid water. According to the data in Table 2, large variations of the calculated frequencies are found among the various QM/MM simulations. It should be noted that these frequencies are highly sensitive to the computational methods, rather than to the structural parameters. In this regard, the results obtained from our HF/MM and ONIOM-XS simulations show good agreement with the recent HF/MM studies.^{33,34}

Self-diffusion coefficients (D) for the central H₂O and its nearest-neighbors were calculated from their center-of-mass VACFs using the Green-Kubo relation,⁵⁷

$$D = \frac{1}{3} \lim_{t \rightarrow \infty} \int_0^t C_v(t) dt. \quad (11)$$

Based on the HF/MM and ONIOM-XS simulations, the D values are estimated to be 3.23×10^{-5} and $2.73 \times 10^{-5} \text{ cm}^2 \cdot \text{s}^{-1}$, respectively. As compared to the experimental value of $2.30 \times 10^{-5} \text{ cm}^2 \cdot \text{s}^{-1}$,^{58,59} the D value resulting from the ONIOM-XS simulation is clearly in better agreement with the experimental observations.

In both the HF/MM and ONIOM-XS simulations, the nonzero first minimum of the O-O RDFs (cf. Figure 1a) clearly suggests an easy exchange of water molecules between those in the first hydration shell of the central H₂O and in the outer region. Such a phenomenon corresponds to the observed large variation of the HB formations in liquid water. The exchange processes of water molecules at each of the hydrogen and oxygen atoms of the central H₂O can be visualized through the plots of the H---O and O---H distances against the simulation time, as depicted in Figures 8 and 9 for the HF/MM and ONIOM-XS simulations, respectively. According to the detailed analyses on the HF/MM and ONIOM-XS trajectories, it is observed that nearest-neighbor waters can be either “loosely” or “tightly” bound to the central H₂O, leading to several water exchange mechanisms, with either “short-lived” or “long-lived” exchange periods. In very recent discussion on the behavior of liquid water,^{60,61} it has been demonstrated that water is inhomogeneous with a fluctuating HB network around two types of structures, strongly

tetrahedral and strongly HB distorted. In this respect, most water molecules favor a closer packing than tetrahedral, with strongly distorted HBs. In Figures 8d and 9d, the variations of the number of all nearest-neighbor waters and those that form hydrogen bonding to the central H_2O , calculated within the O-O distance of 3.20 Å, are also plotted for comparison. These graphs correspond to the plots in Figures 2 and 3, showing that some of the nearest-neighbor waters are not directly hydrogen bonded to the central H_2O . Thus, this leads to an increment of the distribution of 2- and 3-fold HB clusters in liquid water (cf. Figure 3, as compared to Figure 2). In this regard, as can be seen in Figure 3, the presence of 2- and 3-fold HB species becomes more visible in the ONIOM-XS simulation, *i.e.*, compared to the HF/MM results.

The lifetime of HBs and the water exchange processes at the central H_2O was calculated via means residence times (MRT) of the neighboring waters. In this work, the MRT data were calculated using the direct method,⁶² as the product of the average number of nearest-neighbor waters located within the first minimum of the O-O RDFs with the duration of the simulation, divided by the number of exchange events. In this work, since the first peak of the O-O RDFs is not clearly separated from the outer region (cf. Figure 1a), the O-O distance of 3.2 Å was selected, assuming it to be a rough estimate of the first minimum of the O-O RDFs. With respect to time parameters \bar{t} (*i.e.*, the minimum duration of a ligand's displacement from its original coordination shell to be accounted) of 0.0 and 0.5 ps, the calculated MRT values are summarized in Table 3. In general, the MRT data obtained using $\bar{t} = 0.0$ ps are used for an estimation of HB lifetimes, whereas the data obtained with $\bar{t} = 0.5$ ps are considered as a good estimate for sustainable water exchange processes.⁶² With respect to $\bar{t} = 0.0$ ps, both HF/MM and ONIOM-XS simulations reveal rather similar MRT data. However, for $\bar{t} = 0.5$ ps, the ONIOM-XS simulation reveals a relatively smaller MRT value, *i.e.*, compared to the HF/MM data. Consequently, this leads to a different average number of attempts needed to achieve one sustainable exchange event ($N_{ex}^{0.0} / N_{ex}^{0.5}$), being 11.2 and 9.3 for the HF/MM and ONIOM-XS simulations, respectively. Comparing the HF/MM and ONIOM-XS results, these observed differences clearly confirm the important treatment of the ONIOM-XS method in obtaining a more accurate description of this particular system. In this respect, the ONIOM-XS method could be expected to be highly effective for the situation where the number of particles that are

crossing the QM/MM boundary is large, such as in the case of liquid water. According to the simulation data in Table 3, the observed different MRT data can be ascribed to the performance of different QM methods, as well as to the use of different QM sizes and basis sets. For example, with regard to $\bar{t} = 0.0$ ps, the HF/MM, B3LYP/MM and MP2/MM simulations using a similar QM radius (*i.e.*, 3.2 Å for HF/MM and B3LYP/MM, and 3.4 Å for MP2/MM) predicted the MRT values of 0.21, 1.07 and 0.28, respectively.³³ In addition, the HF/MM simulations using QM radii of 3.2 and 5.6 Å yielded different MRT values of 0.21 and 0.33, respectively.^{33,34} Therefore, it should be demonstrated that, in conjunction with the performance of the more accurate ONIOM-XS technique, the QM size and basis set must also be taken into account as the crucial factors in obtaining the correct description of the HBs in liquid water.

4. Conclusion

Conventional HF/MM and ONIOM-XS MD simulations have been performed to investigate the structural and dynamical properties of HBs in liquid water. Based on both HF/MM and ONIOM-XS simulations, it is observed that the HB network in liquid water is highly flexible, in which each water molecule can form various HBs, ranging from 2 to 6, with the prevalent value of 4. In addition, the detailed analyses on the HF/MM and ONIOM-XS's trajectories clearly show that nearest-neighbor waters can be either "loosely" or "tightly" bound to the central water molecule, leading to several water exchange mechanisms, with either "short-live" or "long-live" exchange periods. By means of the ONIOM-XS simulation, as compared to the HF/MM results, it is observed that the structural arrangement of liquid water with respect to 4 HBs decreases significantly and that the distributions of 2- and 3-fold HB species becomes more visible. The results obtained by the ONIOM-XS simulation correspond well to the recent experimental observations, which reported considerable amounts of 2- and 3-fold HB clusters in liquid water. In this context, the observed differences between the HF/MM and ONIOM-XS simulations clearly indicate some deficiencies of the conventional QM/MM scheme, and thus, confirm the need for more accurate simulation techniques, like the ONIOM-XS, in describing the properties of such HBs system.

5. Acknowledgment

This research was supported by grant fund under the program Strategic Scholarships for Frontier Research Network for the Ph.D. Program Thai Doctoral degree from the Commission on Higher Education, Thailand. A.T. also acknowledges support by Suranaree University of Technology (SUT) and the National Research University (NRU) Project of Thailand, Office of the Higher Education Commission. T.K. acknowledges financial support from Mahidol University.

References

- (1) Okhulkov, A. V.; Demianets, Y. N.; Gorbaty, Y. E. *J. Chem. Phys.* **1994**, *100*, 1578.
- (2) Soper, A. K. *Chem. Phys.* **2000**, *258*, 121.
- (3) Soper, A. K.; Bruni, F.; Ricci, M. A. *J. Chem. Phys.* **1997**, *106*, 247.
- (4) Hura, G.; Sorenson, J. M.; Glaeser, R. M.; Head-Gordon, T. *J. Chem. Phys.* **2000**, *113*, 9140.
- (5) Sorenson, J. M.; Hura, G.; Glaeser, R. M.; Head-Gordon, T. *J. Chem. Phys.* **2000**, *113*, 9149.
- (6) Head-Gordon, T.; Hura, G. *Chem. Rev.* **2002**, *102*, 2651.
- (7) Smith, J. D.; Cappa, C. D.; Wilson, K. R.; Messer, B. M.; Cohen, R. C.; Saykally, R. J. *Science* **2004**, *306*, 851.
- (8) Wernet, P.; Nordlund, D.; Bergmann, U.; Cavalleri, M.; Odellius, M.; Ogasawara, H.; Näslund, L. Å.; Hirsch, T. K.; Ojamäe, L.; Glatzel, P.; Pettersson, L. G. M.; Nilsson, A. *Science* **2004**, *304*, 995.
- (9) Myneni, S.; Luo, Y.; Näslund, L. Å.; Cavalleri, M.; Ojamae, L.; Ogasawara, H.; Pelmenchikov, A.; Wernet, P.; Vaterlein, P.; Hesse, C.; Hussain, Z.; Pettersson, L. G. M.; Nilsson, A. *J. Phys.: Condens. Matter* **2002**, *14*, L213.
- (10) Tokushima, T.; Harada, Y.; Takahashi, O.; Senba, Y.; Ohashi, H.; Pettersson, L. G. M.; Nilsson, A.; Shin, S. *Chem. Phys. Lett.* **2008**, *460*, 387.
- (11) Holt, J. *Microfluid. Nanofluid.* **2008**, *5*, 425.
- (12) Tokmakoff, A. *Science* **2007**, *317*, 54.
- (13) Reimers, J. R.; Watts, R. O.; Klein, M. L. *Chem. Phys.* **1982**, *64*, 95.
- (14) Jorgensen, W. L.; Chandrasekhar, J.; Madura, J. D.; Impey, R. W.; Klein, M. L. *J. Chem. Phys.* **1983**, *79*, 926.
- (15) Berendsen, H. J. C.; Grigera, J. R.; Straatsma, T. P. *J. Phys. Chem.* **1987**, *91*, 6269.
- (16) Caldwell, J.; Dang, L. X.; Kollman, P. A. *J. Am. Chem. Soc.* **1990**, *112*, 9144.
- (17) Mahoney, M. W.; Jorgensen, W. L. *J. Chem. Phys.* **2000**, *112*, 8910.
- (18) Stern, H. A.; Rittner, F.; Berne, B. J.; Friesner, R. A. *J. Chem. Phys.* **2001**, *115*, 2237.
- (19) Fanourgakis, G. S.; Xantheas, S. S. *J. Chem. Phys.* **2008**, *128*, 74506.
- (20) Dang, L. X.; Chang, T. *J. Chem. Phys.* **1997**, *106*, 8149.
- (21) Beran, G. J. O. *J. Chem. Phys.* **2009**, *130*, 164115.

- (22) Car, R.; Parrinello, M. *Phys. Rev. Lett.* **1985**, *55*, 2471.
- (23) Grossman, J. C.; Schwegler, E.; Draeger, E. W.; Gygi, F.; Galli, G. *J. Chem. Phys.* **2004**, *120*, 300.
- (24) Izvekov, S.; Voth, G. A. *J. Chem. Phys.* **2002**, *116*, 10372.
- (25) Lee, H.-S.; Tuckerman, M. E. *J. Chem. Phys.* **2006**, *125*, 154507.
- (26) Lee, H.-S.; Tuckerman, M. E. *J. Chem. Phys.* **2007**, *126*, 164501.
- (27) Kuhne, T. D.; Krack, M.; Parrinello, M. *J. Chem. Theory Comput.* **2009**, *5*, 235.
- (28) Yoo, S.; Zeng, X. C.; Xanthous, S. S. *J. Chem. Phys.* **2009**, *130*, 221102.
- (29) Warshel, A.; Levitt, M. *J. Mol. Biol.* **1976**, *103*, 227.
- (30) Singh, U.C.; Kollman, P.A. *J. Comput. Chem.* **1986**, *7*, 718.
- (31) Field, M.J.; Bash, P.A.; Karplus, M. *J. Comput. Chem.* **1990**, *11*, 700.
- (32) Gao, J. *Rev. Comput. Chem.* **1996**, *7*, 119.
- (33) Xenides, D.; Randoif, B. R.; Rode, B. M. *J. Chem. Phys.* **2005**, *122*, 174506.
- (34) Xenides, D.; Randoif, B. R.; Rode, B. M. *J. Mol. Liq.* **2006**, *123*, 61.
- (35) Kerdraroen, T.; Morokuma, K. *Chem. Phys. Lett.* **2002**, *355*, 257.
- (36) Kerdraroen, T.; Morokuma, K. *J. Chem. Phys.* **2003**, *118*, 8856.
- (37) Kerdraroen, T.; Liedl, K.R.; Rode, B.M. *Chem. Phys.* **1996**, *211*, 313.
- (38) Tongraar, A.; Liedl, K.R.; Rode, B.M. *J. Phys. Chem. A* **1998**, *102*, 10340.
- (39) Rode, B.M.; Schwenk, C.F.; Tongraar, A. *J. Mol. Liq.* **2004**, *110*, 105.
- (40) Brooks, B.R.; Brucoleri, R.E.; Olafson, B.D.; States, D.J.; Swaminathan, S.; Karplus, M. *J. Comput. Chem.* **1983**, *4*, 187.
- (41) Svensson, M.; Humbel, S.; Froese, R. D. J.; Mutsabara, T.; Sieber, S.; Morokuma, K. *J. Phys. Chem.* **1996**, *100*, 19357.
- (42) Tasaki, K.; McDonald, S.; Brady, J. W. *J. Comput. Chem.* **1993**, *14*, 278.
- (43) Dunning, T. H. Jr.; Hay, P. J. in *Methods of Electronic Structure Theory*, III, Plenum, New York, 1977.
- (44) Frisch, M. J.; Trucks, G. W.; Schlegel, H. B.; Scuseria, G. E.; Robb, M. A.; Cheeseman, J. R.; Montgomery, J. A.; Vreven, T.; Kudin, K. N.; Burant, J. C.; et al. *GAUSSIAN 03*, Revision D.1; Gaussian, Inc.: Wallingford, CT, 2005.
- (45) Stillinger, F.H.; Rahman, A. *J. Chem. Phys.* **1976**, *68*, 666.
- (46) Bopp, P.; Janesó, G.; Heinzinger, K. *Chem. Phys. Lett.* **1983**, *98*, 129.

- (47) Berendsen, H.J.C.; Postma, J.P.M.; van Gunsteren, W.F.; DiNola, A.; Haak, J.R. *J. Phys. Chem.* **1984**, *81*, 3684.
- (48) Adams, D.J.; Adams, E.H.; Hills, G.J. *Mol. Phys.* **1979**, *38*, 387.
- (49) Soper, A. K. *J. Chem. Phys.* **1994**, *101*, 6888.
- (50) Jedlovsky, P.; Brodholt, J. P.; Bruni, F.; Ricci, M. A.; Soper, A. K.; Vallauri, R. *J. Chem. Phys.* **1998**, *108*, 8528.
- (51) Bopp, P. *Chem. Phys.* **1986**, *106*, 205
- (52) Spohr, E.; Pálfiakás, G.; Heinzinger, K.; Bopp, P.; Probst, M. M. *J. Phys. Chem.* **1988**, *92*, 6754.
- (53) Scott, A. P.; Radow, L. *J. Phys. Chem.* **1996**, *100*, 16502.
- (54) Deak, J. C.; Rhea, S. T.; Iwaki, L. K.; Dlott, D. D. *J. Phys. Chem. A* **2000**, *104*, 4866.
- (55) Lock, A. J.; Woutersen, S.; Bakker, H. J. *J. Phys. Chem. A* **2001**, *105*, 1238.
- (56) Lock, A. J.; Bakker, H. J. *J. Chem. Phys.* **2002**, *117*, 1708.
- (57) McQuarrie, D. A. *Statistical Mechanics*, Harper & Row, New York, 1976.
- (58) Gillen, K. T.; Douglass, D. C.; Hoch, M. J. *J. Chem. Phys.* **1972**, *57*, 5117.
- (59) Woolf, L. A. *J. Chem. Soc. Faraday Trans.* **1975**, *71*, 784.
- (60) Nilsson, A.; Nordlund, D.; Wahyo, I.; Huang, N.; Ogasawara, H.; Kaya, S.; Bergmann, U.; Nisilund, L.-Å.; Öström, H.; Wernet, P.; Andersson, K. J.; Schiros, T.; Pettersson, L. G. M. *J. El. Spec. Rel. Phen.* **2010**, *177*, 99.
- (61) Nilsson, A.; Pettersson, L. G. M. *Chem. Phys.* **2011**, *389*, 1.
- (62) Hofer, T.S.; Tran, H.T.; Schwenk, C.F.; Rode, B.M. *J. Comput. Chem.* **2004**, *25*, 211.
- (63) Tongraar, A.; Rode, B. M. *Chem. Phys. Lett.* **2004**, *385*, 378.
- (64) Lock, A. J.; Woutersen, S.; Bakker, H. J. *Femtochemistry and Femtobiology*, World Scientific, Singapore, 2001.

TABLE CAPTIONS

Table 1 Structural parameters of liquid water, as obtained by various QM/MM MD simulations and experiments.

Table 2 Vibrational frequencies (Q_1 , Q_2 and Q_3) of liquid water, as obtained by various MD simulations and experiments (numbers in parenthesis correspond to the shoulders).

Table 3 Mean residence times ($\tau_{H,O}^*$) of water molecules, calculated within first minimum of the HF/MM and ONIOM-XS's O-O_w RDFs.

FIGURE CAPTIONS

Figure 1 a) O-O, b) O-H, c) H-O and d) H-H radial distribution functions and their corresponding integration numbers, as obtained by the HF/MM and ONIOM-XS MD simulations.

Figure 2 Distributions of coordination numbers, calculated within first minimum of the HF/MM and ONIOM-XS MD's O-O RDFs.

Figure 3 Distributions of number of HBs, calculated according to the geometrical criteria of the H-bond formation.

Figure 4 Some selected HB structures in liquid water, as observed in the ONIOM-XS simulation.

Figure 5 Distributions of O---O---O angles, calculated within first minimum of the HF/MM and ONIOM-XS MD's O-O RDFs (*i.e.*, within O---O distance of 3.2 Å).

Figure 6 Distributions of a) O-H---O and b) O---H-O angles, calculated within first minimum of the HF/MM and ONIOM-XS MD's H-O and O-H RDFs (*i.e.*, within H---O and O---H distances of 2.5 Å).

Figure 7 Fourier transforms of the hydrogen velocity autocorrelation functions (Q_1 , Q_2 and Q_3), as obtained by a) HF/MM and b) ONIOM-XS MD simulations.

Figure 8 Time dependence of a) H1---O, b) H2---O and c) O---H distances, together with d) number of water molecules surrounding the central H₂O (*i.e.*, calculated within O-O distance of 3.20 Å; Red line: number of all nearest-neighbor water molecules, Black line: number of only water molecules forming HBs), as obtained by the HF/MM MD simulation.

Figure 9 Time dependence of a) H1---O, b) H2---O and c) O---H distances, together with d) number of water molecules surrounding the central H₂O (*i.e.*, calculated within O-O distance of 3.20 Å; Red line: number of all nearest-neighbor water molecules, Black line: number of only water molecules forming HBs), as obtained by the ONIOM-XS MD simulation.

Table 3

Method	CN	t_{sim} (ps)	$t^* = 0.0$ ps		$t^* = 0.5$ ps	
			$N_{\text{cr}}^{0.0}$	$\tau_{H_2O}^{0.0}$	$N_{\text{cr}}^{0.5}$	$\tau_{H_2O}^{0.5}$
HF/MM MD*	4.9	40.0	944	0.21	84	2.33
ONIOM-XS MD*	4.7	30.0	607	0.23	65	2.17
HF/MM MD ⁶³	4.6	12.0	292	0.20	31	1.80
HF/MM MD ³⁴	4.2	40.0	515	0.33	112	1.51
MP2/MM MD ³³	4.6	5.0	-	0.28	-	2.45
Experiment ⁶⁴			-	0.5	-	-

* This work

Table 1

Method	R_{O-O} (Å)		R_{O-H} (Å)		R_{H-H} (Å)		CN
	R_{max}	R_{min}	R_{max}	R_{min}	R_{max}	R_{min}	
HF/MM MD*	2.84	3.20	1.90	2.46	2.37	2.98	4.9
ONIOM-XS MD*	2.82	3.22	1.91	2.49	2.35	2.95	4.7
HF/MM MD ³³	2.92	3.41	2.06	2.53	2.59	3.24	4.2
MP2/MM MD ³³	2.87	3.43	1.93	2.61	2.44	2.95	4.7
B3LYP/MM MD ³³	2.81	3.31	1.85	2.42	2.33	2.89	4.2
XS ¹	2.82	-	-	-	-	-	-
XS ⁵	2.72	-	-	-	-	-	3.7
ND ²	2.78	-	1.79	-	-	-	-
ND ³	2.67	-	1.67	-	-	-	4.2
ND ⁴⁹	2.83	-	1.79	-	-	-	4.2
ND ⁵⁰	2.89	-	1.95	-	-	-	-

* This work

Table 2

Method	Q_1 (cm ⁻¹)	Q_2 (cm ⁻¹)	Q_3 (cm ⁻¹)
HF/MM MD*	3624 (3588,3662)	1670	3712 (3678,3730)
ONIOM-XS MD*	3606 (3650)	1660	3720 (3755)
HF/MM MD ³⁴	3770 (3620,3680)	1640	3775 (3615,3675)
MP2/MM MD ³³	3964 (3844)	1640	3964 (3847)
B3LYP/MM MD ³³	3580 (3460)	1622	3553 (3458)
Experiment ³⁴	3400 (3200)	-	-
Experiment ⁵⁵	3410 (3280)	-	-
Experiment ⁵⁶	3400	1643.5	-

* This work

24

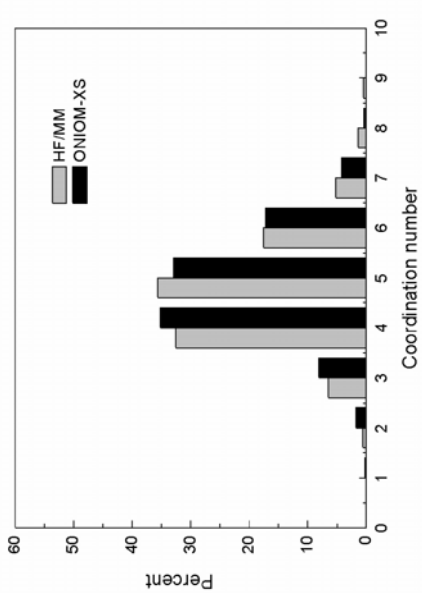


Figure 2

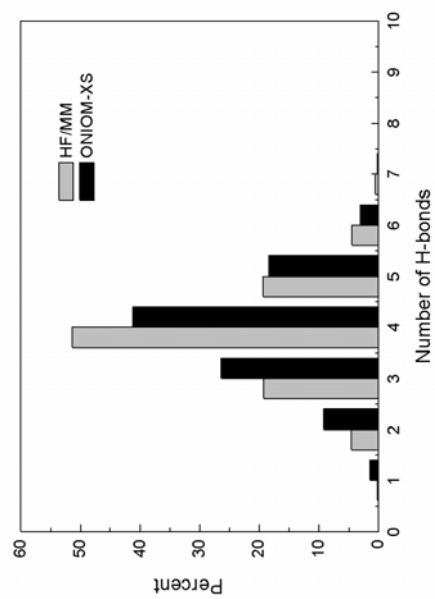


Figure 3

23

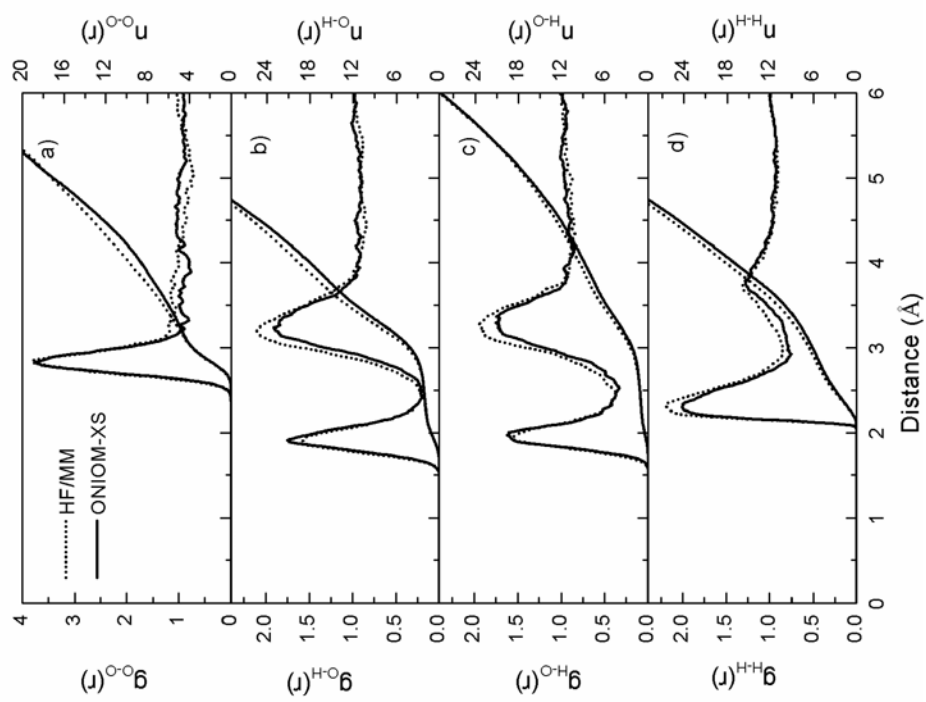
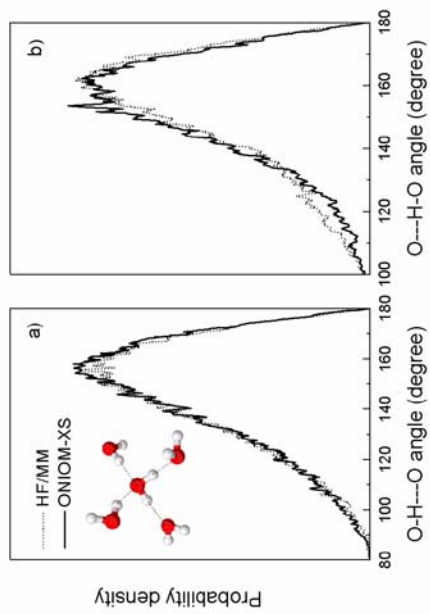


Figure 1



26

Figure 6



25

Figure 4

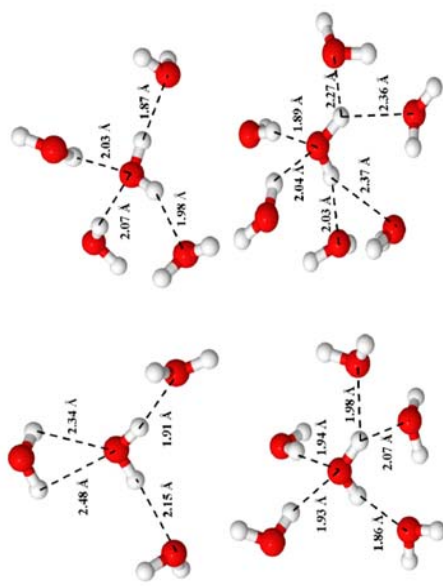


Figure 5

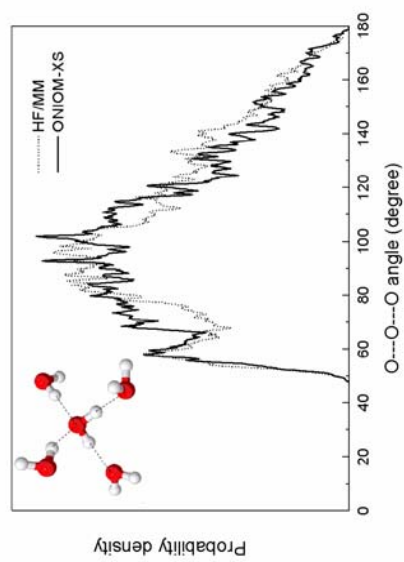


Figure 7

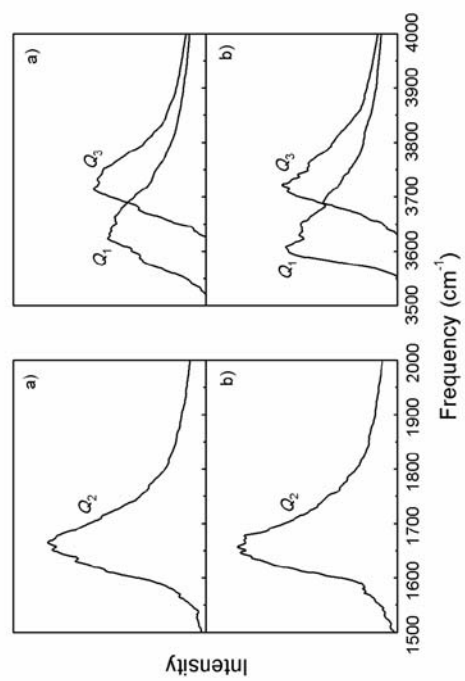


Figure 9

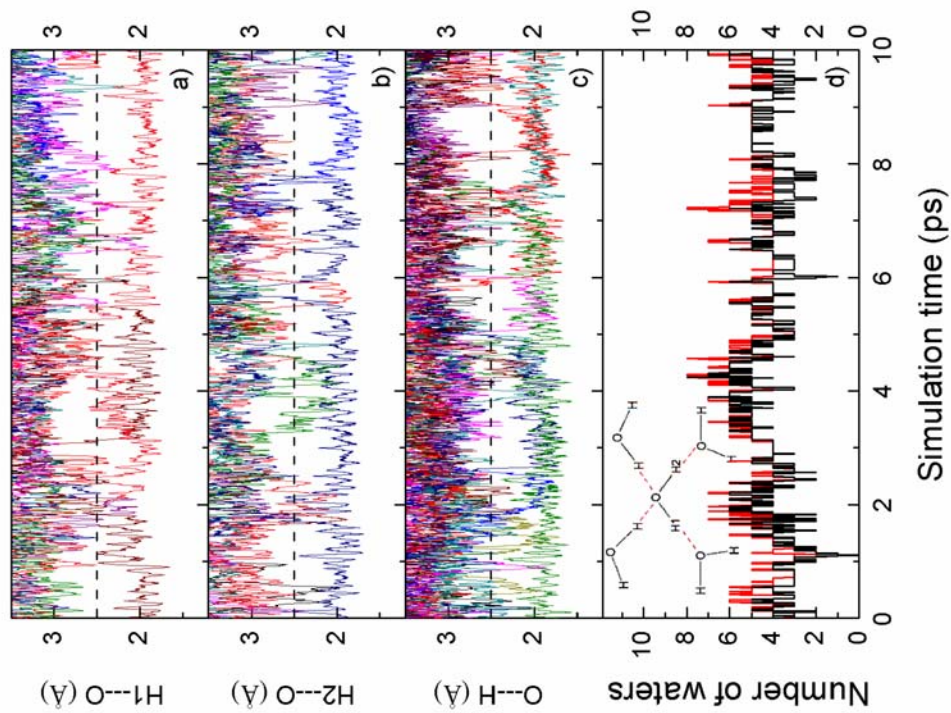
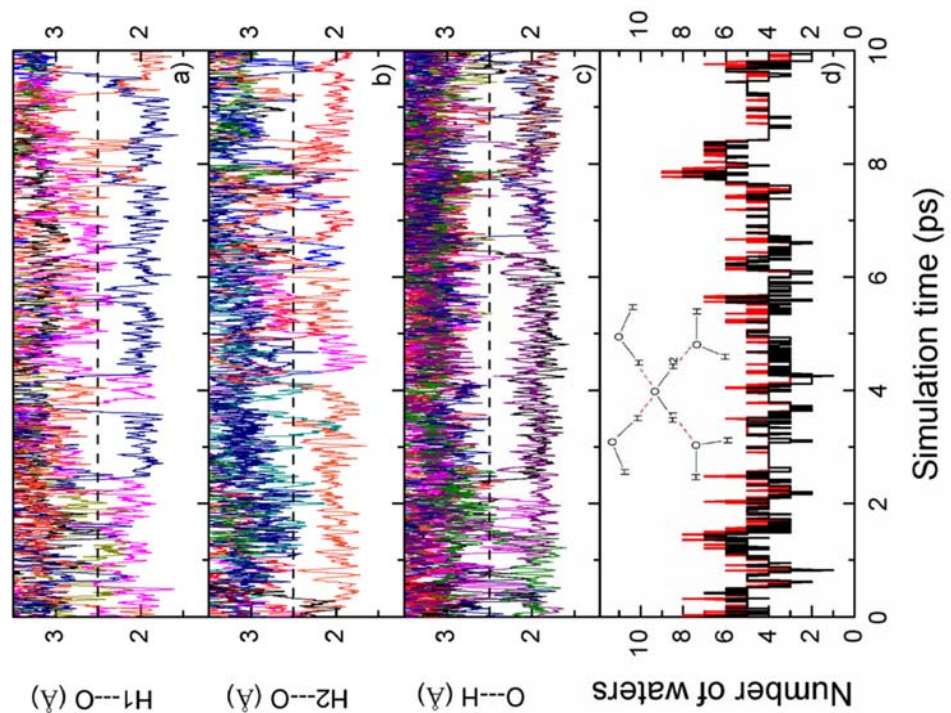


Figure 8



CURRICULUM VITAE

MISS SUKHONTIP THAOMOLA

Education Background:

- 2000-2003 B.Sc. (Physics), Thaksin University, Songkhla, Thailand
- 2004-2007 M.Sc. (Chemistry), Kasetsart University, Bangkok, Thailand
- 2008-2012 Ph.D. Candidate (Chemistry), Suranaree University of Technology,
Nakhon Ratchasima, Thailand

Experiences:

- 2006-2007 Research Assistant, Cheminformatics Research Unit, Kasetsart
University, Bangkok, Thailand
- 2007-2008 Teaching Physics, Faculty of Engineering, North-Chiang Mai
University, Chiang Mai, Thailand
- 2010-2012 Teaching Chemistry, Faculty of Sciences and Technology, Nakhon
Ratchasima Rajabhat University, Nakhon Ratchasima, Thailand

Grant and Fellowships:

- 2004-2005 The Postgraduate on Education and research in Petroleum and
Petrochemical Technology (ADB-MUA)
- 2008-2011 The program Strategic Scholarships for Frontier Research Network
(Thai Doctoral degree) from the Commission on Higher Education,
Thailand